View metadata, citation and similar papers at core.ac.uk

brought to you by CORE

provided by Infoscience - École polytechnique fédérale de Lausanne

COUPLING OF PHOTOCATALYTIC AND BIOLOGICAL PROCESSES AS A CONTRIBUTION TO THE DETOXIFICATION OF WATER: CATALYTIC AND TECHNOLOGICAL ASPECTS

THÈSE N^{O} 2470 (2001)

PRÉSENTÉE AU DÉPARTEMENT DE GÉNIE RURAL

ÉCOLE POLYTECHNIQUE FÉDÉRALE DE LAUSANNE

POUR L'OBTENTION DU GRADE DE DOCTEUR ÈS SCIENCES TECHNIQUES

PAR

Sandra Patricia PARRA CARDONA

chimiste, Universidad del Valle, Cali, Colombie

de nationalité colombienne

acceptée sur proposition du jury:

Dr C. Pulgarin, directeur de thèse
Dr S. Canonica, rapporteur
Prof. C. Comninellis, rapporteur
Dr J. Kiwi, rapporteur
Dr S. Malato, rapporteur
Prof. P. Pichat, rapporteur
Prof. P. Péringer, rapporteur

Lausanne, EPFL
2001

ABSTRACT

This research contributes to the study and development of a new degradation technique that couples solar and biological processes for the treatment of biorecalcitrant, non-biodegradable, and/or toxic organic substances present in the aqueous medium. Efficient physicochemical pretreatments are necessary to modify the structure of the pollutants, by transforming them into less toxic and biodegradable intermediates, allowing then, a biological procedure to complete the degradation of the pollutant load in a shorter time and in a less expensive way. The strategy of coupling photochemical and biological processes implicates among others, the study of some fundamental physicochemical properties, the optimization of a coupled reactor at laboratory scale (2 litres), and the study of solar photocatalytic treatment efficacy under direct sunlight using parabolic collectors of 40 to 200 litres.

The study of the structure effect on the photoreactivity *via* TiO_2 catalysis is studied using several substituted phenols to cover a wide variety of electronic effects, ranging from strong electron-donating (activating) to strong electron-withdrawing (deactivating) groups and herbicides with very similar molecular structures (metobromuron, isoproturon, chlorbromuron, and chlorotoluron). The photoreactivity of these compounds is affected by the electronic nature of the substituents and their positions in the aromatic ring, being higher when there is a greater electronic density. The Hammett constant, which represents the effect that different substituents have on the electronic character of the aromatic studied compounds, appears to give an adequate descriptor of their photocatalytic degradability.

One important consideration in the TiO_2-photocatalysed reactions is the adsorption of the organic compound on the surface of semiconductor particles. The dark adsorption isotherms for complete *p*-halophenols series and four herbicides are measured and correlated with their photoreactivity. The results indicate that no direct correlation exists between the extents of adsorption and the initial photodegradation rates of the studied compounds.

Concerning the optimization and utilization of an integrated photocatalytic-biological process at laboratory scale, two kinds of combined systems are developed using immobilized biomass for the biological step and either diluted Fe^{3+}/H_2O_2 (Fenton reaction) or TiO_2 supported on glass rings for the photocatalytic pre-treatment. The advantages of the latter system are that the catalyst can be re-used and that the pH of the solution remains at neutral values. The photo-Fenton reaction instead, renders the phototreated solution acidic making neutralization necessary.

The photochemical-biological flow reactors mentioned above, are employed to completely mineralize an isoproturon-herbicide solution. Preliminary experiments concerning the chemical and biological characteristics of the phototreated solution, are carried out to determine the moment at which it becomes biocompatible. Two operation modes (continuous or semi-continuous) of the photo-Fenton-biological coupled reactor are compared by studying the efficiency of the photochemical, biological, and overall treatments of *p*-nitro-*o*-toluenesulfonic acid (*p*-NTS) in solution. The two main parameter affecting the performance of the photo-assisted reactor in continuous mode are related to the very low pollutant concentration that characterise this kind of operation mode and to the high residual H_2O_2 concentration after the pretreatment. Thus, a semi-continuous mode was applied to try to overcome these inconveniences. In these conditions, 50 to 70 litres of polluted water can be treated per day per litre of photoreactor.

The last part of this thesis, addresses the study of the solar photocatalytic treatment efficacy under direct sunlight using parabolic concentrating (Helioman reactors) and non-concentrating (CPC) collectors. This part, carried out at the “Plataforma Solar de Almería” (PSA) in Spain, indicates that the solar photocatalytic treatment is effective for the purification of water contaminated by herbicides and other substances of industrial origin like the *p*-NTS. It is demonstrated the utility of both homogeneous (based on Fe^{3+}/H_2O_2 reaction) and heterogeneous photocatalysis (based on TiO_2) as pretreatment methods that can be followed by a biological treatment. Using a coupled system, the treatment of 100 to 300 litres of polluted water per square metre of photoreactor can be envisaged in a sunny day. The low manufacturing, installation, and maintenance costs, and easy operation of the CPC, compared with Helioman collectors, suggest that the former ones are, at present, the best way to apply the solar detoxification technology.

RÉSUMÉ

Cette recherche contribue à l'étude et au développement de nouvelles techniques de traitement photochimique (solaire), biologique et de leur couplage, pour le traitement de composés organiques biorécalcitrants, non-biodégradables, et/ou toxiques présents dans l'eau et qui sont générés par les activités industrielles ou agro-industrielles représentant un risque pour l'environnement. Des procédés de pré-traitements physico-chimiques efficaces, tel que l'irradiation solaire captée par des catalyseurs, sont nécessaires pour modifier la structure des polluants, les rendant moins toxiques et plus facilement biodégradables. Ils permettent ainsi d'acheminer les eaux traitées vers un traitement biologique en peu de temps et à moindre coût. Le développement d'un procédé couplé efficace nécessite l'étude des paramètres chimiques, physico-chimiques et biologiques impliqués dans le processus. Les informations dégagées de ces travaux permettent la mise en place et l'optimisation d'un réacteur couplé à l'échelle de laboratoire (environ 2 litres). La conception modulaire d'un tel système a permis de tester un grand nombre de conditions et de variables par des modifications très simples. Les informations ainsi obtenues permettent de tester et d'évaluer systématiquement l'efficacité des réacteurs de 40 à 200 litres utilisant sur le terrain une irradiation solaire directe.

Cette thèse comporte une étude détaillée des processus physiques et chimiques fondamentaux affectant la dégradation des polluants sous l'effet de la lumière: type des réacteurs, nature du système catalytique (Fe^{3+} ou TiO_2), concentration de la substance, du catalyseur et des accepteur d'électrons, etc. Le lien entre la structure chimique des polluants et leur dégradabilité photochimique est particulièrement étudié. Cela a permis, entre autres, de démontrer que la photoréactivité (*via* TiO_2) de nombreuses substances phénoliques est affectée de manières diverses en fonction du caractère électro-attracteur ou électro-doneur ainsi que des positions des substituants du cycle aromatique. La constante d'Hammett, dont la valeur traduit l'effet électronique des différents substituants sur le cycle aromatique des phénols étudiés, s'est

avéré être le descripteur le plus adéquat, quoique incomplet, de la susceptibilité d'une substance à être dégradée par voie photocatalytique.

Les isothermes d'adsorption d'une série de *p*-halophénols et d'herbicides sont établis. Une tentative de corrélation entre les valeurs d'adsorption obtenues et la vitesse initiale de photodégradation de chacun des composés montre qu'il n'existe pas, dans notre cas, de corrélation directe entre la capacité d'adsorption des substances sur le TiO_2 et leur photodégradabilité.

La mise en marche et optimisation d'un réacteur photochimique et biologique couplé à l'échelle du laboratoire permet d'acquérir des informations techniques et de définir les paramètres hydrodynamiques pour un bon fonctionnement en continu et semi-continu du système. Deux systèmes photocalytiques (Fe^{3+} en solution ou TiO_2 fixé) sont utilisés, couplés à un système biologique constitué d'une colonne à biomasse immobilisée sur un support d'argile expansée. Des études approfondies sur la toxicité et la biodégradabilité de solutions traitées permettent de décider du moment où le traitement photochimique peut laisser place au traitement biologique. L'efficacité du système couplé et sa stabilité pendant des périodes de traitement de quelques semaines est confirmée avec différentes configurations et différentes substances. Les deux principaux facteurs qui affectent l'efficience du système couplé en mode continu (avec Fe^{+3} et H_2O_2) sont la faible réactivité photochimique de la solution traitée qui est toujours diluée par une alimentation continue du photoréacteur et la difficulté à maintenir de faibles concentrations de H_2O_2 qui inhibent le réacteur biologique. Ces difficultés sont surmontées par l'application d'un système semi-continu (batch séquentiel). Ainsi, de 50 à 70 litres d'eau polluée peuvent être traitées par jour et par litre de photoréacteur.

Les études précédentes sont complétées par le traitement photochimique par ensoleillement direct d'eaux contenant différents types de polluants organiques au moyen de collecteurs paraboliques concentrateurs (Helioman) et non-concentrateurs (CPC). Cette dernière partie, effectuée à la Plataforme Solaire Européenne à Almeria en Espagne, permet d'envisager sans réserve le couplage d'un réacteur CPC à un réacteur biologique pour le traitement, par journée ensoleillée, de 100 à 300 litres d'eau polluée par mètre carré de photoréacteur. Cette performance est d'autant plus intéressante que le CPC est un photoréacteur ayant un coût de fabrication, d'installation, d'utilisation et d'entretien très faible.

ACKNOWLEDGMENTS

A Ph.D thesis is simply the culmination of a few years of learning. Throughout these years, I have received much support from my family, teachers, and friends... Indeed, many people believed in me and kept on teaching me many things. It would be impossible to individually acknowledge all those who merit it. However, I will try to express my gratitude to those who made this thesis possible and enriched my life in the past few years.

First of all, to my parents Ana Emilia and Heberth Tulio, and to my Family. I am immensely grateful to “mi madrecita adorada” (my adored little mother) who has always supported me and has been willing to make considerable sacrifices for giving to me all possible advantages in life. I am very grateful to my brother Carlos Fernando, “el hermani” (my little brother) as I call him. Carlos Fernando, who was born when I was 9 year old, is like a son for me. I thank him for his affection, his jokes, and above all, for supporting our mother in difficult moments when I was not present. I am deeply grateful to my aunt Ana Lucia and my uncle Rosmel who “have taken the risk” of backing me in the debt that I acquired with the Colombian government, for my doctoral studies.

To my boyfriend Carlos Andrés, who has always supported me. His love, patience, help, and understanding during the past few years have been determinant for the good development of my work. For this, for his valuable suggestions and comments during the preparation of this manuscript, and for every thing we have shared, my deepest gratitude!.

I am profoundly grateful to César Pulgarin and his family: Jacquelin, Adrian, Leandra, and Mara. They welcome me into their home when I arrived to Switzerland, and taught to me much about living in this country. It was in their home where I first tried “la fondue” and where I learned my first french words. I am very grateful to them. César is much more than a thesis director: he is a good friend and a mentor. César has been able to skilfully manage this research without forgetting the ever essential human relationships. He has always been by my side, ready

to talk and to help in finding ways to overcome problems in my research. Beyond that, César is an inextinguishable source of encouragement when things did not go so well. He always has time for precious advice or for talking about many aspects of life. From deep inside, thank you César for your unconditional and invaluable support, for your sincere friendship, and your always opportune and heartfelt help and guidance.

My acknowledgments to the reviewers of this thesis, Prof. P. Péringer, Prof. C. Comninellis, Dr. J. Kiwi, Dr. S. Malato, Prof. P. Pichat, Dr. S. Canonica, and Prof. A. Mermoud, president of jury, for accepting to read and evaluate my work and for providing valuable suggestions and comments.

During my Ph.D. work, I also performed experiments at the University of Metz, in Saint-Avold, France, and at the “Plataforma Solar de Almería”, in Almería, Spain. I am very grateful to Dr. Didier Robert, Mr. Julián Blanco, and Dr. Sixto Malato for receiving me in their respective laboratories, for their guidance, and for interesting scientific discussions we had for the preparation of scientific papers.

My experience at the LBE has been very enriching. I thank to Professor Paul Péringer not only for receiving me in his laboratory but also for the support and confidence that he has given to César and his research group. I thank all those members of the laboratory who have contributed to make my stay very pleasant. I am particularly grateful to Heidi Bernard, our lab’s secretary, for all her invaluable help and her friendliness. I would like to extend my gratitude to Mrs. Nevenka Adler for her friendliness, help, and our useful discussions about work and many other subjects. I thank very much Jean-Pierre Kradolfer for his skilful technical assistance. My gratitude to Sylvie Marcacci and Katia Szynalsky for her friendship and preoccupation for the security of our laboratory. I am also grateful to Chantal Seignez, Jean-Paul Schwitzguebel, and Marc Deront for their help and encouragement. I also express my gratitude to the Colombian colleagues and friends of the “chemical-biological coupled process group”: Guiovana Rincon, Victor Sarria, and Ricardo Torres for their support, help, and friendship. I am very grateful to all of them for contributing to make my stay at the LBE so pleasant and enriching.

To all former students at the LBE who have contributed, in one way or another, to the realisation of this work: Marie-Laure Thevenaz, Isabelle Rappaz, Marco Invernizzi, Kim Ng,

Milena Lapertot, Yannick Bischoff, Seydina Diouf, Alexandre Audergon, and Lhasen Menkari. To all of them my great gratitude for their contributions and the moments we shared.

I am profoundly grateful to all my Colombian friends who were like a family throughout the last few years. I thank them for their friendship, support, help, encouragement, for all the experiences and moments shared, and for our interesting discussions about our Colombia, science, computers, religion, life,...

I want to thank particularly Adona Oviedo and José Luis Bermúdez, “Los Chuchis”. They are a couple that I admire and love very much. All the moments (goods and not so) shared with them are very special and important to me. Thanks to “Los Chuchis” for their sincere friendship and unconditional support.

I am also very grateful to Luis Berardo Borda for his friendship and our discussions during the coffee’s brake at the “Arcadie”.

I can not forget Norberto Benitez, a very special friend who supported me during the first part of my stay in Switzerland. Thanks to Norberto for his friendship.

During the writing of this thesis, the help of Nora Eugenia Restrepo was invaluable. I am profoundly grateful to Nora not only for the time and effort spent proofreading this manuscript and for her valuable suggestions and comments, but also for her unconditional friendship and help. I also want thank all the people who help me in the preparation and correction of several papers: María de la Fuente, Nevenka Adler, David Fermín, and Carlos Andrés Peña.

This project has been carried out within the framework of the cooperation program, in the environmental field, between the Swiss Federal Institute of Technology in Lausanne (EPFL)-Switzerland and the “Universidad del Valle”, Colombia. The support of the Colombian Institute for the Science and Technology Development “Francisco José de Caldas (COLCIENCIAS), of the Cooperation Center (especially to J-M. Plancherel and J-C Bolay) and the Social Service (especially to C. Vinckenbosh and A. Jaccard) of the EPFL , and of each one of the concerned Swiss and Colombian institutions, have been the key for the good development of this thesis and I am sincerely grateful to them.

LIST OF SYMBOLS

AM	Air Mass ratio
AOP	Advanced Oxidation Processes
AOS	Average Oxidation State
BOD	Biological Oxygen Demand
c	Light speed
CB	Chlorbromuron
$\mathbf{C_{eq}}$	Equilibrium concentration
$\mathbf{C_i}$	Initial concentration
COD	Chemical Oxygen Demand
CPC	Compound Parabolic Collector
CR	Concentration Ratio
CT	Chlorotoluron
DOC	Dissolved Organic Carbon
$\mathbf{E_{bg}}$	Semiconductor band-gap energy
$\mathbf{EC_{50}}$	Effective Concentration at which 50% of light is lost
$\mathbf{E_{HOMO}}$	Energy of the Highest Occupied Molecular Orbital
$\mathbf{E_{LUMO}}$	Energy of the Lowest Unoccupied Molecular Orbital
HM	Helioman collector
HPLC	High Performance Liquid Chromatography
I	Photon flux density
IP	Isoproturon
k	First-order rate constant
K	Adsorption constant

K_{OW}	1-octanol water partition coefficient
l	Litre
LBE	Laboratory of Environmental Engineering
L-H	Langmuir Hinshelwood model
λ	Wavelength
MB	Metobromuron
MW	Molecular Weight
NHE	Normal Hydrogen Electrode
pKa	Acid dissociation constant
***p*-NTS**	*p*-nitrotoluene-*o*-sulfonic acid
PSA	Plataforma Solar de Almería
PTC	Parabolic Trough Collector
PZC	Point of Zero Charge
σ	Hammett constant
t_r	Residence time
V	Volume
v_o	Initial degradation rate
V_{TOT}	Total volume
UV_D	Direct ultraviolet light
UV_G	Global ultraviolet light
VB	Valence Band

TABLE OF CONTENTS

ABSTRACT i

RÉSUMÉ iii

ACKNOWLEDGMENTS v

LIST OF SYMBOLS ix

LIST OF FIGURES xv

LIST OF TABLES xix

CHAPTER 1

INTRODUCTION 1

1.1 Generalities 1

1.2 Overview 3

1.3 Background 5

1.3.1 Heterogeneous photocatalysis 6

Mechanism of the TiO_2 - photocatalysed degradation 9

Influence of some fundamental parameters on the kinetics of TiO_2 photocatalysis 11

1.3.2 Homogeneous photodegradation 14

Fenton and Fenton photo-assisted reactions 16

1.3.3 Application of heterogeneous photocatalysis and Fenton reaction to water treatment 18

1.4 The studied substances 19

1.4.1 Substituted phenols 20

1.4.2 Phenylurea herbicides 20

1.4.3 p-nitrotoluene-o-sulfonic acid (p-NTS) 22

1.5 Bibliography 22

CHAPTER 2

STRUCTURAL PROPERTIES AND PHOTOREACTIVITY RELATIONSHIPS **27**

2.1 Introduction **27**

2.2 Experimental **29**

2.2.1 Materials **29**

2.2.2 Photodegradation experiments **29**

2.2.3 Chemical and biological analysis **30**

High Performance Liquid Chromatography (HPLC) **30**
Dissolved Organic Carbon (DOC) **30**
Chemical Oxygen Demand (COD) **30**
Biological Oxygen Demand (BOD) **31**

2.2.4 Adsorption isotherms **31**

2.2.5 Structure-photoreactivity relationships. Computational details **32**

Model construction **32**

2.3 Results and Discussion **33**

2.3.1 Photocatalytic degradability of substituted phenols via TiO_2 catalysis **33**

Influence of the substituent nature at para- position **33**
Effect of the substituent position **36**

2.3.2 Photocatalytic degradability of p-halophenols via TiO_2 catalysis **38**

Influence of physicochemical characteristics on p-halophenols photodegradability **39**

2.3.3 Molecular structure and biodegradability relationship **45**

2.3.4 Photocatalytic degradability of four phenylurea herbicides **47**

Direct photolysis essay **47**
Some parameters affecting the herbicides photodegradation via TiO_2 catalysis **48**
Comparison of the photocatalytic degradability of the four herbicides **51**
Influence of physicochemical characteristics of herbicides on their photodegradability **53**

2.4 Conclusions **59**

2.5 Bibliography **61**

CHAPTER 3

INTEGRATED PHOTOCATALYTIC-BIOLOGICAL PROCESS **65**

3.1 Introduction **65**

3.1.1 General strategy for coupling photochemical and biological treatments **66**

3.2 Experimental **68**

3.2.1 Materials **68**

3.2.2 Coupled photochemical-biological flow reactor. Procedures **68**

Coiled photochemical reactor **69**
Coaxial photocatalytic reactor **70**
Biological reactor **70**

3.2.3 Chemical and biological analysis **71**

Dissolved Organic Carbon (DOC) **71**
Chemical Oxygen Demand (COD) **71**
High Performance Liquid Chromatography (HPLC) **72**
Biological Oxygen Demand (BOD) **72**
Zahn-Wellens biodegradability test **73**
Microtox® rapid toxicity testing system **73**
Hydrogen peroxide analysis **74**

3.3 Results and discussions **74**

3.3.1 Biodegradability of metobromuron, isoproturon, and p-NTS initial solutions **74**

3.3.2 Photochemical-biological flow system for p-nitro-o-toluenesulfonic acid treatment **77**

Continuous versus batch photo-Fenton process **77**
Chemical and biological characteristics of the phototreated p-NTS solution **82**
Mineralization with the coupled reactor **84**

3.3.3 Photochemical-biological flow system for metobromuron and isoproturon herbicides treatment **90**

Optimal photodegradation conditions **90**
Chemical and biological characteristics of the phototreated solutions **93**
Isoproturon mineralization by the coupled reactor in semi-continuous mode **97**

3.3.4 Mineralization of isoproturon using supported TiO_2 for the photochemical stage **100**

Supported versus suspended TiO_2 **100**
Supported TiO_2 durability **101**
Chemical and biological characteristics of the phototreated isoproturon solution **101**
Photochemical-biological coupled flow treatment **103**

3.4 Conclusions **105**

3.5 Bibliography **107**

CHAPTER 4

APPLICATION OF THE SOLAR FIELD SCALE TECHNOLOGY **109**

4.1 Introduction **109**

4.1.1 Solar radiation **109**

4.1.2 Solar collector technology **112**

4.1.3 Solar water detoxification collectors **115**

Parabolic trough collectors **118**
One-sun collectors **119**
Compound Parabolic Concentrator (CPC) **120**

4.1.4 Application of solar photocatalysis to wastewater decontamination **122**

4.2 Experimental **123**

4.2.1 Materials **123**

4.2.2 Solar collectors **123**

Helioman collector **124**
Compound parabolic collector **124**

4.2.3 Evaluation of solar UV radiation **126**

4.2.4 Chemical analysis **126**

4.3 Results and discussions **127**

4.3.1 Comparison between CPC and HM reactors during the photodegradation of isoproturon and p-NTS via suspended TiO_2 **127**

4.3.2 Comparison of different advanced oxidation processes in a CPC reactor **129**

Photodegradation of isoproturon **129**
Photodegradation of p-nitrotoluene-o-sulfonic acid **131**

4.3.3 Perspectives for the coupling of a CPC-biological system at field pilot scale **133**

The photo-Fenton reaction as pre-treatment. **133**
The TiO_2 photo-assisted process as pre-treatment. **135**

4.4 Conclusions **138**

4.5 Bibliography **139**

GENERAL CONCLUSIONS AND PERSPECTIVES **141**

CURRICULUM VITAE **145**

LIST OF FIGURES

INTRODUCTION

A simplified view of the water cycle. **2**

Scheme illustrating the different parts studied in the thesis work. **4**

Illumination of a semiconductor. **7**

TiO_2-semiconductor photocatalysis process. **10**

Yearly distribution of the references on TiO_2 photocatalysis. **19**

Para-substituted phenols. **20**

General structure of urea herbicides. **21**

Chemical structure, chemical name, and molecular formula of the herbicides studied. **21**

Chemical structure of p-nitrotoluene-o-sulfonic acid (p-NTS). **22**

STRUCTURAL PROPERTIES AND PHOTOREACTIVITY RELATIONSHIPS

Relationship between the initial degradation rate (v_o) and Hammett constants (σ) of p-substituted phenols. **35**

Representation of keto-enol tautomeric equilibrium for hydroquinone and benzoquinone. **36**

Photodegradation of catechol, resorcinol, and hydroquinone. **37**

Schematic representation of the activation of the aromatic cycle by the -OH groups. **37**

Photocatalytic degradation of p-halophenols. **39**

Relationship between the initial degradation rate and the carbon halide bonds strengths of p-halophenols. **40**

Relationship between the initial degradation rate and Hammett constants of p-halophenols. **41**

Relationship between the initial degradation rate and the 1-octanol-water partition coefficient. **42**

Relationship between K_{ow} and the extent of adsorption of p-halophenols on TiO_2 ($n_2^s{}_{max}$). **43**

p-halophenols adsorption isotherms on TiO_2. **44**

UV spectra between 190 and 400 nm of herbicides and suntest lamp light. **48**

Effect of TiO_2 concentration on the initial degradation rates of herbicides. **49**

Influence of the initial concentration on the photodegradation of MB with 1.0 g l^{-1} of TiO_2. **50**

Variations of the initial degradation rates of MB as a function of its initial concentration. **51**

Photodegradation of herbicide solutions (0.1 mmol l^{-1}) in presence of TiO_2 (1.0 g l^{-1}). **52**

Chemical structure of herbicides. **54**

Molecular electrostatic potential (MEP) maps for herbicides. **56**

Herbicides adsorption isotherms on TiO_2. **57**

INTEGRATED PHOTOCATALYTIC-BIOLOGICAL PROCESS

Scheme of the coupled photochemical-biological flow reactor. **69**

Zahn-Wellens biodegradability test of MB and IP. **75**

Zahn-Wellens biodegradability test of p-NTS. **76**

DOC evolution as a function of time at different flow rates. **78**

Energy consumption in kW h l^{-1} for the treatment of a p-NTS solution **80**

Photo-Fenton batch degradation of a p-NTS solution at different Fe^{3+} concentrations. **81**

DOC evolution during the photo-Fenton treatment of a p-NTS solution. **82**

Phototreatment of a p-NTS solution by Fenton reaction. **83**

DOC remotion by photochemical, biological, and coupled (overall) treatment of p-NTS. **90**

Rate constant of IP and MB oxidation at different Fe^{3+} concentrations. **92**

Rate constant of MB oxidation at different H_2O_2 concentrations. **93**

Phototreatment of a MB solution using suspended TiO_2 catalyst. **94**

Phototreatment of a IP solution using suspended TiO_2 catalyst. **96**

Average Oxidation State evolution as a function of time for the photodegradation of IP. **97**

Photocatalytic degradation of IP by supported (open points) and suspended (full points) TiO_2. **100**

Phototreatment of an IP solution using supported TiO_2 catalyst. **102**

Coupled photocatalytic and biological process for the mineralization of IP. **103**

UV spectra between 190 and 400 nm of a phototreated solution of IP. **104**

APPLICATION OF THE SOLAR FIELD SCALE TECHNOLOGY

Solar radiation spectrum plotted from 0.2 to 4.5 μm. **110**

Air mass and solar components. **111**

Ultraviolet spectrum on the earth surface (standard ASTM). **112**

Non-concentrating solar collectors for domestic heat water application. **113**

Medium-concentrating solar collectors. PTC type (PSA, Spain). **114**

High concentrating solar collector. Parabolic dish solar collector (PSA, Spain). **114**

Relation between the photocatalytic reaction rate and the intensity of the radiation received. **116**

Solar reflection on a CPC collector. **121**

HM-type collector in tracking position. **124**

View of the CPC used for the solar driven experiments at the PSA. **125**

Linear transform of the kinetic curves of IP photodegradation in CPC and HM reactors. **127**

Treatment of IP in different degradation systems. **130**

Treatment of p-NTS in different degradation systems. **131**

Phototreatment of (a) MB and (b) IP in a CPC reactor. **134**

Degradation of p-NTS (0.5 mmol l^{-1}) in a CPC reactor with 0.2 g l^{-1} of TiO_2. **136**

Degradation of IP (0.1 mmol l^{-1}) in a CPC reactor. **137**

LIST OF TABLES

INTRODUCTION

Band positions of some common semiconductor photocatalysts in aqueous solution at pH=1. **8**

STRUCTURAL PROPERTIES AND PHOTOREACTIVITY RELATIONSHIPS

Initial photodegradation rates (v_o) and first order rate constants (k) relative to phenol for the abatement of p-substituted phenols. **34**

Molecular characteristics of the p-halophenols. **39**

Dark adsorption parameters of the four p-halophenols. **45**

Biodegradability of different substituted phenols. **46**

Photodegradation of IP, CT, MB, and CB herbicides in different reactors. **53**

Dark adsorption parameters of the four herbicides. **58**

INTEGRATED PHOTOCATALYTIC-BIOLOGICAL PROCESS

Attempts of biodegradation of a p-NTS solution in a fixed bed biological reactor. **76**

Performance of the coiled photochemical reactor operated in continuous mode at four different flow rates for degradation of a p-NTS solution (330 mg C l^{-1}). **79**

Performances for p-NTS degradation by the coupled photochemical (coiled) - biological reactor in continuous mode at three different flow rates. **87**

Performances for p-NTS degradation by the coupled photochemical (coiled) - biological reactor in semi-continuous mode at five different flow rates. **88**

Performances for IP degradation by the coupled photochemical (coiled) - biological reactor in semi-continuous mode. **99**

Performances for IP degradation by the coupled photochemical (coaxial)- biological reactor using supported TiO_2 and fixed bacteria. **105**

APPLICATION OF THE SOLAR FIELD SCALE TECHNOLOGY

CHAPTER 1

INTRODUCTION

1.1 Generalities

The whole amount of water existing on earth (oceans, lakes, rivers, polar regions, glaciers, underground water, water of the biosphere and atmosphere) is around 1.4×10^9 km^3 from where only ~0.8 – 1.0% (i.e., ~1.3×10^7 km^3) corresponds to total drinking water [1]. World water consumption per year is about 9×10^3 km^3 and at present, the quantity of available potential drinking water per year is between 10 and 30×10^3 km^3. This numbers clearly illustrates how even a small shortage of water could become a threat to mankind. Besides, the world suffers from growing health and hygienic problems and a high percentage of diseases in developing countries is caused by a deficient water supply.

The drinking water is not only rare and limited, but also the central element of all the vital, social, and economic processes in the frame of the closed water cycle shown in Figure 1.1. This cycle is in crisis because of the development of a consumer society that entails the augmentation of industrial or agro-industrial activities. These activities generate an enormous diversity (~200.000) of commercialized chemical substances that arrive in huge quantities to the water cycle by different ways, endangering the fragile natural equilibrium of which all animals, including humans, are tributary.

One of the most alarming phenomena is the growing accumulation of hardly-biodegradable anthropogenic substances under the saturated auto-depurative conditions of such perturbed and overloaded cycle. The situation worsens by the lack, or insufficiency, of adequate water treatment systems capable of diminishing the concentration of toxic substances that

represent a chronic chemical risk. It can be said that badly-treated wastewaters lead inevitably to a deterioration of water sources quality and consequently, of drinking water.

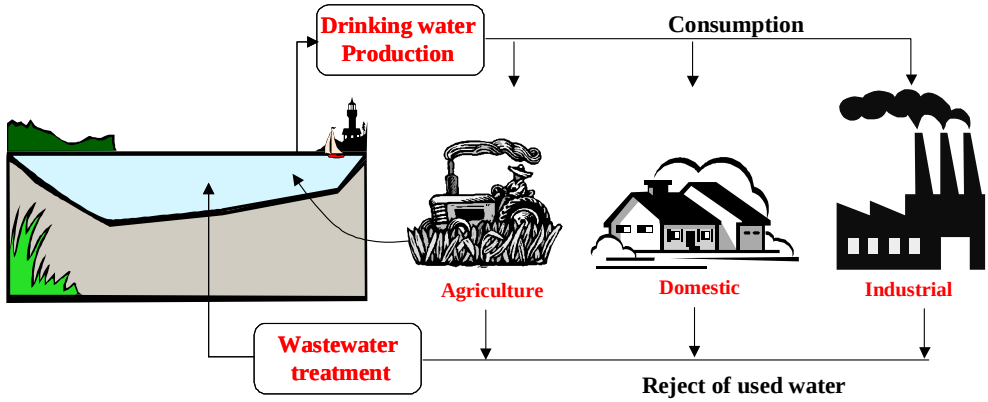

FIGURE 1.1 *A simplified view of the water cycle.*

Two strategies of water treatment have to be forced in order to counterbalance these growing environmental problems:

- the development of appropriate methods for contaminated drinking, ground, and surface waters, and mainly

- the development of appropriate methods for wastewaters containing toxic or non-biodegradable compounds.

The incapability of conventional wastewater treatment methods to effectively remove many biorecalcitrant pollutants evidences that new efficient treatment systems are needed. Besides biological processes, several oxidation systems are currently used or in different stages of development. For the last 25 years the water purification research has been extensively growing. Rigorous pollution control and legislation in many countries have resulted in an intensive search for new and more efficient water treatment technologies.

Chemical treatment methods known as Advanced Oxidation Processes (AOP) are an attractive alternative for the treatment of contaminated ground, surface, and waste waters containing hardly-biodegradable anthropogenic substances as well as for the purification and

disinfection of drinking waters [2-6]. These AOP are useful complements to well established techniques like flocculation, precipitation, adsorption on granular activated carbon, air stripping or reverse osmosis, combustion, and aerobic biological oxidation. Some of these latter techniques could transfer pollutants from the aqueous phase to a second one, but they do not destroy the pollutant. Others may be selective but slow to moderate in destruction rate, or rapid but not selective, thus generating appreciable reactor or energy costs. Aerobic biological oxidation is limited when the feeding water contains substances either recalcitrant to biodegradation, or inhibitory or toxic to the bioculture. Other conversion processes can be limited by economic reasons, oxidative potential, effluent characteristics, or tendency to form harmful disinfection by-products as, for example, the case of formation of trihalomethanes (THMs) when a chlorination procedure is used for drinking water treatment.

Although AOP are cheaper than combustion or wet oxidation technologies, a serious drawback of AOP is their relatively high operational costs compared to those of biological treatments. However, their use as a pretreatment step for the enhancement of the biodegradability of wastewater containing recalcitrant or inhibitory compounds can be justified when the intermediates resulting from the reaction can be readily degraded by microorganisms. Therefore, combinations of AOP as preliminary treatments with inexpensive biological processes, seem very promising from an economical point of view.

One of the most important research subjects of the Laboratory of Environmental Biotechnology (LBE), where this study is carried out, is the combination of AOP and biological processes to treat different types of wastewaters, mainly those coming from the production of flavours, dyes, pharmaceutical goods, or pesticides.

1.2 Overview

This research contributes to the study and development of a new degradation technique that couples solar and biological processes for the treatment of non-biodegradable organic substances present in aqueous milieu. Efficient physicochemical pretreatments (using TiO_2 or Fe^{3+} as catalyst) are necessary to modify the structure of the pollutants, by transforming them into less toxic and easily biodegradable intermediates, allowing then a biological procedure to complete the degradation of the pollutant load. Figure 1.2 illustrates the ensemble of specific

tasks, developed in this doctoral thesis, which together allow the accomplishment of this general purpose.

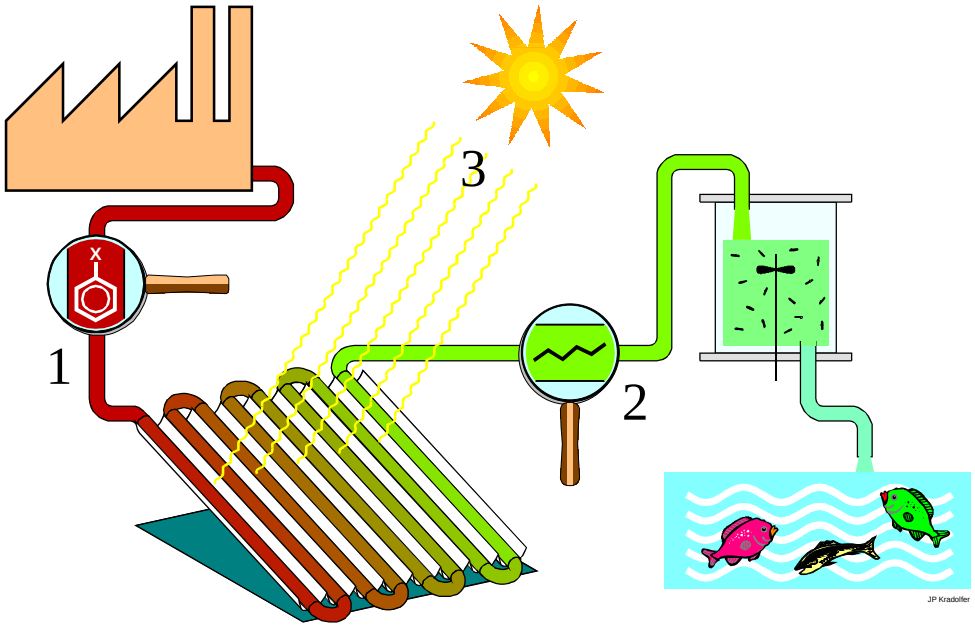

FIGURE 1.2 *Scheme illustrating the different parts studied in the thesis work. (1) Physicochemical properties of pollutants and their photoreactivity, (2) integrated photocatalytic-biological process, and (3) application of the solar field scale technology.*

The presentation of the work has been divided in four chapters, the first one including the background related to the thesis. The second chapter presents the study of some fundamental physicochemical processes such as effects of some classical parameters and chemical structure (or properties) of some substituted phenols and herbicides, on their photochemical degradability.

The third part (chapter 3), concerns to the optimization of a coupled photochemical-biological flow reactor at laboratory scale. This process provides technical information about engineering parameters necessary for an optimal performance in continuous or semi-continuous mode. Further studies about the toxicity and the biodegradability of the solutions under treatment will help to determine the optimum moment to go from the photochemical treatment to the biological process.

The last part (chapter 4) addresses the study of the efficacy of the solar photocatalytic treatment under direct sunlight using parabolic collectors. This part, carried out at the "Plataforma Solar de Almeria" (PSA) in Spain, allows to analyse the possible application of the solar technology in countries with high sun irradiation levels.

1.3 Background

The most recent advances in water purification concern the oxidation of persistent organic compounds dissolved in water, generally refractory to common biological detoxification processes. Methods based on chemical and photolytic catalysis have been included in a group of new technologies denominated Advanced Oxidation Processes (AOP), which produce highly degrading hydroxyl radicals ($^{\bullet}OH$). These radicals are produced by different combinations of ozone, hydrogen peroxide, UV radiation [2, 6-8] and titanium dioxide [5, 9-12], and also by the combination of hydrogen peroxide with ferrous ions in the so-called Fenton's reagent [13-16]. The $^{\bullet}OH$ radicals are generated in solution and due to its strong oxidative nature, they are responsible for the oxidation of organic compounds mainly by hydrogen abstraction generating free organic radicals $R^{\bullet}$ (Equation 1.1). These latter radicals can react with molecular oxygen forming peroxyradicals (Equation 1.2), starting a series of oxidative degradation reactions that can give lead to the complete mineralization of the organic compound.

$$OH + RH \rightarrow R^{\bullet} + H_2O \qquad \textbf{(Eq. 1.1)}$$

$$R^{\bullet} + O_2 \rightarrow RO_2^{\bullet} \rightarrow \text{Products and } CO_2 \qquad \textbf{(Eq. 1.2)}$$

Hydroxyl radicals in presence of an organic substrate, can also follow electrophilic addition (Equation 1.3) and single electron transfer (Equation 1.4) mechanisms.

$$OH + PhX \rightarrow HOPhX^{\bullet} \qquad \textbf{(Eq. 1.3)}$$

$$^{\bullet}OH + RX \rightarrow R^{+\bullet} + HO^{-} \qquad \textbf{(Eq. 1.4)}$$

It must also be taken into account radical-radical recombination (Equation 1.5) and hydroperoxyl radicals production in presence of excess of H_2O_2, (Equation 1.6), which are much less reactive and do not appear to contribute to the oxidative degradation of organic substrates.

$$OH + {}^{\bullet}OH \rightarrow H_2O_2 \qquad \textbf{(EQ. 1.5)}$$

$$H_2O_2 + {}^{\bullet}OH \rightarrow H_2O + HO_2^{\bullet} \qquad \textbf{(EQ. 1.6)}$$

The above mentioned combined methods for $^{\bullet}OH$ radicals production, have been reported by several authors for the decomposition of a wide variety of organic contaminants [5, 17, 18] and are of special interest since some of them can use solar energy. A common problem to all of the AOP is their high cost, fundamentally due to the high demand of electric energy either for ozonizers and/or UV lamps. Application of solar irradiation to the photochemical process reduces costs but this is only possible for catalysed homogeneous and heterogeneous reactions using iron ions [15, 19, 20] and titanium dioxide [21-23] respectively. These catalysts absorb at wavelengths of the solar spectrum while ozone and hydrogen peroxide do not absorb above 300 nm, which is the most important condition for the use of sunlight.

1.3.1 Heterogeneous photocatalysis

Heterogeneous photocatalysis is a technology based on the irradiation of a catalyst, usually a semiconductor, which may be photoexcited to form electron-donor sites (reducing sites) and electron-acceptor sites (oxidising sites), providing great scope as redox reagents. The process is heterogeneous because there are two active phases, solid and liquid.

The molecular orbitals of semiconductors have a band structure. The bands of interest in photocatalysis are the occupied valence band (VB) and the unoccupied conductance band (CB), separated by an energy distance referred to as the band gap (E_{bg}). When the semiconductor is illuminated with light ($h\upsilon$) of greater energy than that of the band gap, an electron is promoted from the VB to the CB leaving a positive hole in the valence band as illustrated in Figure 1.3. After separation, the electron (e^-) and hole (h^+) pair may recombine generating heat or can

become involved in electron transfer reactions with other species in solution, as for example the oxidation or reduction of, respectively, electron-donor (D) or electron-acceptor (A) species shown in Figure 1.3.

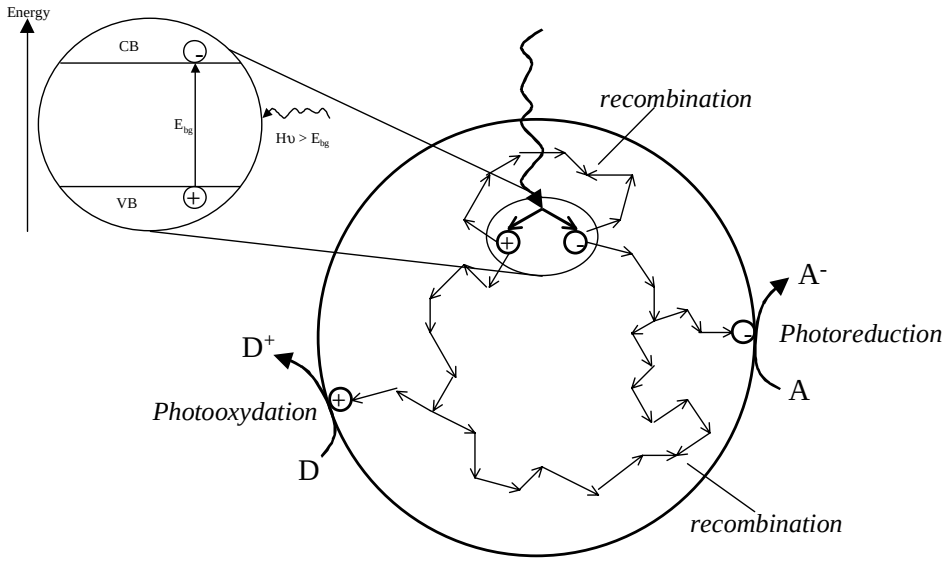

FIGURE 1.3 *Illumination of a semiconductor. Promotion of an electron from the VB to the CB and fate of electrons and holes generated in presence of electron acceptors (A) and donors (D).*

For oxidation reactions to occur, the VB must have a higher oxidation potential than the material under consideration. The redox potential of the VB and the CB for different semiconductors varies between +4.0 and -1.5 volts versus Normal Hydrogen Electrode (NHE) respectively. Therefore, by careful selection of the semiconductor photocatalyst, a wide range of species can be treated *via* these processes.

Metal oxides and sulphides represent a large class of semiconductor materials suitable for photocatalytic purposes [3]. Table 1.1 lists some selected semiconductor materials, which have been used for photocatalytic reactions, together with the VB and CB potentials and the band gap energy and wavelength required to activate the catalyst. To produce this gap, the radiation must be of a λ equal or lower than the calculated by the Planck's equation (Equation 1.7).

$$\lambda = \frac{hc}{E_{bg}} \qquad \textbf{(EQ. 1.7)}$$

where E_{bg} is the semiconductor band-gap energy, *h* is the Planck's constant and *c* is the speed of light.

TABLE 1.1. *Band positions of some common semiconductor photocatalysts in aqueous solution at pH=1.*

Semiconductor	Valence Band (V *vs* NHE)	Conductance band (V *vs* NHE)	Band gap (eV)	Band gap wavelength (nm)
TiO_2	+3.1	-0.1	3.2	387
SnO_2	+4.1	+0.3	3.9	318
ZnO	+3.0	-0.2	3.2	387
ZnS	+1.4	-2.3	3.7	335
WO_3	+3.0	+0.2	2.8	443
CdS	+2.1	-0.4	2.5	496
CdSe	+1.6	-0.1	1.7	729
GaAs	+1.0	-0.4	1.4	886
GaP	+1.3	-1.0	2.3	539

Among the listed semiconductors, TiO_2 has proven to be the most suitable for widespread environmental applications. Titanium dioxide is biologically and chemically inert; it is stable to photo- and chemical corrosion, and inexpensive. Furthermore, TiO_2 is of special interest since it can use natural (solar) UV radiation. This is because TiO_2 has an appropriate energetic separation between its valence and conduction bands, which can be surpassed by the energy of a solar photon. The VB and CB energies of the TiO_2 are estimated to be +3.1 and -0.1 volts, respectively, which means that its band gap energy is 3.2 eV and therefore absorbs in the near UV light (λ<387 nm). Although ZnO seems to be a suitable alternative to TiO_2, it dissolves in acidic solutions and can therefore not be used for technical applications [24]. Other semiconductor particles (e.g., CdS or GaP) absorb larger fractions of the solar spectrum than TiO_2 and can form chemically activated surface-bond intermediates, but unfortunately, such catalysts are degraded during the repeated catalytic cycles usually involved in heterogeneous photocatalysis.

Titanium dioxide is widely used as white paint pigment, as sun blocking material, as cosmetic, or as builder in vitamin tablets, among many other uses. This semiconductor exists in three crystalline forms: anatase, rutile, and brookite. Anatase and rutile are the most common forms and the former is the most effective in wastewater treatment [25]. The band gap energies are approximately 3.2 eV for anatase and 3.0 eV for rutile but the driving force for oxidative processes are similar. Anatase is thermodynamically less stable than rutile, but its formation is kinetically favoured at lower temperature (<600^{o}C), which could explain its higher surface area, and its higher surface density of active sites for adsorption and for catalysis.

Titanium dioxide Degussa P-25 has become the standard for photoreactivity in environmental applications [4, 26, 27]. It is produced through high-temperature (greater than 1200^{o}C) flame hydrolysis of $TiCl_4$ in the presence of hydrogen and oxygen. The TiO_2 so formed, is treated with steam to remove HCl which is also produced as part of the reaction. The product is 99.5% pure TiO_2 (anatase:rutile ratio, 70:30), which is non-porous, with rounded edges cubic particles. The P-25 TiO_2 powder has a surface area of 50 ± 15 m^2 g^{-1} and an average particle diameter of 21 nm. It is important to notice that 90% of the material does not exist as isolated particles, but rather as irreducible complex primary aggregates, typically of approximately 0.1 μm in diameter. The VB and CB positions for Degussa P-25 have been calculated as +2.9 and -0.3 V, respectively, at pH=0 [28].

1.3.1.1 Mechanism of the TiO_2 - photocatalysed degradation

To date, there is evidence supporting the idea that hydroxyl radical ($^{\bullet}$OH) is the main oxidizing species responsible for photo-oxidation of the majority of the studied organic compounds [2]. The first event, after absorption of near ultraviolet radiation at λ<380 nm, is the generation of electron/hole pairs (Equation 1.8) separated between the CB and VB as shown in Figure 1.4.

$$TiO_2 + h\upsilon \rightarrow TiO_2(e^- + h^+) \qquad \textbf{(EQ. 1.8)}$$

Some of the many events which take place after the UV light absorption by TiO_2 particles and the subsequent generation and separation of electrons (e^-_{CB}) and holes (h^+_{VB}) are

summarized in equations 1.9 to 1.16 and Figure 1.4. Three oxidation reactions have been experimentally observed: electron transfer from RX (Equation 1.9), H_2O (Equation 1.10), and ^-OH (Equation 1.11) adsorbed on the catalyst surface. Reactions 1.10 and 1.11 appear to be of great importance in oxidative degradation processes, most probably due to the high concentration of ^-OH and H_2O adsorbed on the TiO_2 surface.

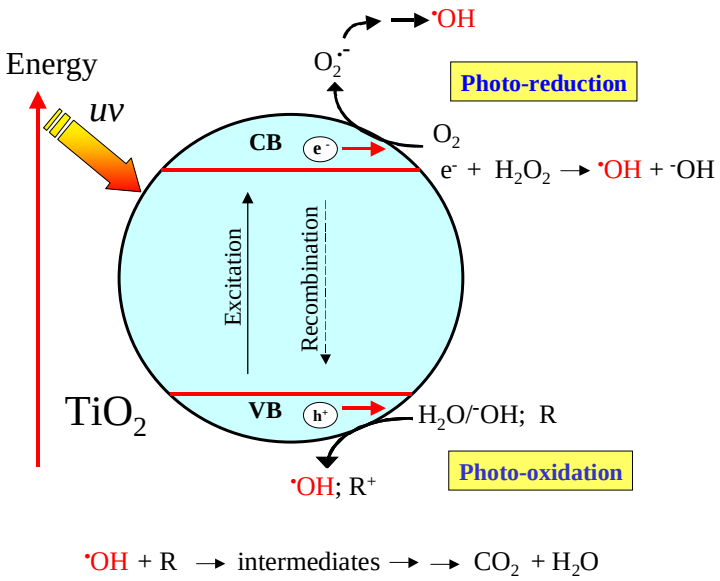

FIGURE 1.4 *TiO_2-semiconductor photocatalysis process. Scheme showing some of photochemical and photophysical events that might be taking place on an irradiated semiconductor particle.*

(EQ. 1.9)

$$iO_2(h^+) + H_2O_{ad} \rightarrow TiO_2 + {}^\bullet OH_{ad} + H^+ \qquad \textbf{(EQ. 1.10)}$$

$$iO_2(h^+) + {}^-OH_{ad} \rightarrow TiO_2 + {}^\bullet OH_{ad} \qquad \textbf{(EQ. 1.11)}$$

Molecular oxygen, which must be present in all oxidative degradation process is the acceptor species in an electron-transfer reaction with the photocatalyst CB (Equation 1.12). Superoxide anion and its protonated form subsequently dismute to yield hydrogen peroxide or peroxide anion. (Equations 1.13, 1.14, 1.15).

$$TiO_2(e^-) + O_2 \rightarrow TiO_2 + O_2^{\bullet -} \quad \textbf{(EQ. 1.12)}$$

$$O_2^{\bullet -} + H^+ \rightarrow HO_2^{\bullet} \quad \textbf{(EQ. 1.13)}$$

$$O_2^{\bullet -} + HO_2^{\bullet} \rightarrow {}^{\bullet}OH + O_2 + H_2O_2 \quad \textbf{(EQ. 1.14)}$$

$$2HO_2^{\bullet} \rightarrow O_2 + H_2O_2 \quad \textbf{(EQ. 1.15)}$$

It has also been shown that hydrogen peroxide addition considerably enhances the photodegradation rate, most probably *via* reaction 1.16, or by surface-catalysed dismutation of H_2O_2 [29, 30].

$$TiO_2(e^-) + H_2O_2 \rightarrow TiO_2 + {}^{-}OH + {}^{\bullet}OH \quad \textbf{(EQ. 1.16)}$$

Organic pollutants adsorbed on TiO_2 particles surface will then be oxidized by $^{\bullet}OH$ radicals. It has been found that the heterogeneous photoprocess is affected by several factors, some of which are presented in the next section.

1.3.1.2 Influence of some fundamental parameters on the kinetics of TiO_2 photocatalysis

This part describes several of the fundamental parameters related to heterogeneous photocatalysis reactions. Some examples that allow a better comprehension of the influence of catalyst and initial substrate concentration, and radiation intensity are also given in chapter 2.

1.3.1.2.1 Catalyst concentration

Either in static, or in slurry or dynamic flow photoreactors, the initial reaction rates are directly proportional to the catalyst mass (*m*) indicating a true heterogeneous catalytic regime. However, above a certain *m* limit value, the reaction rate levels off and becomes independent of *m*. This limit depends on the nature of the compound to be treated and on the geometry and

working conditions of the photoreactor corresponding to the maximum TiO_2 concentration in which all the particles (i.e., all the surface exposed) are totally illuminated. At higher catalyst concentration, a screening effect of exceeding particles masks part of the photosensitive surface. The optimal catalyst concentrations that ensure a total adsorption of efficient photons for TiO_2 Degussa P-25 range from 0.1 to 5.0 g l^{-1} [31-34].

1.3.1.2.2 Initial compound concentration

Generally, the degradation kinetics of compounds follows a Langmuir-Hinshelwood mechanism with a reaction rate (r) varying proportionally to the fraction of surface covered by the substrate (θ) as follows:

$$r = k\theta = k\left(\frac{KC}{1+KC}\right) \quad \textbf{(EQ. 1.17)}$$

where k is the reaction rate constant, K is the compound adsorption constant, and C the initial compound concentration. For diluted solutions, KC becomes <<1 and the reaction is of apparent first order, whereas for higher concentrations, KC>>1 and the reaction rate is maximum and of zero order [35-37].

1.3.1.2.3 Temperature and pH

Most of photoreactions are not sensitive to small variations in temperature. Very few cases have shown an Arrhenius dependence during detoxification [38, 39]. The pH of the aqueous solution significantly affects the particle size, the surface charge, and the band edge positions of the TiO_2 due to its amphoteric character [40]. The Zero Point Charge (pH_{ZPC}) or pH at which the surface of an oxide is uncharged, for TiO_2 is around 7. Above and below this value, the catalyst is negatively or positively charged according to Equations 1.18 and 1.19. In consequence the photocatalytic degradation of organic compounds is affected by the pH.

$$TiOH_2^+ \leftrightarrow TiOH + H^+ \quad \textbf{(EQ. 1.18)}$$

$$TiOH \leftrightarrow TiO^- + H^+ \quad \textbf{(EQ. 1.19)}$$

1.3.1.2.4 Inorganic ions

Some anions commonly found in natural or polluted waters (e.g., chloride, bromide, sulphate, phosphate) have an inhibiting effect on the photodegradation process if they are bound to TiO_2 or close to its surface [38, 41, 42]. Consequently, the pH and pH_{PZC} should be determining properties for the ions effect, as well as the chemical affinities of the ions for TiO_2. Significant inhibition in the degradation rate of different compounds has been observed in presence of chloride at pH=3 [43]. According to Equation 1.18, at acidic pH, $TiOH_2^+$ and TiOH are the main species on the catalyst surface, and the chloride ions compete whit organic compounds for active sites lowering the degradation rates. At higher pH, the negatively charged catalyst surface (Equation 1.19) repulse the approach of chloride ions and no inhibiting effect is observed. Nitrate ions, with charge similar to that of chloride, only slightly inhibit the reaction at pH=3, indicating the role of individual ions.

1.3.1.2.5 Light intensity

It has been reported that degradation rate is proportional to light intensity, which confirms the photo-induced nature of the catalytic process activation, with the participation of photo-induced electrical charges (electrons and holes) in the reaction mechanism [44]. However, at high light intensity the degradation rate becomes proportional to the square root of this parameter [33]. The optimal light power utilization corresponds to the domain where the degradation rate is proportional to light intensity. More details of this effect are given in section 4.1.3.

1.3.1.2.6 Oxygen

The rates and efficiencies of photo-assisted degradation of organic substrates are reported as significantly improved in the presence of oxygen or by the addition of several oxidizing species such as peroxydisulfate or peroxides [2, 45]. The oxygen concentration dependence has been explained by involvement of O_2 adsorption and depletion, both in the dark and during illumination at the photocatalyst surface. Molecular oxygen acts as a conduction band electron trap, suppressing totally or partially the surface electron-hole recombination as shown in

Equation 1.12. The superoxide ($O_2^{\bullet -}$) formed is an effective oxidant agent. Alternatively, the sequence shown in Equations 1.13 to 1.16 generates hydrogen peroxide to form $^{\bullet}OH$ radicals which also initiate oxidative reactions.

1.3.1.2.7 Wavelength

The variation of the reaction rate as a function of the wavelength follows the catalyst absorption spectrum, with a threshold corresponding to its band gap energy. Titanium dioxide, having a band gap energy of 3.2 eV, absorbs in the near-UV at $\lambda < 387$ nm. In addition, it must be checked that the reactants do not absorb at that wavelength to conserve the exclusive catalyst photoactivation for a true heterogeneous catalytic regime (no homogeneous nor photochemistry in the adsorbed phase) [35].

1.3.1.2.8 Adsorption

One important consideration in the TiO_2 photocatalyzed reactions is the adsorption of the organic compounds on the surface of the semiconductor particles. The Langmuir-type relationship between degradation rates and initial organic compound concentrations (section 1.3.1.2.2), indicates that adsorption plays a role in the photocatalytic reaction. However, this role on the photocatalyzed degradation rate is still uncertain. Some examples illustrating the controversial adsorption effect on the photodegradation of four herbicides and *p*-halophenols are presented in chapter 2.

1.3.2 Homogeneous photodegradation

The former applications of homogeneous photodegradation (single-phase system) to treat contaminated waters, concerned the use of UV/ozone and UV/H_2O_2. The use of UV light for photodegradation of pollutants can be classified into two principal areas: (1) direct photodegradation, which proceeds following direct excitation of the pollutant by UV light and (2) photo-oxidation, where light drives oxidative processes principally initiated by hydroxyl radicals. The latter process involves the use of an oxidant to generate radicals, which attack the

organic pollutants to initiate oxidation. Three major oxidants used are: hydrogen peroxide, ozone, and Photo-Fenton system (Fe^{+3}/H_2O_2).

The most commonly accepted mechanism for the photolysis of H_2O_2 is the cleavage of the molecule into hydroxyl radicals with a quantum yield of two $^{\bullet}OH$ radicals formed per quantum of radiation absorbed (Equation 1.20). This reaction is observed only at $\lambda < 300$ nm for concentrations of H_2O_2 of 10^{-1} mol l^{-1}. On the other hand, H_2O_2 is known to dismute producing $^{\bullet}OH$ radicals (Equation 1.21) with maximum rate at the pH of its pKa value, (i.e., 11.4).

$$H_2O_2 + h\upsilon \rightarrow \quad 2^{\bullet}OH \qquad \textbf{(EQ. 1.20)}$$

$$_2O_2 + HO_2^- \rightarrow O_2 + H_2O_2 + \quad ^{\bullet}OH \qquad \textbf{(EQ. 1.21)}$$

The use of hydrogen peroxide is very common for the treatment of contaminated water due to several practical advantages: (i) H_2O_2 is available as an easily handled solution that can be diluted in water to give a wide range of concentrations, (ii) there are no air emissions, and (iii) a high-quantum yield of hydroxyl radicals is generated. The major drawback of using H_2O_2 is its low molar extinction coefficient at the near UV-region [2]. The H_2O_2/UV photoprocess needs low pressure mercury lamps emitting short UV-radiation (254 nm), which is not available in the solar radiation. The high operation costs of the UV-C lamps reduce the feasibility of application of this system on a large scale [46].

Photolysis of ozone dissolved in water leads to the production of hydrogen peroxide (Equation 1.22) and the subsequent formation of $^{\bullet}OH$, which oxidizes the organic compounds. Direct oxidation of the pollutants by O_3 is also involved in the oxidative mechanism of this process. The O_3/UV process is considered as an advanced water treatment for the effective oxidation and destruction of toxic and refractory organics, bacteria, and viruses in water but it has the same problem as hydrogen peroxide process for the use of solar energy since O_3 does not absorb light at λ>300 nm.

$$O_3 + H_2O + h\upsilon \rightarrow O_2 + H_2O_2 \qquad \textbf{(EQ. 1.22)}$$

Application of solar irradiation to the homogeneous photochemical process, is only possible for the photo-Fenton reaction, which can be active to wavelengths up to 600 nm (35% of the solar irradiation) as explained below.

1.3.2.1 Fenton and Fenton photo-assisted reactions

The Fenton reaction was discovered by H.J.H Fenton in 1894 [47]. Forty years later the Haber-Weis mechanism was postulated [48], which revealed that the effective oxidative agent in the Fenton reaction is the hydroxyl radical ($^{\bullet}OH$). Since then, some groups have tried to explain the whole mechanism [13, 49, 50]. The Fenton reaction can be outlined as follows:

$$^{n+} + H_2O_2 \rightarrow M^{(n+1)+} + {}^{-}OH + {}^{\bullet}OH \qquad \textbf{(EQ. 1.23)}$$

where M is a transition metal as Fe or Cu.

In absence of light and complexing ligands other than water, the most accepted mechanism of H_2O_2 decomposition in acid homogeneous aqueous solution, involves the formation of hydroxyperoxyl ($HO_2^{\bullet}/O_2^{-}$) and hydroxyl radicals ($^{\bullet}OH$) [51, 52].

The $^{\bullet}OH$ radical, once in solution attacks almost every organic compound. The metal regeneration can follow different paths. For Fe^{+2}, the most accepted scheme is described in Equations 1.24 to 1.30 [49].

$$e^{2+} + H_2O_2 \rightarrow Fe^{3+} + {}^{-}OH + {}^{\bullet}OH \qquad \textbf{(EQ. 1.24)}$$

$$e^{3+} + H_2O_2 \rightarrow Fe^{2+} + HO_2^{\bullet} + H^{+} \qquad \textbf{(EQ. 1.25)}$$

$$e^{2+} + {}^{\bullet}OH \rightarrow Fe^{3+} + {}^{-}OH \qquad \textbf{(EQ. 1.26)}$$

$$^{\bullet}OH + H_2O_2 \rightarrow HO_2^{\bullet} + H_2O \qquad \textbf{(EQ. 1.27)}$$

$$Fe^{3+} + HO_2^{\bullet} \rightarrow Fe^{2+} + H^{+} + O_2 \qquad \textbf{(EQ. 1.28)}$$

$$Fe^{3+} + O_2^{\bullet -} \rightarrow Fe^{2+} + O_2 \quad \textbf{(EQ. 1.29)}$$

$$e^{2+} + HO_2^{\bullet} \rightarrow Fe^{3+} + HO_2^{-} \quad \textbf{(EQ. 1.30)}$$

Fenton reaction rates are strongly increased by irradiation with UV/visible light [14, 53, 54]. During the reaction, Fe^{+3} ions are accumulated in the system and after Fe^{+2} are consumed, the reaction practically stops. Photochemical regeneration (Equation 1.31) of ferrous ions (Fe^{+2}) by photoreduction of ferric ions (Fe^{3+}) is then proposed [55]. The new generated ferrous ion reacts with H_2O_2 generating a second $^{\bullet}OH$ radical and ferric ion, and the cycle continues.

$$Fe^{3+} + H_2O + h\upsilon \rightarrow Fe^{2+} + {}^{\bullet}OH \quad \textbf{(EQ. 1.31)}$$

Fenton and photo-Fenton reactions depend not only on H_2O_2 concentration and iron added, but also on the operating pH value as indicated in the next section.

1.3.2.1.1 Effect of the pH

The Fenton and photo-Fenton systems have a maximum catalytic activity at pH of about 2.8. The pH value influences the generation of $^{\bullet}OH$ radicals and thus the oxidation efficiency. For pH values above 4 the degradation strongly decreases since iron precipitates as hydroxide derivate, reducing the Fe^{2+} availability and the radiation transmission [55, 56].

1.3.2.1.2 Influence of initial hydrogen peroxide concentration

Degradation rates increase with H_2O_2 concentration which is explained by the effect of the additionally produced $^{\bullet}OH$ radicals [57]. However, above a certain H_2O_2 concentration, the reaction rate levels off and sometimes is negatively affected, by the progressive increase of the hydrogen peroxide. This may be due to auto-decomposition of H_2O_2 to oxygen and water and recombination of $^{\bullet}OH$ radicals (Equation 1.27). Therefore, H_2O_2 should be added at an optimal concentration to achieve the best degradation. This optimal H_2O_2 concentration depends on the nature and concentration of the compound to treat and on the iron concentration.

1.3.2.1.3 Effect of the amount of iron salt

As in the case of H_2O_2, degradation rates increase with iron salt amount, but after a determined iron concentration the efficiency decreases. This may be due to the increase of a brown turbidity that hinders the absorption of the light required for the photo-Fenton process or by the recombination of $^{\bullet}OH$ radicals. In this case, Fe^{2+} reacts with $^{\bullet}OH$ radicals as a scavenger (Equation 1.26).

It is desirable for the ratio of H_2O_2 to Fe^{2+} or Fe^{3+} to be as small as possible, so recombination can be avoided and iron complex production reduced. An optimal H_2O_2/iron molar ratio between 10 and 25 has been proposed by several authors [8, 58, 59]. The effect that H_2O_2 and iron concentrations have on the degradation of some herbicides is discussed in section 3.3.3.1.

1.3.3 Application of heterogeneous photocatalysis and Fenton reaction to water treatment

The application of heterogeneous catalysis using irradiated TiO_2 for the remediation of waters containing different pollutants has grown exponentially during the last 10 years as shown in Figure 1.5, which summarizes four exhaustive reviews made by Blake [18] reporting more than 3000 studies carried out between 1970 and 1998.

Some of the most studied pollutants are: alkanes, aliphatic alcohols, aliphatic carboxylic acids, alkenes, phenols, aromatic carboxylic acids, dyes, PCB's, simple aromatics, halogenated alkanes and alkenes, surfactants, pesticides, and hazardous metal ions. The most currently investigated topics are among others, the photodegradation kinetics and pathways for different compounds, the modification and immobilisation of the catalyst, the use of oxidants other than oxygen, and the scale-up of photocatalytic processes.

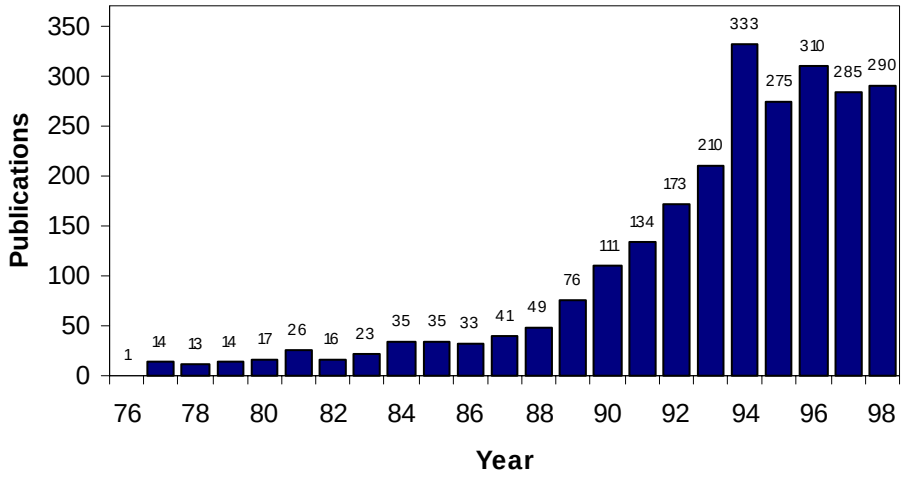

FIGURE 1.5 *Yearly distribution of the references on TiO_2 photocatalysis. Reviewed by Blake between 1976 and 1998. (Taken from reference [60]).*

Regarding the application of the Fenton and photo-Fenton reactions to water detoxification, they have been wide and successfully used for the complete mineralization of hardly-degradable pollutants such as pesticides [17, 19], phenols [56, 58, 61], and dyes as orange II [62, 63], *p*-coumaric acid [64], or uniblue A and ramazol brilliant blue R [65]. These reactions have also been employed as water pretreatment methods prior to biological treatments by Pulgarin's group [57, 66, 67]. One main limitation of these reactions in homogeneous solution, where all the reactants including the catalyst are in solution, is that the recovery of iron is not easy or cheap. One of the last advances in this field, the immobilization of Fe^{+3} ion on Nafion®, allows to overcome this inconvenience [46, 68, 69].

1.4 The studied substances

Substituted phenols, phenylurea herbicides, and *p*-nitrotoluene-*o*-sulfonic acid (*p*-NTS) have been chosen for this study. The substituted phenols as model substances with similar chemical structure representative of a large number of chemical compounds used for industrial and domestic activities, which are often found in the natural environment, and the herbicides

and *p*-NTS as non-biodegradable substances requiring physicochemical treatments to be degraded.

1.4.1 Substituted phenols

Phenolic compounds pose a significant threat to the environment and are commonly found as dilute contaminants in ground- and surface water. Figure 1.6 shows the *para*-substituted phenols used to study the structure-photoreactivity relationship. Several *para*-substituted phenols are used in order to cover a wide variety of electronic effects, ranging from strong electron-donating to strong electrons-withdrawing groups.

Experiments using substituted phenols with Cl, NO_2, COOH, and OH at *ortho*-, *meta*-, and *para*- positions are carried out to study the directing effect of a single substituent on the photodegradability.

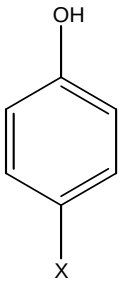

X = OH, OCH_3, $OCH_2CH_2CH_3$, COOH, COH, $COCH_3$, NO_2, SO_3H, CN, CF_3, F, Cl, Br, I

FIGURE 1.6 *Para-substituted phenols.*

1.4.2 Phenylurea herbicides

The presence of herbicides in ground waters, surface waters, effluents of wastewater treatment plants, and other sources of drinking water, indicates that many of these compounds are recalcitrant and/or non-biodegradable and can persist for long periods in the environment

representing a risk to living beings. Pesticides of the urea type are worldwide used as herbicides and plant growth regulators. The general structure of urea herbicides is presented in Figure 1.7.

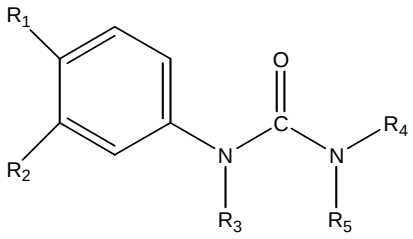

FIGURE 1.7 *General structure of urea herbicides.*

Among these urea herbicides, metobromuron (MB), isoproturon (IP), chlorbromuron (CB), and chlorotoluron (CT) were chosen in this study. Figure 1.8 presents the chemical structure of these herbicides together with the IUPAC name and the molecular formula.

Isoproturon
3-(4-Isopropylphenyl)-
1,1-dimethylurea
$C_{12}H_{18}N_2O$

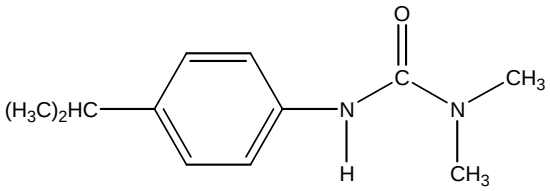

Metobromuron
3-(4-Bromophenyl)-
1-methoxy-1-methylurea
$C_9H_{11}BrN_2O_2$

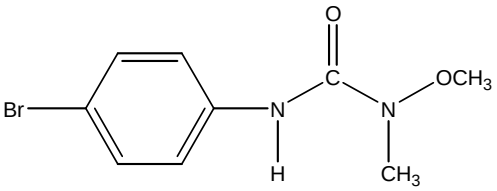

Chlorotoluron
3-(3-Chloro-4-methylphenyl)-
1,1-dimethylurea
$C_{10}H_{13}ClN_2O$

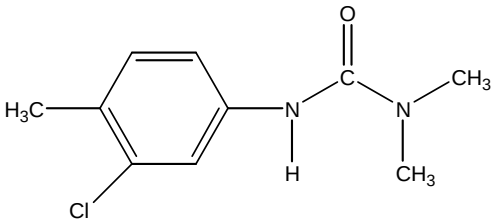

Chlorbromuron
3-(4-Bromo-3-chlorophenyl)-
1-methoxy-1-methylurea
$C_9H_{10}BrClN_2O_2$

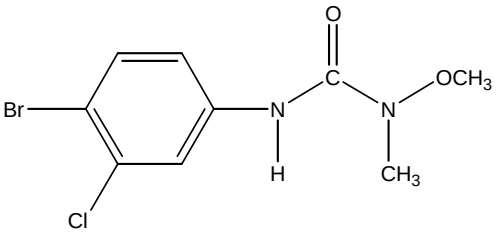

FIGURE 1.8 *Chemical structure, chemical name, and molecular formula of the herbicides studied.*

1.4.3 *p*-nitrotoluene-*o*-sulfonic acid (*p*-NTS)

The *p*-NTS is used by chemical industries in the manufacture of dyes, surfactants, brighteners, and is therefore often found in effluents. The chemical structure if this compound is given in Figure 1.9.

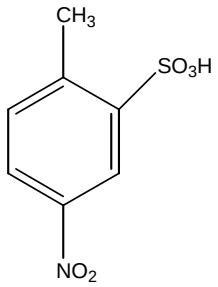

FIGURE 1.9 *Chemical structure of p-nitrotoluene-o-sulfonic acid (p-NTS).*

1.5 Bibliography

1. World Resources Institute 1994-95, N.Y.O., 1994.

2. Legrini, O., E. Oliveros, and A.M. Braun, *Photochemical Processes for Water-Treatment.* Chem Rev, 1993. 93(2): p. 671-698.

3. Robertson, P., *Semiconductor photocatalysis: an environmentally acceptable alternative production technique and effluent treatment process.* J. Cleaner Prod., 1996. 4(3-4): p. 203-212.

4. Hoffmann, M., *et al., Environmental Applications of semiconductor catalysis.* Chem. Rev., 1995. 95: p. 69-96.

5. Bahnemann, D., *et al., Photocatalytic Treatment of Waters,* in *Aquatic and Surface Photochemistry,* G.R. Helz, R.G. Zepp, and D.G. Crosby, Editors. 1994, Lewis Publishiers: Boca Raton. p. 261-316.

6. Bolton, J.R. and S.R. Cater, *Homogeneous photodegradation of pollutants in contaminated water: an introduction.,* in *Aquatic and Surface Photochemistry,* G.R. Helz, R.G. Zepp, and D.G. Crosby, Editors. 1994, Lewis Publishiers: Boca Raton. p. 467-490.

7. Beltran, F.J., J.M. Encinar, and J. Gonzalez, F., *Industrial wastewater advanced oxidation. Ozone combined with hydrogen peroxide or UV radiation.* Water research, 1997. 31(10): p. 2415-2448.

8. Beltran-Heredia, J., *et al., Comparison of the degradation of p-hydroxybenzoic acid in aqueous solution by several oxidation process.* Chemosphere, 2001. 42: p. 351-359.

9. Ollis, D.F., E. Pelizzetti, and N. Serpone, *Heterogeneous Photocatalysis in the environment: Application to Water purification*, in *Photocatalysis: Fundamentals and applications*, N. Serpone and E. Pelizzetti, Editors. 1989, Wiley: Nex York. p. 603-637.

10. Pichat, P., *Partial or complete heterogeneous photocatalytic oxidatation of organic compounds in liquid organic or aqueous phase*. Catalysis Today, 1994. 19: p. 313-334.

11. Fox, M.A. and M.T. Dulay, *Heterogeneous photocatalysis.* Chem. Rev., 1993. 93: p. 341-357.

12. Serpone, N., *Brief introductory remarks on heterogeneous photocatalysis.* Solar energy materials and solar cells, 1995. 38: p. 369-379.

13. Walling, C., *Fenton's reagent revisited.* Acc. Chem. Res., 1975. 8: p. 125-131.

14. Sun, Y.F. and J.J. Pignatello, *Photochemical-Reactions Involved in the Total Mineralization of 2,4-D by Fe-3+/H2O2/UV.* Environ Sci Technol, 1993. 27(2): p. 304-310.

15. Bauer, R. and H. Fallmann, *The photo-Fenton oxidation -a cheap and efficient wastewater treatment method.* Res. Chem. Intermed, 1997. 23(4): p. 341-354.

16. Bossmann, S.H., *et al., new evidence against hydroxyl radicals as reactive intermediates in the thermal and photochemically enhanced Fenton reactions.* J. Phys. Chem, 1998. 102: p. 5542-5550.

17. Huston, P.L. and J.J. Pignatello, *Degradation of Selected Pesticide Active Ingredients and Commercial Formulations in Water by the Photo-Assisted Fenton Reaction.* Water Res, 1999. 33(5): p. 1238-1246.

18. Blake, D., *Bibliography of work on the heterogeneous photocatalytic removal of hazardous compounds from water and air. Update number 3 to january 1999, NREL/TP-570-26797. National Technical Information Service (NTIS), U.S. Department of comerce, Springfield, VA 22161*. 1999.

19. Fallmann, H., *et al., Applicability of the Photo-Fenton method for treating water containing pesticides.* Catalysis Today, 1999. 54(2-3): p. 309-319.

20. Spacek, W., R. Bauer, and G. Heisler, *Heterogeneous and homogeneous wastewater treatment - comparison between photodegradation with TiO2 and the photo-Fenton reaction.* Chemosphere, 1995. 30(3): p. 447-484.

21. Blanco, J., S. Malato, and C. Richter, *Solar chemistry technology*, in *Solar Thermal Test Facilities*. 1996, CIEMAT: Madrid. p. 145-164.

22. Bockelmann, D., *et al., Concentrating Versus Non-Concentrating Reactors for Solar Water Detoxification.* Solar Energ Mater Solar Cells, 1995. 38(1-4): p. 441-451.

23. Minero, C., *et al., Large Solar Plant Photocatalytic Water Decontamination - Degradation of Pentachlorophenol.* Chemosphere, 1993. 26(12): p. 2103-2119.

24. Bahnemann, D., D. Bockelmann, and R. Goslich, *Mechanistic studies of water detoxification in illuminated TiO2 suspensions.* Solar Energy materials, 1991. 24: p. 564-483.

25. Matthews, R.W., *Environment: photochemical and photocatalytic process. Degradation of organic compounds.*, in *Photochemical conversion and storage of solar energy*, E. Pelizzetti and M. Schiavello, Editors. 1991, Kluwer academic publishers: Dadrecht, The Netherlands. p. 427-449.

26. Mills, A. and S. Le Hunte, *An overview of semiconductor photocatalysis.* Journal of Photochemistry and Photobiology A: Chemistry, 1997. 108: p. 1-35.

27. Litter, M., *Heterogeneous photocatalysis transition metals ions in photocatalytic systems.* Applied Catalysis B: Environmental, 1999. 23: p. 89-114.

28. Martin, S., H. Herrmann, and M. Hoffmann, *Time-resolved microwave conductivity, Part 2. Quantum sized TiO2 and the effect of adsorbates and light intensity on charge-carrier dynamics.* J. Chem. Soc. Faraday Trans., 1994. 90(21): p. 3323-3330.

29. Pichat, P., *et al.*, *Assessment of the Importance of the Role of H2O2 and O-2(O-) in the Photocatalytic Degradation of 1,2- Dimethoxybenzene.* Solar Energ Mater Solar Cells, 1995. 38(1-4): p. 391-399.

30. Wolfrum, E.J. and D.F. Ollis, *Hydrogen peroxide in heterogeneous photocatalysis.*, in *Aquatic and Surface Photochemistry*, G.R. Helz, R.G. Zepp, and D.G. Crosby, Editors. 1994, Lewis Publishiers: Boca Raton. p. 451-463.

31. Gimenez, J., D. Curco, and M.A. Queral, *Photocatalytic treatment of phenol and 2,4-dichlorophenol in a solar plant in the way to scaling-up.* Catalysis Today, 1999. 54(2-3): p. 229-243.

32. Chen, D. and A.K. Ray, *Photocatalytic kinetics of phenol and its derivates over UV irradiated TiO2.* Applied Catalysis B: Environmental, 1999. 23: p. 143-157.

33. Al-Sayyed, G., J.C. D'Oliveira, and P. Pichat, *Semiconductor-sensitized photodegradation of 4-chlorophenol in water.* Journal of Photochemistry and Photobiology A: Chemistry, 1991. 58: p. 99-114.

34. Percherancier, J.P., R. Chapelon, and B. Pouyet, *Semiconductor-sensitized photodegradation of pesticides in water: the case of carbetamide.* Journal of Photochemistry and Photobiology A: Chemistry, 1995. 87: p. 261-266.

35. Herrmann, J.M., *Heterogeneous photocatalysis: fundamentals and applications to the removal of various types of aqueous pollutants.* Catalysis Today, 1999. 53: p. 115-129.

36. Inel, Y. and A.N. Okte, *Photocatalytic degradation of malonic acid in aqueous suspension of titanium dioxide: an initial kinetic investigation of CO2 photogeneration.* Journal of Photochemistry and Photobiology A: Chemistry, 1996. 96: p. 175-180.

37. Arslan, I., I.A. Balcioglu, and D.W. Banheman, *Heterogeneous photocatalytic treatment of simulated dyehouse effluents using novel TiO2 photocatalysts.* Applied Catalysis B: Environmental, 2000. 26: p. 193-206.

38. Herrmann, J.M., C. Guillard, and P. Pichat, *Heterogeneous photocatalysis: an emerging technology for water treatment.* Catalysis Today, 1993. 17: p. 7-20.

39. Zhang, T., *et al.*, *Photooxidative N-demethylation of methylene blue in aqueous TiO2 dispersions under UV irradiation.* Journal of Photochemistry and Photobiology A: Chemistry, 2001. 140: p. 163-172.

40. Fernandez-Ibanez, P., F.J. de las Nieves, and S. Malato, *Titanium dioxide/electrolyte solution interface: electron transfer phenomena.* Journal of Colloid and Interface Science, 2000. 227: p. 510-516.

41. Pelizzetti, E., *Concluding remarks on heterogeneous solar photocatalysis.* Solar energy materials and solar cells, 1995. 38: p. 453-457.

42. Wang, K.H., *et al.*, *The pH and anion effects on the heterogeneous photocatalytic degradation of o-methylbenzoic acid in TiO2 aqueous suspension.* Chemosphere, 2000. 40: p. 389-394.

43. Wang, K.H., *et al.*, *Photocatalytic degradation of 2-chloro and 2-nitrophenol by titanium dioxide suspensions in aqueous solution.* Applied Catalysis B: Environmental, 1999. 21: p. 1-8.

44. Ollis, D.F., *Solar-assisted photocatalysis for water purification: issues, data, questions,* in *Photochemical conversion and storage of solar energy.* 1991, Kluwer Academic Publishers. p. 593-622.

45. Wang, y. and C.S. Hong, *TiO2-mediated photomineralization of 2-chlorobiphenyl : the role of O2.* Water research, 2000. 34(10): p. 2791-2797.

46. Bauer, R., *et al.*, *The photo-Fenton reaction and the TiO2/UV process for waste water treatment - novel developments.* Catalysis Today, 1999. 53: p. 131-144.

47. Fenton, H.J.H., *Oxidation of tartaric acid in presence of iron.* J. Chem. Soc. Trans., 1894. 65: p. 899-910.

48. Haber, W.G. and J. Waiser, *The catalytic decomposition of hydrogen peroxide by iron salts.* J. Proc. Roy. Soc. London, 1934. A147: p. 332.

49. Sychev, A.Y. and V.G. Isak, *Iron compounds and the mechanisms of the homogeneous catalysis of the activation of O2 and H2O2 and of the ativation of organic substrates.* Russian Chemical Reviews, 1995. 64(12): p. 1105-1129.

50. Prousek, J., J. Chem. Lisy., 1995. 89: p. 11-21.

51. De Laat, J. and H. Gallard, *Catalytic decomposition of hydrogen peroxide by Fe(III) in homogeneous aqueous solution: mechanism and kinetic modeling.* Environmental Science and Technology, 1999. 33: p. 2726-2732.

52. Gallard, H. and J. De Laat, *Kinetic modelling of Fe(III)/H2O2 oxidation reactions in dilute aqueous solution using atrazine as a model organic compound.* Water research, 2000. 34(12): p. 3107-3116.

53. Rupert, G., R. Bauer, and G. Heisler, *The photo-Fenton reaction - an effective photochemical wastewater treatment process.* Journal of Photochemistry and Photobiology A: Chemistry, 1993. 73: p. 75-78.

54. Bandara, J., *et al.*, *Degradation/Decoloration of Concentrated-Solutions of Orange-II - Kinetics and Quantum Yield for Sunlight- Induced Reactions via Fenton Type Reagents.* J Photochem Photobiol A. Chem, 1996. 99(1): p. 57-66.

55. Faust, B.C. and J. Hoigne, *Photolysis of Fe(III) - hydroxy complexes as sources of OH radicals in clouds, fog and rain.* Atmos. Environ., 1990. 24A(1): p. 79-89.

56. Ghaly, M.Y., *et al.*, *Photochemical oxidation of p-chlrophenol by UV/H2O2 and photo-Fenton process. A comparative study.* Waste Management, 2001. 21: p. 41-47.

57. Parra, S., *et al., Photochemical versus coupled photochemical-biological flow system for the treatment of two biorecalcitrant herbicides: metobromuron and isoproturon.* Applied Catalysis B: Environmental, 2000. 27: p. 153-168.

58. Tang, W.Z. and C.P. Huang, *2,4-dichlorophenol oxidation kinetics by Fenton's reagent.* Environ. Technol., 1996. 17: p. 1371-1378.

59. Kim, S.M., S.U. Geissen, and A. Vogelpohl, *Landfill leachate treatment by a photoassisted Fenton reaction.* Water science and technology, 1997. 35(4): p. 239-248.

60. Maldonado, M.I., *Descontaminación de aguas de lavado de envases de plaguicidas mediante fotocatálisis solar*, in *Departamento de Ingeniería Química*. 2000, Universidad de Almeria: Almeria, Spain.

61. Kiwi, J., C. Pulgarin, and P. Peringer, *Effect of Fenton and Photo-Fenton Reactions on the Degradation and Biodegradability of 2-Nitrophenols and 4- Nitrophenols in Water-Treatment.* Applied Catalysis B: Environmental, 1994. 3(4): p. 335-350.

62. Bandara, J., J.A. Mielczarski, and J. Kiwi, *1. Molecular mechanism of surface recognition. Azo dyes degradation on Fe, Ti, and Al oxides through metal sulfonate complexes.* Langmuir, 1999. 15: p. 7670-7679.

63. Bandara, J., *Abatement of azo-dyes and bichlorophenols mediated by iron-oxides: mechanism and flow reactor studies*, in *Département de Chimie*. 1999, Ecole Polytechnique Fédérale de Lausanne: Lausanne, Switzerland.

64. Herrera, F., *et al., Accelerated Photooxidation of Concentrated P-Coumaric Acid in Homogeneous Solution - Mechanistic Studies, Intermediates and Precursors Formed in the Dark.* Appl Catal B-Environ, 1998. 17(1-2): p. 141-156.

65. Herrera, F., *Degradation of Uniblue A and Remazol Brilliant Blue R by iron: Fenton photo-assisted process and hematite,* in *Département de Chimie*. 1999, Ecole Polytechnique Fédéral de Lausanne: Lausanne, Switzerland.

66. Bandara, J., *et al., Chemical (Photo-Activated) Coupled Biological Homogeneous Degradation of p-Nitro-o-toluene-sulfonic Acid in a Flow Reactor.* J Photochem Photobiol A. Chem, 1997. 111(1-3): p. 253-263.

67. Pulgarin, C., *et al., Strategy for the coupling of photochemical and biological flow reactors useful in mineralization of biorecalcitrant industrial pollutants.* Catalysis Today, 1999. 54(2-3): p. 341-352.

68. Balanosky, E., *et al., Degradation of membrane concentrates of the textile industry by Fenton like reactions in iron-free solutions at biocompatible pH values.* Water science and technology, 1999. 40(4-5): p. 417-424.

69. Fernandez, J., *et al., Photoassisted Fenton degradation of non biodegradable azo dye (orange II) in Fe-free solutions mediated by cation transfer membranes.* Langmuir, 1999. 15: p. 185-192.

CHAPTER 2

STRUCTURAL PROPERTIES AND PHOTOREACTIVITY RELATIONSHIPS

2.1 Introduction

As mentioned in chapter 1, the photocatalytic treatment of water with TiO_2 is efficient for the destruction of many organic pollutants. The photocatalytic degradation rate of different compounds depends on various parameters, such as temperature, pH, initial concentration of the pollutant, TiO_2 concentration, light intensity, and chemical nature (structure) of the reactant, among others. In this chapter, special attention is given to the effect of the structure and consequently of some of the physicochemical properties of different compounds on their photoreactivity *via* TiO_2 aqueous suspensions.

Various studies have reported that the photocatalytic reactivity of aromatic compounds can be affected by the number of substituents, their electronic nature, and their positions in the aromatic ring [1-7], but only few of those studies correlate the measured photodegradation rates to some parameters characterizing the compounds to degrade. The photocatalytic degradability of some compounds have been principally correlated to the Hammett constant (σ) and to the 1-octanol-water partition coefficient (K_{ow}). Hammett constant represents the effect that different substituents have on the electronic character of a given aromatic system, while K_{ow} reflects the hydrophobicity and is considered to be related to the extent of adsorption of the organic compound on TiO_2. Among the chemical families of compounds studied are dichloro- and trichlorophenols [1], methoxybenzenes (anisoles) substituted at *meta*- and *para*- positions by F, Cl, NO_2, OH, NH_2 [3], and phenols substituted at *para*- positions by OCH_3, CH_3, F, Cl, Br, I, CF_3, $COCH_3$, CN [2]. In general, these studies show that the kinetics of the photocatalytic degradation of aromatic pollutants is faster for compounds with electron-donating substituents

and that the hydrophobicity, reflecting the extent of adsorption on the catalyst, plays an important role on the photocatalytic reactions.

In other oxidation processes, such as the UV/H_2O_2 system, the Fenton reaction, and pyrylium salt-photosensitized degradation, it has also been found that the reaction rate strongly depends on the basic structure of the molecules to be degraded. It has been reported, for example, that the oxidation rate of chlorinated phenols by Fenton reagent decreases linearly as the number of chlorine content increases [8]. For Fenton reaction degraded monochlorophenols, the oxidation rate decreases in the order 3-chlorophenol > 4-chlorophenol > 2-chlorophenol [9]. As for the case of TiO_2 photocatalytic systems, the presence of electron-donating substituents increases the reactivity of the compounds, effect that has been illustrated by the pyrylium salt-photosensitized degradation study of phenolic contaminants derived from cinnamic acid [10]. Substrates as ferulic and caffeic acid, with two electron-donating groups, react faster than *p*-coumaric acid, which has only one activating substituent; while the non-activated cinnamic acid is nearly unreactive.

In this chapter, the effect of the structure on the photoreactivity *via* TiO_2 catalysis is studied using several substituted phenols to cover a wide variety of electronic effects, ranging from strong electron-donating (activating) to strong electron-withdrawing (deactivating) groups. First, the effect of the nature of the substituent is studied at a single position (*para*-) and secondly, the directing effect (*ortho*-, *meta*-, *and para*-) is examined for some substituents. The photocatalytic degradability of *p*-halophenols is discussed in detail and some physicochemical characteristics such as electronegativity of the halide substituent, carbon-halide bond strengths, and hydrophobicity are used to explain the found photodegradability order.

The photodegradability of four phenylurea herbicides (metobromuron, isoproturon, chlorotoluron, and chlorbromuron) with very close molecular structure is presented in this thesis. Some physicochemical properties of these herbicides, such as donor or withdrawing character of substituents, dipolar moment, and extent of adsorption of molecules, are employed to assess their photodegradability order when a solution of the compound is irradiated in presence of TiO_2. Structure-Activity relationships are used to understand the involved mechanisms and the molecular descriptors responsible for such events.

One important consideration in the TiO_2-photocatalysed reactions is the adsorption of the organic compounds on the surface of semiconductor particles. It has been often reported that adsorption is a prerequisite for the photodegradation of organic compounds. However, the role of adsorption on the photocatalytic degradation rate is still uncertain. In this work, the dark adsorption isotherms for the *p*-halophenols and herbicides are measured and correlated with their photoreactivity. The results show that no direct correlation exists between the measured extents of adsorption and the initial photodegradation rates of the studied compounds.

2.2 Experimental

2.2.1 Materials

All chemicals are used as received. Phenol, catechol, resorcinol, hydroquinone, hydroquinone monomethyl ether, hydroquinone monopropyl ether, 2-hydroxybenzoic acid, 3-hydroxybenzoic acid, 4-hydroxybenzoic acid, 4-hydroxyacetophenone, 4-hydroxybenzaldehyde, 4-hydroxybenzotrifluoride, 4-hydroxybenzonitrile, 2-nitrophenol, 3-nitrophenol, 4-nitrophenol, phenol-4-sulfonic acid, 4-iodophenol, 4-fluorophenol, 4-bromophenol, 2-chlorophenol, 3-chlorophenol, and 4-chlorophenol were obtained from Fluka.

Metobromuron (MB), chlorotoluron (CT), chlorbromuron (CB), and isoproturon (IP) were obtained from Ciba (Monthey-Switzerland). TiO_2 is Degussa P-25, mainly anatase with a surface area of 50 m^2g^{-1}. The chemicals for HPLC analysis were obtained from Fluka. Milli-Q water was used throughout for the preparation of aqueous solutions or as a component of the mixed water-acetonitrile (HPLC grade) mobile phase in HPLC analysis.

2.2.2 Photodegradation experiments

The photocatalytic experiments were performed using 40 ml Pyrex flask with a cut-off at λ = 290 nm placed into a Hanau Suntest Simulator. The radiation source employed is a xenon lamp where the total radiant flux (40 mW cm^{-2}) was measured with a YSI Corporation powermeter. The lamp has a λ distribution with about 0.5% of the emitted photons at

wavelengths shorter than 300 nm and about 7% between 300 and 400 nm. The profile of the photons emitted between 400 and 800 nm followed the solar spectrum. The aqueous suspensions were magnetically stirred throughout irradiation, opened to air. Extreme care was taken to ensure uniform experimental conditions during the degradation rate determination. Samples were taken periodically and the disappearance of each substance was monitored by high performance liquid chromatography after filtration with millipore filters (0.45 μm) to remove the catalyst.

2.2.3 Chemical and biological analysis

2.2.3.1 High Performance Liquid Chromatography (HPLC)

The equipment used is a Varian 9065 unit provided with a Varian 9012 solvent delivery system, an automatic injector 9100, and a Varian Pro Star variable (200-400 nm) diode array detector 9065 Polychrom. All the modules are piloted with a PC computer with the Varian Star 5.3 software for liquid chromatography. A reverse phase Spherisorb silica column ODS-2 and acetonitrile/water as mobile phase are used to run the chromatography.

2.2.3.2 Dissolved Organic Carbon (DOC)

A Shimadzu, model 5050A, TOC analyser is used for DOC measurements. The instrument is equipped with an ASI automatic sample injector and it uses potassium phthalate solution as calibration standard. Acidification and stripping before analysis were sometimes necessary to keep the solutions free of atmospheric CO_2.

2.2.3.3 Chemical Oxygen Demand (COD)

The COD is used as a measure of the oxygen equivalent of the organic matter content of a sample that is susceptible to oxidation by a strong chemical oxidant. This analysis is carried out via a Hach-2000 spectrophotometer using dichromate solution as the oxidant in strong acid

medium. Test solution (2 ml) is pipetted into the dichromate reagent and digested at 150°C for two hours. Colour is developed during the oxidation and measured against a water blank using a Hach DR/890 colorimeter. The optical density for the change of colour of the dichromate solution was determined at λ = 430 nm.

2.2.3.4 Biological Oxygen Demand (BOD)

The BOD measures the oxygen required for the biochemical degradation of organic material. This analysis is made by means of a Hg free WTW 2000 Oxytop unit thermostated at 20°C. The pH of the samples are adjusted between 6.8 and 7.5 followed by addition (20% v/v) of decanted sludge (inoculum) from the biological plant of Vidy, Lausanne, Switzerland and of nutrients substances necessary for the bacterial activity. More details about this test are presented in section 3.2.3.4.

2.2.4 Adsorption isotherms

All equilibrium experiments were conducted in the dark. Measurements were made on TiO_2 suspensions with various *p*-halophenols or herbicides concentrations at natural pH (5-6). The TiO_2 concentration is of 10 g l^{-1}. Preliminary experiments, performed during 24 h under constant magnetic stirring, demonstrated that the equilibrium is reached after 1 h. The equilibrium concentrations were determined by liquid chromatography after centrifugation and filtration (0.45 μm Millipore filters) of the suspension.

The number of molecules adsorbed per gram of TiO_2 (n_2^s in mol g^{-1}) is calculated as follows:

$$n_2^s = \frac{V \times \Delta C}{W} \qquad \textbf{(EQ. 2.1)}$$

where ΔC = (initial concentration, C_i – equilibrium concentration, C_{eq}), V is the volume (0.02 l), and W is TiO_2 weight (0.2 g).

2.2.5 Structure-photoreactivity relationships. Computational details

Computer modelling procedures used in this study were performed using Hyperchem 5.1 (Hypercube Inc, 1996). The compounds in the data set were entered as two-dimensional sketches into Hyperchem and stored as atomic coordinates. Full optimization geometry and calculation of the positive and negative molecular electrostatic potential for the best conformer was performed using the semi empirical method AM1 [11] running on Hyperchem. Electronic properties were calculated from single point calculations and moments of inertia from optimized structures. Calculated molecular descriptors included the total and electronic energy, the Energy of the Highest Occupied (E_{HOMO}) and the Lowest Unoccupied (E_{LUMO}) Molecular Orbitals, the dipolar moment (DM), the most positive and the most negative charge, the moments of inertia I, II, and III, and the molecular weight (MW).

2.2.5.1 Model construction

Structure-photoreactivity relationships were developed for the initial photodegradation rate (v_o) of four herbicides. Molecular reactivity was expressed as a function of the electronic architecture and some geometrical descriptors of the molecule. A linear regression equation was obtained using stepwise regression in which the kinetic data and the molecular descriptors were used as dependent and independent variables, respectively. The low number of molecules in the data set allowed the presence of only one descriptor in the model. Accordingly, partial correlation was performed to study the influence of confounding variables in the predictability of v_o by molecular descriptors.

2.3 Results and Discussion

2.3.1 Photocatalytic degradability of substituted phenols *via* TiO_2 catalysis

The reactivity of phenolic compounds can be drastically affected by the electronic nature of substituents and by their positions in the aromatic ring. In this work, structure effect on the photoreactivity *via* TiO_2 catalysis is studied using several substituted phenols in order to cover a wide variety of electronic effects, ranging from strong electron-donating (activating) to strong electron-withdrawing (deactivating) groups: OH, OCH_3, $OCH_2CH_2CH_3$, COOH, COH, $COCH_3$, NO_2, SO_3H, CN, CF_3, F, Cl, Br, and I. First, the substituent-nature effect is studied at a single position (*para*-) and secondly, the directing effect (*ortho*-, *meta*-, *and para*-) is examined for some substituents (OH, Cl, NO_2, COOH).

2.3.1.1 Influence of the substituent nature at *para*- position

The influence of the *para*-substituents on the photocatalytic degradation of the substituted phenols is investigated by comparing their initial degradation rates (v_o), which is the decay of the *p*-halophenol concentration at 10 minutes of the photoreaction. In all the cases studied, for phenols concentration of 0.4 mmol l^{-1} and 1.0 g l^{-1} of TiO_2, a first-order kinetics is observed. Table 2.1 presents the initial degradation rates and the first order rate constants of the *para*-substituted phenols relative to phenol, which is used as reference compound. The last column in the table presents the literature Hammett constant (σ) for each compound [12, 13].

TABLE 2.1 *Initial photodegradation rates (v_o) and first order rate constants (k) relative to phenol for the abatement of p-substituted phenols. Unsubstituted phenol is used as reference compound.*

substituent (X)	v_o relative to phenol	k relative to phenol	σ
p-H	1.00	1.00	0
p-OH	0.44	0.82	-0.38
p-OCH_3	1.85	1.87	-0.28
p-$OCH_2CH_2CH_3$	1.80	1.23	-0.25
p-COOH	0.99	1.07	0.44
p-COH	1.18	0.93	0.22
p-$COCH_3$	0.91	0.66	0.47
p-NO_2	0.74	0.78	0.81
p-SO_3H	0.97	1.07	0.50
p-CN	0.87	0.91	0.70
p-CF_3	0.94	0.82	0.53
p-F	0.99	1.06	0.15
p-Cl	0.87	0.94	0.24
p-Br	0.63	0.52	0.26
p-I	0.65	0.55	0.28

The Hammett constant represents the effect that different substituents have on the electronic character of a given aromatic system [12]. A positive value of σ indicates an electron-withdrawing group while a negative value indicates an electron-donating group. Hammett constants are then used to establish a correlation with the initial degradation rates for the *para*-substituted phenols (Figure 2.1).

Although the plot of σ *vs* v_o shows a poor correlation when considering all the substituted phenols, when the *p*-halophenols are evaluated separately and the hydroquinone (OH substituent) is not taken into account, good correlations are observed in both groups of data. The *p*-halophenols exhibit a different behaviour possibly due to the strong electronegative character

of the halo-substituents. A more detailed study of the *p*-halophenols degradation is presented in section 2.3.2.

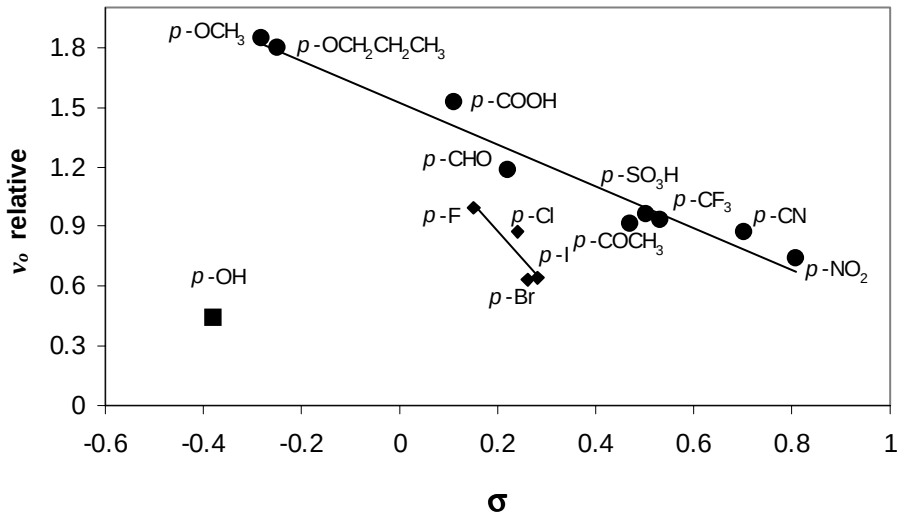

FIGURE 2.1 *Relationship between the initial degradation rate (v_o) and Hammett constants (σ) of p-substituted phenols.*
Circles, triangles, and the square represent the non-halogens, halogens, and the hydroxy substituents, respectively.

The good correlation observed between σ and v_o for the non-halogenated *p*-substituted phenols indicates the electrophilic nature of the photocatalytic reaction. The photodegradation rates depend principally on the activating or deactivating effect of the substituents on the aromatic ring which is accelerated by electron-donating groups and retarded by electron-withdrawing groups. For each electronic category, the effect on photodegradation depends on the activating or deactivating ability of each substituent, which is directly related with the σ value as shown in Figure 2.1.

Hydroquinone, even having two strongly activating groups, is not the most reactive of the compounds studied. It has been reported [14] that the delay in the degradation of hydroquinone could be related to a keto-enolic oxydo-reductive tautomeric effect as illustrated in Figure 2.2. Due to this effect, the oxidation of hydroquinone to benzoquinone by photogenerated holes in

the valence band of the TiO_2 semiconductor might be followed by electron capture from the conduction band by benzoquinone, giving rise to a recombination reaction.

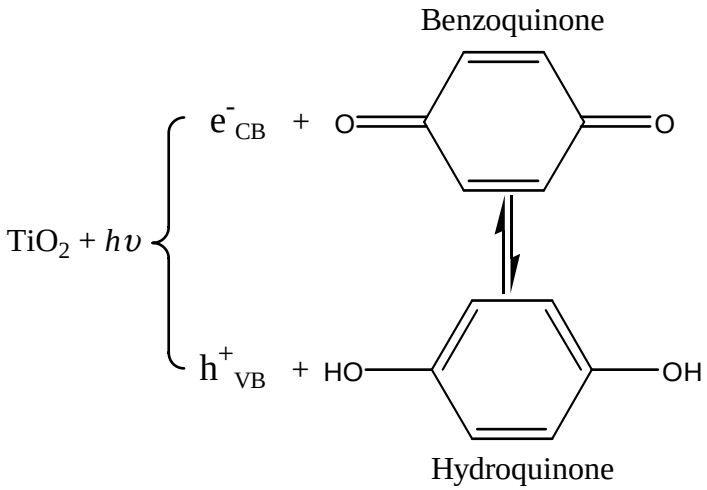

FIGURE 2.2 *Representation of keto-enol tautomeric equilibrium for hydroquinone and benzoquinone.*
(adapted from reference [14]).

2.3.1.2 Effect of the substituent position

Experiments using substituted phenols with NO_2, Cl, OH, and COOH as substituents at the three positions (*ortho*-, *meta*-, and *para*-) were carried out to study the directing effect on the photodegradability. It is found that the substituent position does not influence the photocatalytic degradation, except in the case of dihydroxybenzenes (catechol, resorcinol, and hydroquinone). Although it has been reported that the photodegradation of *p*-chlorophenol is faster than that of *o*-chlorophenol, and *m*-chlorophenol in TiO_2 aqueous suspension [1, 5], in this study none effect of the Cl position in chlorophenols degradation is observed.

Figure 2.3 shows the evolution of the three compounds (4.0 mmol l^{-1}) as a function of the irradiation time in presence of 1 g l^{-1} of TiO_2. A first order kinetics is observed for the three isomers with degradation efficiencies decreasing in the order: resorcinol > hydroquinone > catechol.

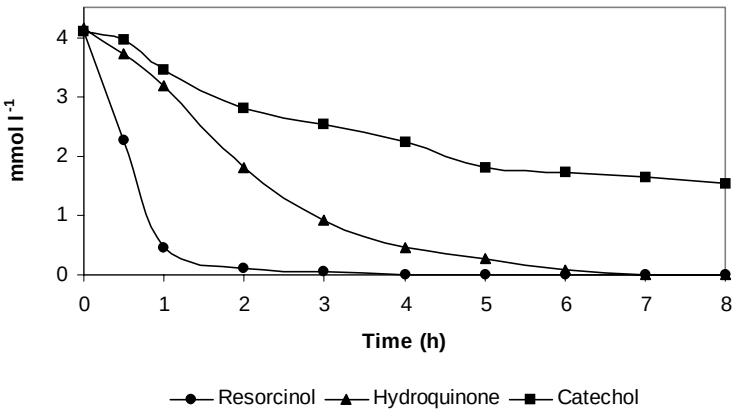

FIGURE 2.3 *Photodegradation of catechol, resorcinol, and hydroquinone. Initial concentration of the three isomers: 4.0 mmol l^{-1}.*

As mentioned before, the OH group being an electron-donating substituent is considered as strong activating and *ortho - para* directing for the aromatic ring. The activation degree of the dihydroxybenzene compounds depends on the position of the second OH group as shown in Figure 2.4.

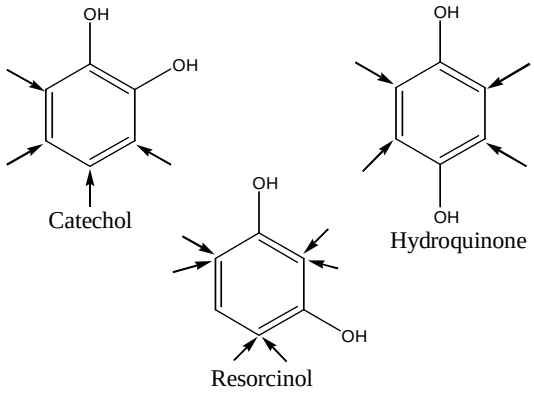

FIGURE 2.4 *Schematic representation of the activation of the aromatic cycle by the -OH groups.*

Resorcinol, which has three double activated positions, reacts faster than catechol and hydroquinone, which have the unsubstituted positions activated only once. Delay in catechol

photodegradation can be also due to a keto-enolic oxydo-reductive tautomeric effect as in the case of hydroquinone (Figure 2.2). Such equilibrium is not present in resorcinol.

2.3.2 Photocatalytic degradability of *p*-halophenols *via* TiO_2 catalysis

As mentioned in section 2.3.1.1, the *p*-halophenols exhibit a different photocatalytic behaviour with respect to the non-halogenated *p*-substituted phenols, which could be due to the strong electronegative character of the halogens. However, among them, it is observed a good correlation between photodegradability and the respective Hammett constants. Besides the electronegativity of the halide substituent represented by the Hammett constants, other physicochemical characteristics of these compounds such as carbon-halide bond strengths and hydrophobicity of the solutes are used to try to explain the photodegradability order of the four *p*-halophenols.

Figure 2.5 shows the kinetics of disappearance, as a function of time, of illuminated *p*-halophenols with an initial concentration of 0.4 mmol l^{-1} and 1.0 g l^{-1} of TiO_2. In all the cases, a first-order kinetics is observed, which is confirmed by the linear transform shown in the figure insert.

The initial degradation rates (v_o) of the *p*-halophenols were compared to estimate the effect of the halogen substituent. The last four rows of Table 2.1 presents v_o values and the first-order rate constants (k) for the four *p*-halophenols relative to phenol. The k values represent the curve slopes in Figure 2.5 insert and v_o, the decay of the *p*-halophenol concentration at 10 minutes of photoreaction.

In Figure 2.5, the evolution of *p*-halophenols as a function of time indicates two groups: *p*-fluorophenol and *p*-chlorophenol, which are eliminated within approximately 6 hours, whereas *p*-bromophenol and *p*-iodophenol are eliminated after 8 hours. Initial degradation rates decrease in the following order: *p*-fluorophenol ≥ *p*-chlorophenol >> *p*-iodophenol ≥ *p*-bromophenol.

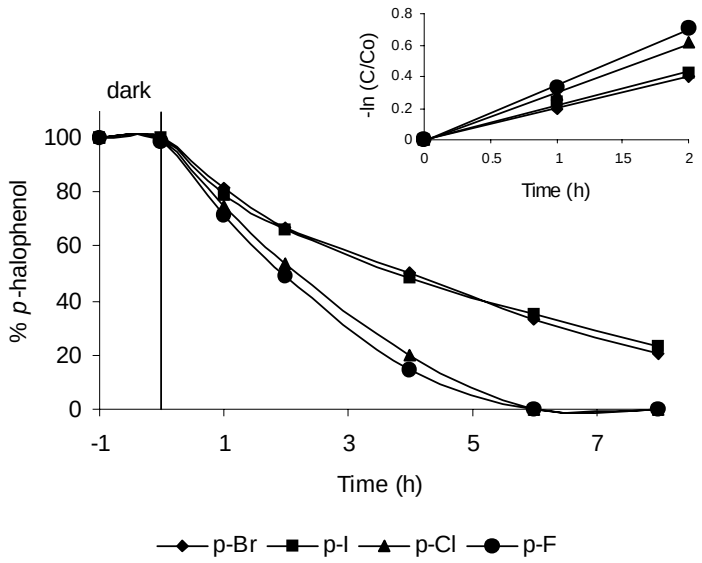

FIGURE 2.5 *Photocatalytic degradation of p-halophenols. Compounds and TiO_2 concentration of 0.4 mmol l^{-1} and 1.0 g l^{-1}, respectively. The insert represents the linear transform -ln(C/Co)=f(time).*

2.3.2.1 Influence of physicochemical characteristics on *p*-halophenols photodegradability

Physicochemical characteristics presented in Table 2.2 have been taken into account to try to explain the *p*-halophenols photoreactivity order observed in the precedent section.

TABLE 2.2 *Molecular characteristics of the p-halophenols.*

***p*-halophenol**	**C-Halide Bond energy (kcal mol^{-1})**	**log K_{ow}**	**σ**
p-Fluorophenol	125	1.77	0.15
p-Chlorophenol	95	2.39	0.24
p-Bromophenol	80	2.59	0.26
p-Iodophenol	65	2.91	0.28

2.3.2.1.1 Carbon-halide bond strength

As shown in Figure 2.6, there is a good correlation between the *p*-halophenol initial degradation rate (v_o) and its carbon-halide bond strength. However, the observed trend suggests that halide elimination is not the rate-determining step, since, contrary to expected, v_o is higher when carbon-halide bond is stronger.

Formation of an intermediate has been suggested [2] to rationalize the observed relative reactivities of the *p*-halophenols. In this way, the intermediate formed being either a complex between the halide and TiO_2, or a radical, or an excited stated, will be more reactive when *p*-halophenol carbon-halide bond is stronger.

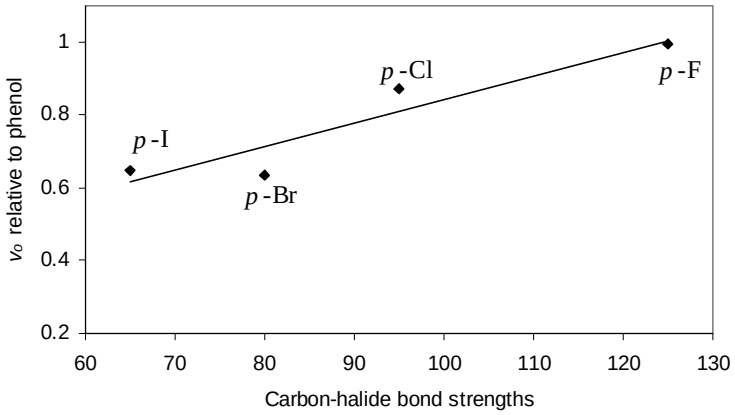

FIGURE 2.6 *Relationship between the initial degradation rate and the carbon halide bonds strengths of p- halophenols.*

2.3.2.1.2 Electronic effect of the halide substituent

As mentioned before, a direct relationship is observed between the photodegradability of *p*-substituted monohalogenated phenols and their respective Hammett constants (σ). This correlation is shown in Figure 2.7. The initial degradation rate of these compounds changes systematically with the electronic influence (represented by σ) of the individual halides on the aromatic ring.

The observed correlation suggests that the monohalogenated phenols follow analogous photodegradation mechanisms, which may involve an attack by electrophilic reagents (as hydroxyl radicals), or the formation of a positively charged reaction centre by the loss of one electron, or the formation of an intermediate as mentioned before. The dehalogenation of halosubstituted phenols has been explained by the addition of hydroxyl radical followed by halide elimination [15].

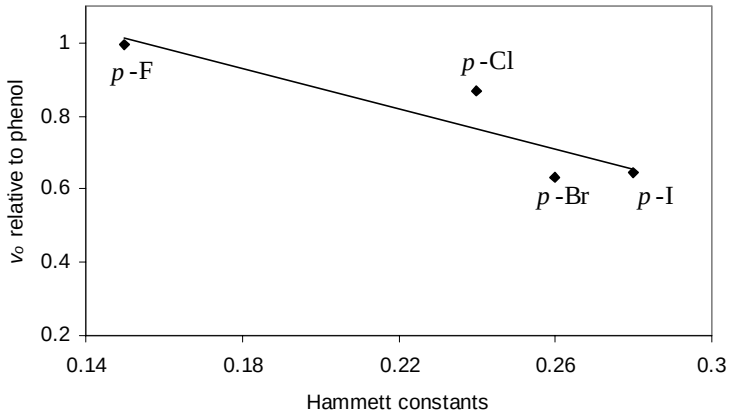

FIGURE 2.7 *Relationship between the initial degradation rate and Hammett constants of p-halophenols.*

There are two types of halogen electronic effects: resonance (or mesomeric) and field (or inductive). On the one hand, the halide unshared pair can migrate to the ring by resonance effect, then "donating" electrons and activating the ring. On the other hand, by field effect, the halide atom "withdraws" electrons, deactivating the aromatic ring. If the field effect overcomes the resonance one, *p*-halophenol is deactivated towards electrophilic attack as compared to phenol. Conversely, when the molecules have undergone the attack, the resulting radical is stabilized by the electronegative group. Thus, *p*-fluorophenol initial degradation rate is the highest being fluoride the most electronegative.

2.3.2.1.3 Hydrophobicity of *p*-halophenols

The logarithm of 1-octanol-water partition coefficient (K_{ow}) reflects the hydrophobicity of a solute. Water solubility expresses the pollutants trend to remain in or escape from the

solvent. Thus, it is reasonable to assume that the closer the pollutant to the photocatalyst surface (i.e., low water solubility and high K_{ow}) the higher the probability of reaction with holes or oxidizing species formed on that surface. It should be then expected an increase of pollutants degradation rate with the increase of log K_{ow} values. Table 2.2 presents literature *p*-halophenols log K_{ow} values [16].

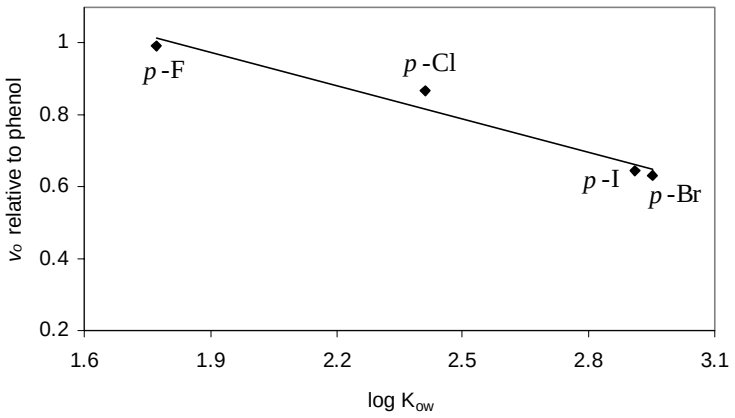

FIGURE 2.8 *Relationship between the initial degradation rate and the 1-octanol-water partition coefficient.*

As shown in Figure 2.8, there is a good correlation between *p*-halophenols initial degradation rate (v_o) and log K_{ow} but the observed trend is contrary to expected. Although *p*-fluorophenol log K_{ow} is the lowest, its relative initial degradation rate is higher than those of the others substrates. These results do not explain the photocatalytic degradation order found but they indicate that less adsorbed molecules turn out to be eliminated faster. Assuming that some active species escape from the surface, they could react with poorly adsorbing pollutants situated in near-surface regions. This same phenomenon is observed for studied herbicides photodegradation as will be discussed later.

The adsorption extent of *p*-halophenols on TiO_2 is also measured in this study to ensure the proportional correlation between log K_{ow} and adsorption on the catalyst. As expected, Figure 2.9 shows that these parameters are correlated. Notice that $n_2^s{}_{(max)}$ represents the number of organic molecules that can be adsorbed onto a gram of TiO_2 as explained below.

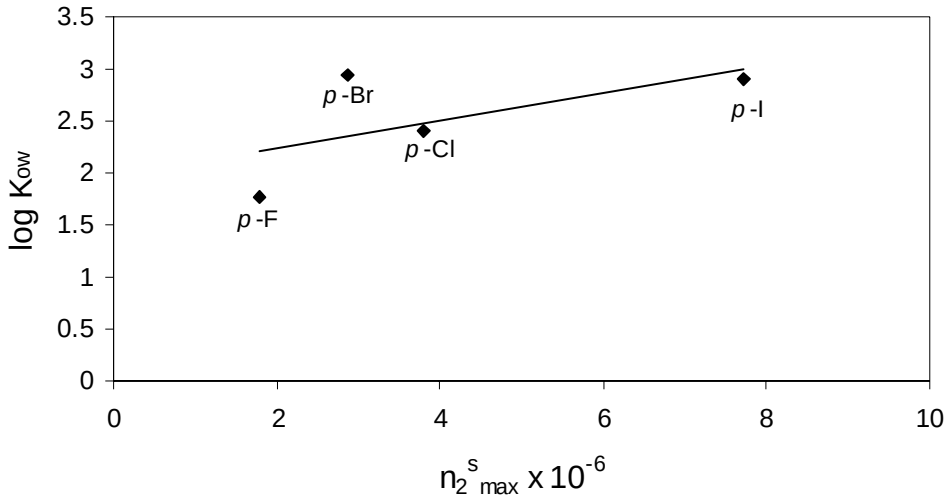

FIGURE 2.9 *Relationship between K_{ow} and the extent of adsorption of p-halophenols on TiO_2 ($n_2^s{}_{max}$).*
Latter values are presented in table 2.3.

Figure 2.10 illustrates the results obtained for the equilibrium extent of adsorption of *p*-halophenols on TiO_2 as a function of C_{eq}, the concentration remaining in bulk solution upon attainment of adsorption/desorption equilibrium in the dark. The behaviour of the number of *p*-halophenols molecules adsorbed per gram of TiO_2 (n_2^s) is usually stated as a function of the equilibrium concentration C_{eq} as follows:

$$n_2^s \approx \frac{n^s \cdot K \cdot C_{eq}}{1 + K \cdot C_{eq}} \qquad \textbf{(EQ. 2.2)}$$

where n^s is the number of adsorption sites on TiO_2 and K is the equilibrium constant for *p*-halophenols adsorption. It has been proposed [17] that due to competition with solvent molecules it is unrealistic to expect for all the available sites on the TiO_2 surface to be occupied by organic molecules. In this case, n^s can be expressed as $n_2^s{}_{max}$ giving the limited number of organic molecules that can be adsorbed onto a gram of TiO_2. Thus, the adsorption data is linearized by:

$$\frac{C_{eq}}{n_2^s} = \frac{1}{K \cdot n_{2(max)}^s} + \frac{C_{eq}}{n_{2(max)}^s} \qquad \textbf{(EQ. 2.3)}$$

$$\frac{C_{eq}}{n_2^s} = \frac{N_A \cdot \sigma^o}{A_{sp} \cdot K} + \frac{N_A \cdot \sigma^o}{A_{sp}} \cdot C_{eq} \qquad \textbf{(EQ. 2.4)}$$

In the latter equation, σ^o is the average area occupied by each *p*-halophenol molecule on the surface monolayer, A_{sp} is the specific TiO_2 surface area (50 m^2 g^{-1}), and N_A is the Avogadro's number. The plots of C_{eq}/n_2^s *versus* C_{eq} are shown for the four *p*-halophenols using the right-side scale in Figure 2.10. The values of $n_2^s{}_{(max)}$ and σ^o are calculated from the slope of straight plots in Figure 2.10 according to Equations 2.3 and 2.4. These values are presented in Table 2.3. Note that $1/\sigma^o$ represents the number of molecules adsorbed by nm^2 of catalyst area.

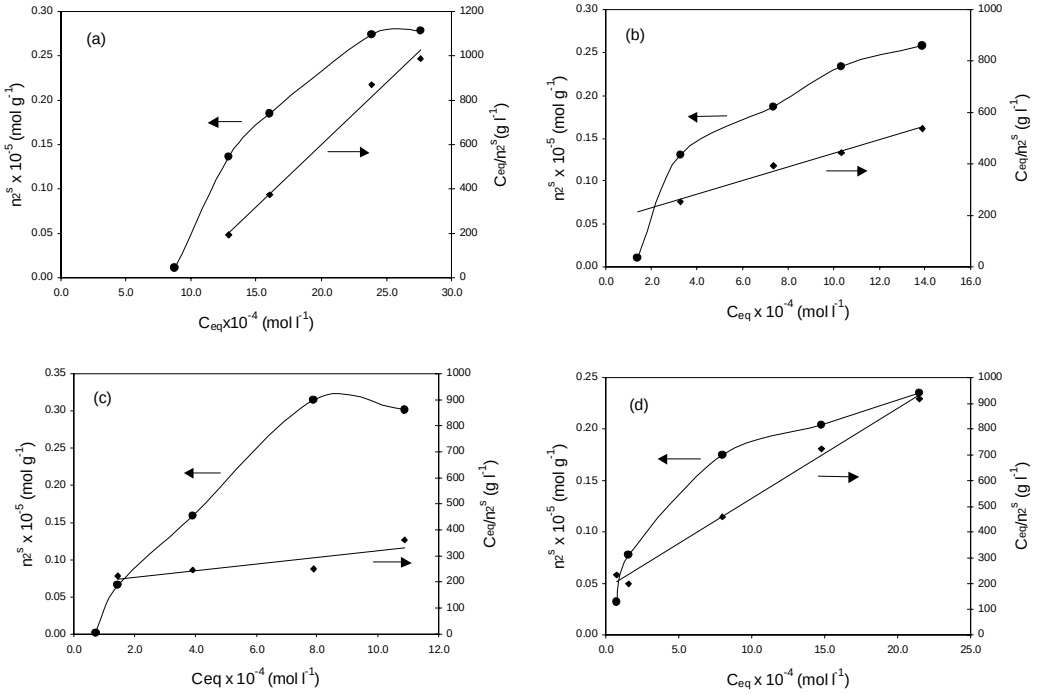

FIGURE 2.10 *p-halophenols adsorption isotherms on TiO_2.*
(a) p-fluorophenol; (b) p-chlorophenol; (c) p-iodophenol; (d) p-bromophenol. Circle data points correspond to the extent of adsorption, n_2^s, as a function of equilibrium concentration, C_{eq}. Triangle data points illustrate the linearization of data when plotted in accordance with Equation 2.3.

TABLE 2.3 *Dark adsorption parameters of the four p-halophenols.*

Phenol substituent	$n_2^s{}_{(max)}$ x 10^{-6} mol g^{-1}	Molecules adsorbed by nm^2 of TiO_2 ($1/\sigma^o$) x 10^{-2}
p-F	1.80	2.17
p-Cl	3.80	4.58
p-Br	2.87	3.46
p-I	7.71	9.29

Considering that the geometric area of one molecule of *p*-halophenol is almost 0.5 nm^2 (20 to 25% larger than benzene i.e., 0.4 nm^2), two molecules are needed to cover 1 nm^2 of catalyst. A comparison with the number of molecules effectively adsorbed indicates a low coverage, varying from 1.0 to 4.5%. This phenomenon results from the adsorption of solvated molecules. Pollutant molecules need to break the H_2O tridimensional net at TiO_2 surface and to reorganize the water molecules around them. This creates difficult thermodynamic changes, which also depend on their localization (monolayer or bulk). The number of adsorbed molecules decreases in the order: *p*-iodophenol > *p*-chlorophenol > *p*-bromophenol > *p*-fluorophenol.

Among the physicochemical characteristics evaluated, only the electronic effect represented by the Hammett constant, is directly correlated with the photodegradability order found for the *p*-halophenols.

2.3.3 Molecular structure and biodegradability relationship

The knowledge of structure-biodegradability relationship of organic compounds makes possible the estimation of biological treatability of wastewaters and removability of organic compounds by the treatment process. For substituted aromatic compounds, good correlations between biodegradability and electronic effects (expressed by the Hammett constant) of the substituents have been reported [18]. These correlations make possible the prediction of biodegradation rates of organic compounds in the environment, and facilitate the understanding of the biological degradation mechanism.

The biodegradability of aromatic compounds is influenced by the nature, number, and position of the substituents on the aromatic ring. To try to clarify this aspect, the biodegradability of substituted phenols with NO_2, Cl, COOH, and OH at *ortho*-, *meta*-, and *para*- positions is tested. The ratio of Biological Oxygen Demand (BOD) to Chemical Oxygen Demand (COD), representative of the solution biocompatibility, is summarized in Table 2.4 for the initial substituted phenol solutions and for those resulting from the photochemical treatment. The BOD values are obtained after 5 days incubation period, i.e., BOD_5. It should be noticed that BOD_5/COD ratios higher than 0.4 indicate a readily and rapidly degradable solution, while ratios below 0.4 involve the presence of slowly degradable compounds.

TABLE 2.4 *Biodegradability of different substituted phenols.*

Substituent	**BOD_5/COD**	
	Initial solutions	after phototreatment
o-NO_2	0.12	0.50
m-NO_2	0.53	0.74
p-NO_2	0.71	0.86
o-Cl	0.02	0.46
m-Cl	0.10	0.54
p-Cl	0.57	0.77
o-COOH	0.29	0.43
m-COOH	0.44	0.83
p-COOH	0.77	0.77
o-OH	0.60	0.63
m-OH	0.50	0.56
p-OH	0.78	0.57

The results presented in Table 2.4, agree with those reported in literature [18]: for a same position, the presence of OH and COOH groups facilitates the biodegradation while substituents as NO_2 and halogens decrease it. Generally, the biodegradation-increasing group includes primarily substituents that can augment the aromatic ring electron density while the biodegradation-decreasing group includes substituents diminishing electron density. These substituents activate or deactivate the aromatic ring to electrophilic attack by oxygen.

The effect of position isomerism can not be evaluated independently of the nature of substituents. As a general rule, it can be considered that compounds having free sites for biological *ortho*-hydroxylation are readily degradable, as is also the case for compounds whose individual groups can be either easy biochemically transformed to the hydroxy group or eliminated yielding free sites for the biological hydroxylation. In this sense, deactivating substituents as NO_2 and Cl in *ortho*- positions, render the compounds more difficulty biodegradable with respect to those having the same substituent in *meta*- or *para*- positions (Table 2.4). With phenolic compounds containing substituents of the biodegradation-increasing group (e.g., OH and COOH), no considerable differences are observed in the biodegradation rate depending on the position of the substituents.

It is not observed a direct correlation between the structure of the substituted phenols and the biodegradability of their phototreated solutions. However, all the phototreated solutions evaluated exhibit BOD_5/COD ratios greater than 0.4, which is an indication of the positive effect of the phototreatment applied, since easily biodegradable intermediates are formed.

2.3.4 Photocatalytic degradability of four phenylurea herbicides

2.3.4.1 Direct photolysis essay

For eight hours of irraditation, no direct photodegradation is observed for metobromuron (MB), isoproturon (IP), chlorotoluron (CT), and chlorbromuron (CB) herbicides because their molar absorptivities are very low at the radiation wavelength range used. Figure 2.11 shows that herbicides spectra do not (or very slightly) overlap the UV spectrum of the suntest lamp used for the experiments. Consequently, there is no place for a possible photoalteration process of the molecules. Thus, degradation of these herbicides, presented within this work, is exclusively due to photoactivation of the TiO_2 catalyst.

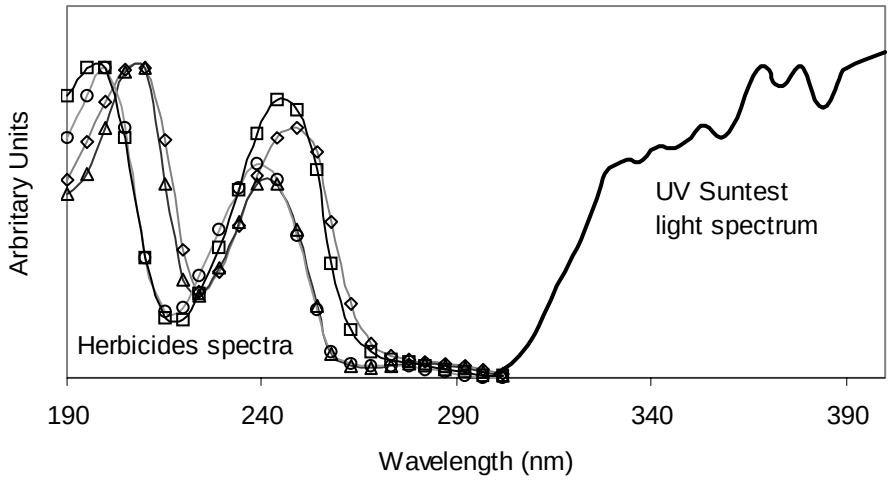

FIGURE 2.11 *UV spectra between 190 and 400 nm of herbicides and suntest lamp light. Chlorbromuron (diamonds); Isoproturon (circles); Chlorotoluron (triangles); Metobromuron (squares).*

2.3.4.2 Some parameters affecting the herbicides photodegradation *via* TiO_2 catalysis

2.3.4.2.1 Effect of TiO_2 concentration

In slurry photocatalytic processes, TiO_2 dosage is an important parameter that can affect the degradation rate. The optimal catalyst concentrations reported in the literature for TiO_2 Degussa P-25 range from 0.1 to 5.0 g l^{-1} depending on the nature of the compounds and the photoreactor geometry [19-22]. Figure 2.12 shows a plot of the initial reaction rate (v_o), which is the herbicide concentration decay at 10 minutes of photoreaction, as a function of the catalyst concentration for the four herbicides under suntest illumination. It can be observed that the initial degradation rate increases proportionally to TiO_2 concentration up to a plateau indicating a progressive saturation of the photonic absorption for a given incident radiant flux. The most efficient TiO_2 concentration is not the same for all compounds. However, above 1.0 g l^{-1} of

TiO_2, the initial rate of herbicide oxidation is negatively affected by the progressive increase of TiO_2. This phenomenon may be due to the aggregation of TiO_2 particles at high concentrations, causing a decrease in the number of surface active sites. Several authors [23-25] relate this phenomenon to the light scattering and consequent reduction in light penetration through the solution induced by lightproof suspended catalyst.

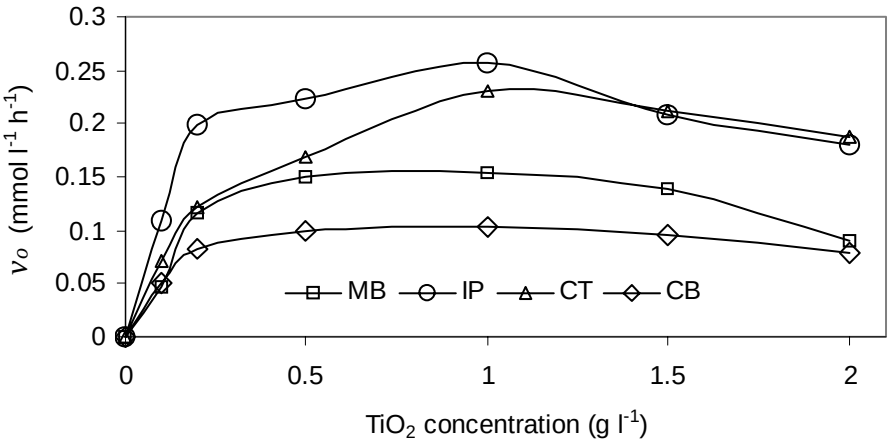

FIGURE 2.12 *Effect of TiO_2 concentration on the initial degradation rates of herbicides.*

The maximal initial degradation rate appears at a TiO_2 concentration of around 0.5 g l^{-1} in the case of CB and MB, and at values of around 1.0 g l^{-1} in the case of IP and CT. To study the structure-photoreactivity relationship, the degradation rates of different compounds have to be compared using the same optimal TiO_2 concentration for each substrate. For this reason, according to Figure 2.12 values, a TiO_2 concentration of 1.0 g l^{-1} was used in this study.

2.3.4.2.2 Effect of initial metobromuron concentration

Figure 2.13 presents the evolution of illuminated suspensions containing different concentrations of MB and 1.0 g l^{-1} of TiO_2 at natural pH as a function of time. The elimination of MB proceeds in a shorter time period at lower concentrations of initial substrate as expected.

The quasi-exponential decay observed during the degradation indicates a pseudo-first order kinetics strongly dependent on substrate initial concentration.

In Figure 2.14, it is shown that the initial degradation rate (v_o) increases at the beginning with the increase of MB concentration to then attain a plateau at around 0.4 mmol l^{-1}, indicative of a saturation-type Langmuir kinetics. This is confirmed by the linear plots of $1/v_o$ *vs* $1/[MB]_o$ (insert in Figure 2.14) with an intercept on the ordinate in agreement with equations 2.5 and 2.6.

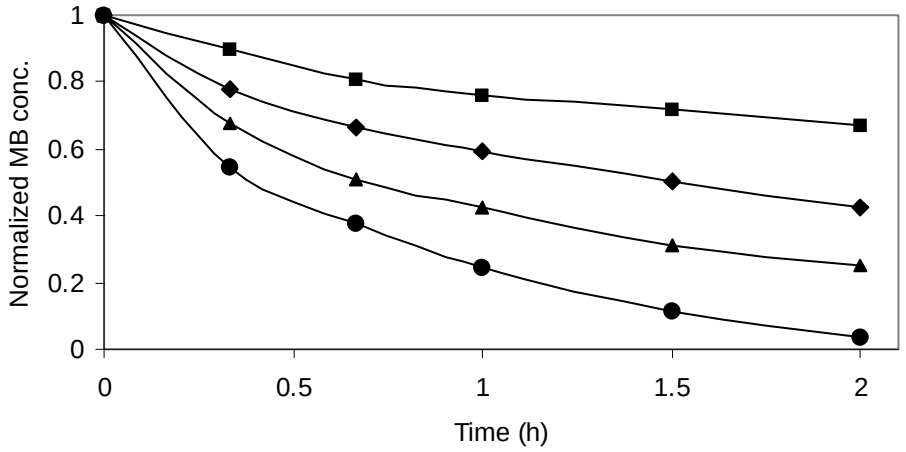

FIGURE 2.13 *Influence of the initial concentration on the photodegradation of MB with 1.0 g l^{-1} of TiO_2.*
MB initial concentrations: 0.10 (circles), 0.20 (triangles), 0.40 (diamonds), and 0.86 (squares) mmol l^{-1}.

$$v_o = \frac{k_{L-H} K^* [MB]_o}{1 + K^* [MB]_o} \qquad \textbf{(EQ. 2.5)}$$

hence

$$\frac{1}{v_o} = \frac{1}{k_{L-H} K^* [MB]_o} + \frac{1}{k_{L-H}} \qquad \textbf{(EQ. 2.6)}$$

where $[MB]_o$ is MB initial concentration, $k_{L\text{-}H}$ is often interpreted in the literature [17] as a pseudo-first-order Langmuir-Hinshelwood-type rate coefficient relating to TiO_2-sensitized primary oxidation events in a surface monolayer (0.33 mmol $l^{-1}h^{-1}$) and K^* is a pseudo-

equilibrium constant related to monolayer adsorption (7.0 x 10^3 l mol^{-1}). This Langmuir-type relationship between the initial degradation rate and concentration, reported also by other authors [22, 25, 26], indicates that adsorption plays a role in the photocatalytic reaction. Nevertheless, the extent of adsorption is not necessarily decisive in the evolution of the photochemical process as is discussed later in section 2.3.4.4.3.

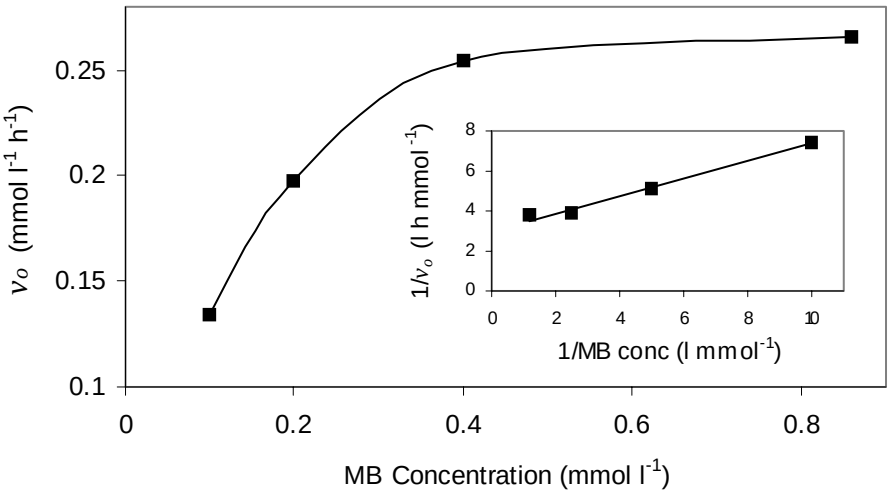

FIGURE 2.14 *Variations of the initial degradation rates of MB as a function of its initial concentration.*
The insert shows the linear transform of the Langmuir-type expression.

2.3.4.3 Comparison of the photocatalytic degradability of the four herbicides

Figure 2.15 shows the kinetics of disappearance, as a function of time, of illuminated herbicides with an initial concentration of 0.1 mmol l^{-1} and 1.0 g l^{-1} of TiO_2. The curves behave as first order processes as confirmed by the linear transform shown in the figure insert. The total photodegradation of herbicides is reached in approximately 1 h for IP and CT, and 2 h for MB and CT. For all compounds, a 70 - 80% of mineralization is obtained in 4 h as showed also in Figure 2.15. The differences between the DOC and compound concentration during the photodegradation indicate a higher accumulation of intermediates in the case of degradation of IP and CT than in degradation of MB and CT.

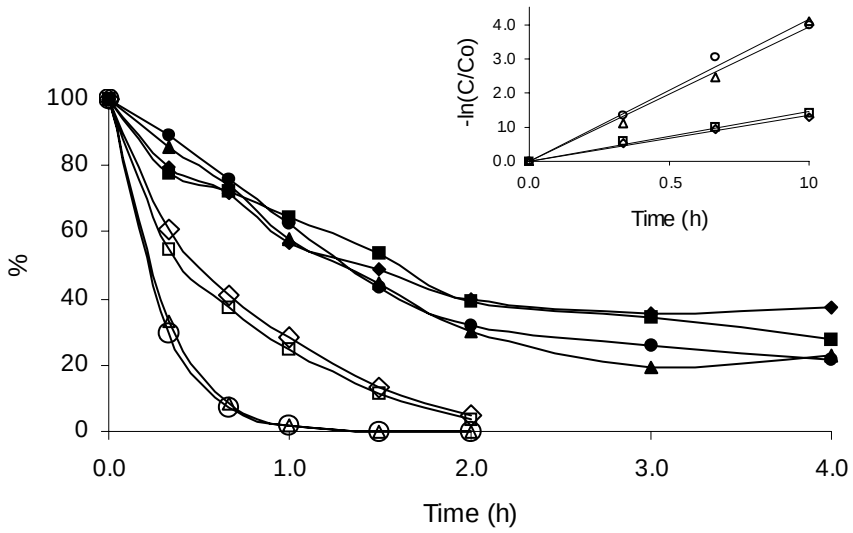

FIGURE 2.15 *Photodegradation of herbicide solutions (0.1 mmol l^{-1}) in presence of TiO_2 (1.0 g l^{-1}).*
Evolution of the initial compound (open points) and of the DOC (dark points): CB (diamonds); IP (circles); CT (triangles); MB (squares); The insert represents the linear transform $-ln(C/C_o) = f(time)$

The initial degradation rates (v_o) and the first-order rate constants (k) for the four herbicides in different reactors are presented in Table 2.5. The k values represent the curve slopes in Figure 2.15 insert and v_o, the decay of herbicide concentration during a short period time (first 10 minutes) at the beginning of the reaction.

To study the structure effect on the photodegradation, v_o has been used as comparison parameter. Although from Figure 2.15 it seems that there exists a similar degradation rate between IP and CT, and MB and CB, the v_o values of herbicides into each group are slightly different. The photoreactivity of the four herbicides can then be ranked in the following order: IP ≥ CT >> MB ≥ CB.

TABLE 2.5 *Photodegradation of IP, CT, MB, and CB herbicides in different reactors.*

Herbicide	Suntest simulator Suspended TiO_2		Coaxial reactor Supported TiO_2	CPC collector Suspended TiO_2
	v_o (mmol $l^{-1}h^{-1}$)	k (h^{-1})	v_o (mmol $l^{-1}h^{-1}$)	v_o (mmol $l^{-1}h^{-1}$)
IP	0.21	4.14	0.49	0.21
CT	0.19	3.91	0.44	0.20
MB	0.14	1.45	0.38	0.14
CB	0.11	1.33	0.31	0.10

2.3.4.4 Influence of physicochemical characteristics of herbicides on their photodegradability

2.3.4.4.1 Electron donor or withdrawing effect

The differences in photoreactivity discussed in the precedent section suggest that v_o is directly related to the electron-donor or electron-withdrawing character of the different substituents in the herbicides aromatic ring, which can activate or deactivate the ring with respect to electrophilic attack of the $^{\bullet}OH$ radical. To explain these results, only the effect of substituents in positions 3 and 4 (Figure 2.16) is taken into account since the substituent in position 1 is similar in all cases.

Isoproturon is the most reactive substance due probably to the presence of the $CH(CH_3)_2$ group, which is benzene ring activating, and to the absence of halogen substituents (Figure 2.16). The other three herbicides contain halogen groups that are considered as deactivating. Some studies [1, 5] concerning the photodegradation of mono-, di-, and tri-chlorophenols indicate that the photocatalytic degradation of these compounds proceeds by the attack of electrophilic species such as $^{\bullet}OH$ and that it should be faster with a greater aromatic ring electron density. Consequently, the degradation rates of the chlorophenols decrease with the

degree of chlorination increase. The results obtained in the current work are explained by analogy with this fact.

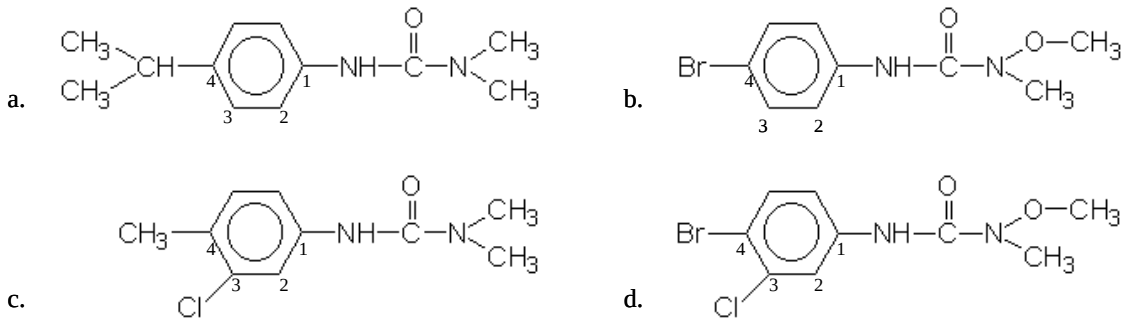

FIGURE 2.16 *Chemical structure of herbicides.*
(a) isoproturon; (b) metobromuron; (c) chlorotoluron; (d) chlorbromuron.

Chlorbromuron has two halogen groups (Br and Cl) bound to the aromatic ring and this could explain its lower reactivity when compared with the other herbicides. Only one halogen group is present in the molecular structure of CT (Cl) and MB (Br) and the difference in their photoreactivity is probably due to the presence of a CH_3 activating group in the CT herbicide. As it is known, the activating character of a CH_3 group prevails over the deactivating character of a Cl group explaining why CT reacts faster than MB.

The photocatalytic degradation of these same herbicides was also carried out in a coaxial photocatalytic reactor (refer to 3.2.2.2) with supported TiO_2 and at pilot scale in a compound parabolic collector (refer to section 4.2.2.2) with suspended TiO_2. The initial degradation rates (v_o), presented in Table 2.5 for the four herbicides are different for each system. However, they can be ranked in the same order independently of the photodegradation system employed. Note that the initial degradation rates are almost identical when using suspended TiO_2 with both simulated (suntest) or natural (CPC reactor) solar irradiation.

2.3.4.4.2 Computer-based structure-activity relationships

Molecular structure-based electronic and geometrical properties for all the tested compounds are statistically associated with their respective initial photo-degradation rates (v_o)

using multiple linear regression. The criteria for the selection of the best regression model are the square of the correlation coefficient (R^2), the standard error of the estimate (SE), the F-ratio, and the probability level (P). The best prediction model obtained is shown below.

$$v_o = (0.274 \pm 0.019).E_{HOMO} + (2.572 \pm 0.171)$$

R^2=0.985, SE=0.006, F-Ratio=197.85, P=0.005

E_{HOMO} is the best descriptor responsible for the degradation rate of herbicides. However, E_{HOMO} is a parameter highly dependent on molecular size, as observed from the correlation with molecular weight (r = 0.999, P = 0.001). In order to obtain the best descriptor associated with the degradation rate but independent of molecular weight (MW), partial correlations were performed controlling for MW. The greater partial correlation between v_o and the molecular descriptors was obtained for the dipolar moment (R = -0.908, p = 0.275), suggesting that an increase in charge separation decreased the v_o. Interestingly, after controlling for MW, the correlation between v_o and E_{HOMO} was highly reduced (R = 0.635, p = 0.562). The data are in agreement with the donor or withdrawing effect discussed above where the presence of the electronegative group attached to the phenyl moiety determines the behaviour of v_o.

The effect of the presence of the electronegative group on v_o is clearly shown in the Hyperchem-derived Molecular Electrostatic Potentials (MEPs) computed on the AM1-optimized structures of the molecules taken at a plane off set 1Å over the surface of the aromatic ring.

Figure 2.17 shows that the negative electrostatic potential on the aromatic ring increases its size in the order IP > CT > MB > CB, property that is directly proportional with the photoreactivity of the herbicides [27]. This approach has also been used to design novel insect repellents [28].

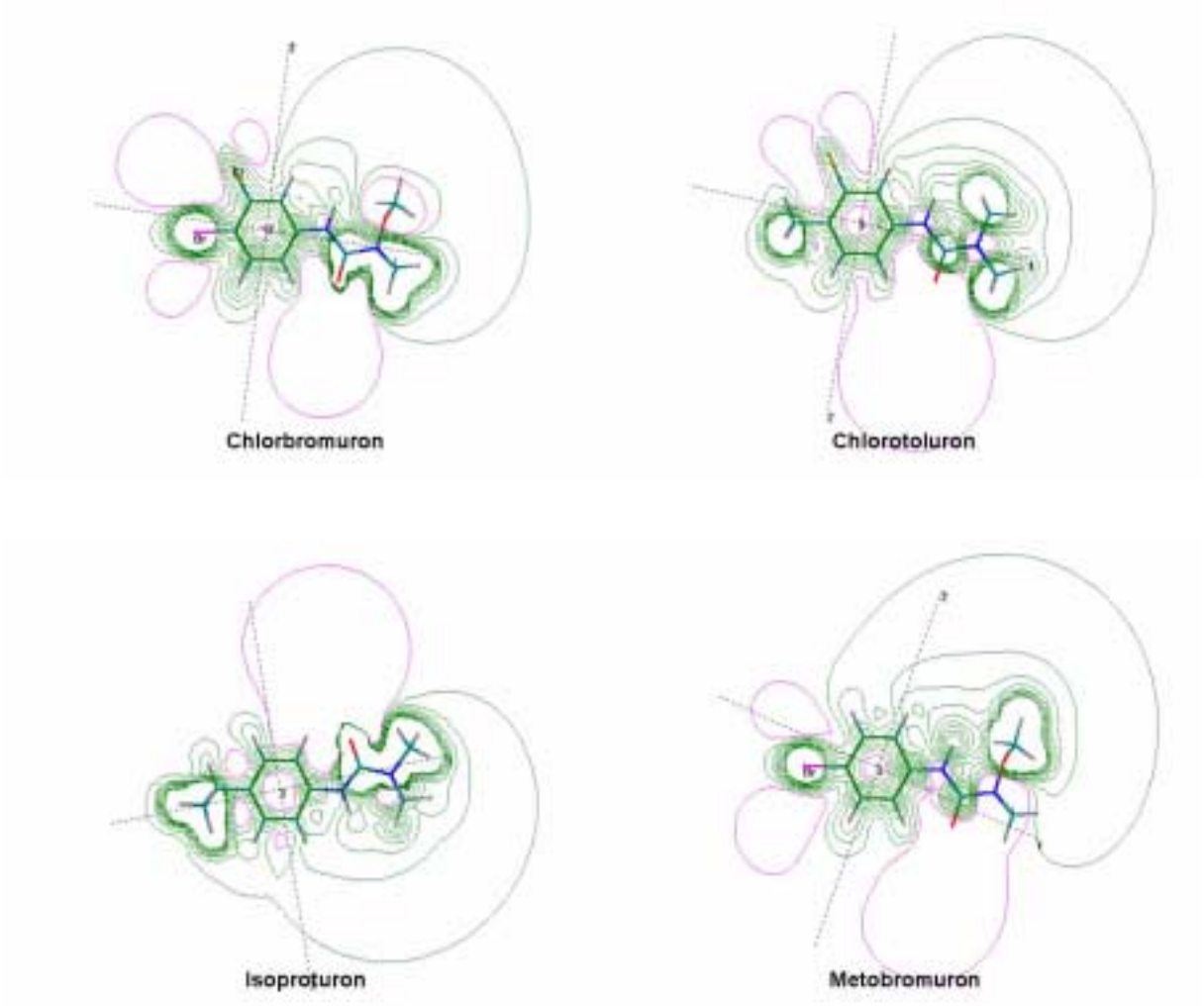

FIGURE 2.17 *Molecular electrostatic potential (MEP) maps for herbicides. Electronegative and electropositive potential contours are shown in red and green, respectively. MEPs were recorded after full structure optimization by the semi-empirical method AM1 (Hyperchem) and the countor levels taken at a starting value of -0.005 a.u.e., increments of 0.01 a.u.e. and a plane off set at 1 Anstrong.*

2.3.4.4.3 Herbicides adsorption on TiO_2

The herbicides adsorption on TiO_2 is assessed to determine how their structure affects the adsorption on the catalyst. In Figure 2.18, it appears that the adsorption increases toward a plateau in all cases as the concentration of the herbicide does. The experiments were made (but

not shown) using a wider concentration range for each herbicide than those presented in Figure 2.18. In such case, it was noted that beyond a maximal concentration, specific to each substance isotherm, a sharp rise of the adsorption is observed. This corresponds to the transition from a monolayer to a multilayer adsorption as suggested by several authors [29, 30] for other compounds.

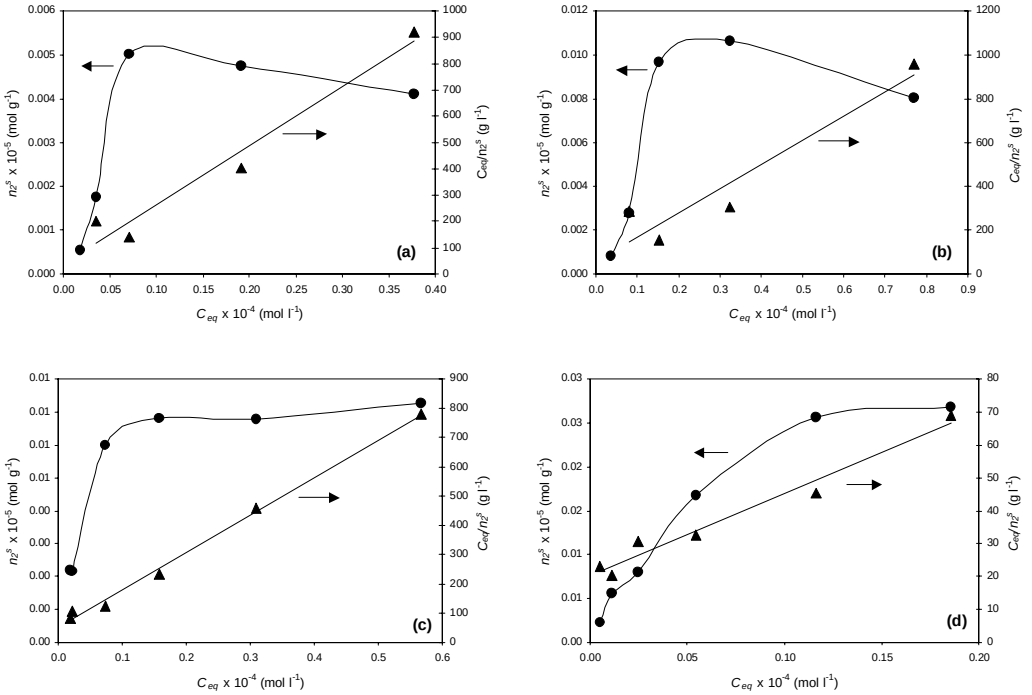

FIGURE 2.18 *Herbicides adsorption isotherms on TiO_2.*
(a) Isoproturon, (b) metobromuron, (c) chlorotoluron, and (d) chlorbromuron. Circle data points correspond to the extent of adsorption, n_2^s, as a function of equilibrium concentration, C_{eq}. Triangle data points illustrate the linearization of data when plotted in accordance with Equation 2.3.

The behaviour of number of herbicide molecules adsorbed per gram of TiO_2 (n_2^s) is usually stated as a function of the herbicide equilibrium concentration C_{eq} following the Equation 2.2. As mentioned in section 2.3.2.1.3, the adsorption data can be linearized by Equations 2.3 and 2.4. The plots of C_{eq}/n_2^s *versus* C_{eq} are shown for the four herbicides using the right-side scale in Figure 2.18. The values of $n_2^s{}_{(max)}$, K, and σ^o are calculated from the

slope and intercept of straight plots in Figure 2.18 according to Equations 2.3 and 2.4. These values are presented in Table 2.6.

TABLE 2.6 *Dark adsorption parameters of the four herbicides.*

Herbicide	$n_2^s{}_{(max)}$ x 10^{-4} mol g^{-1}	K x 10^2 l mol^{-1}	σ^o nm^2
IP	0.45	0.60	1.84
CT	0.78	0.25	1.06
MB	0.90	0.18	0.92
CB	1.42	0.16	0.58

In comparison with the pseudo-equilibrium constant (K^* = 7.0 x 10^3 l mol^{-1}) measured under irradiation for MB in section 2.3.4.2.2, the *K* measured in the dark for the same compound is about 280 times smaller. This result is in agreement with that reported by other authors, whom have shown that the adsorption constant determined in photocatalytic degradation experiments is always greater than the adsorption constant measured in the dark: for instance, 13 times fold has been observed for benzyl alcohol [17] and 220 times fold for *p*-chlorophenol [31]. The apparent variability in the adsorption constant may be related to the changes in the absorptive sites of the TiO_2 surface upon irradiation. The possibilities of significant photoadsorption and/ or involvement of reaction steps occurring in the double layer could not be ruled out [32]. Furthermore, Xu and Langford [33] have demonstrated that the adsorption constant is a function of the light intensity and that the electronic properties of the TiO_2 surface will undergo dramatic changes upon illumination, altering the adsorption sites as well.

The average area occupied by each molecule of herbicide (σ^o values in Table 2.6) on the surface monolayer of the TiO_2 is much larger than the geometric cross section (typically 0.2-0.3 nm^2) of a non-solvated herbicide molecule. Assuming that each H_2O molecule requires a surface space of 0.02 nm^2, the total cross section (1.84 nm^2) deduced per adsorbed IP molecule at saturation (Table 2.6) indicates that each molecule could be surrounded by around 80 H_2O molecules.

The values of $n_2^s{}_{(max)}$ in Table 2.6 provide an adsorption capacity in the dark for the four herbicides in the order CB > MB > CT > IP, which is inversely proportional to the

photodegradability order shown in section 2.3.4.3. Nevertheless, it can not be defined, in a general way, that there is an inverse relationship between these two parameters. Indeed, it is well known that photocatalytic reactions can occur independently of the degree of adsorption of organic compounds on TiO_2 either in the dark or during the photocatalytic process. These results demonstrate that a large extent of adsorption is not an indication of a highly efficient photodegradation of the herbicides or *vice versa*. The radical species produced during irradiation can react with herbicides on the surface of the TiO_2 but also in the bulk of the solution when they are neither adsorbed (or little) nor chemi-adsorbed. It has been suggested [34] that in the case of radical formation on an UV-illuminated TiO_2 surface, adsorption of the organic contaminant would increase the reaction rates, but it is not a requirement for the reaction to occur since the reactive $^{\bullet}OH$ radicals and other oxidizing species can diffuse into the solution bulk to react with the organic pollutant. In the case of well-adsorbing organic pollutants presenting a poorly degradation rate, it has been proposed [17] that the inhibition of the photocatalytic degradation occurs either *via* blockage of reaction sites on TiO_2 surface or through their action as locations for surface recombinations of photogenerated holes and electrons.

2.4 Conclusions

The influence of substituted phenols and herbicides substituents on the TiO_2-catalysed photodegradation is investigated. It is clearly demonstrated that the photoreactivity of such compounds can be drastically affected by the electronic nature of the substituents and the substitution pattern.

Whether the photocatalytic degradation proceeds by the formation of organic cations or by the direct attack of electrophilic species such as hydroxy radicals, the initial degradation rate of the *p*-substituted phenols is higher with a greater electron density on the aromatic ring. In this sense, the Hammett constant is an adequate descriptor of the photocatalytic degradability of such compounds.

Good Hammett correlations are observed for the initial degradation rates of the non-halogenated and halogenated *p*-substituted phenols when these two families are separately evaluated. *Para*-halophenols are degraded following a first-order kinetics with initial

degradation rates decreasing in the following order: *p*-fluorophenol ≥ *p*-chlorophenol >> *p*-iodophenol ≥ *p*-bromophenol. Among the physicochemical characteristics (carbon-halide bond strengths, hydrophobicity, and halogen substituent electronic effect) evaluated to explain the found photoreactivity order, only the halogen substituent effect represented by the Hammett constant, allows to assess the photodegradability order of these compounds.

The hydroxybenzenes are the only group for which is observed an effect of OH group position on photodegradation in TiO_2 aqueous suspensions. The three isomers follow a first-order kinetics with degradation efficiencies decreasing in the following order: resorcinol > hydroquinone > catechol.

The effect of the nature and position of the substituents on the aromatic ring is also noticed in the biodegradation of some substituted phenols. The same as in the case of the photodegradation, the biodegradation is faster when there is a greater electronic density on the aromatic ring, since it is activated towards an electrophilic attack by oxygen.

The photodegradation rate of the studied herbicides is affected by the TiO_2 dosage. A Langmuir-type relationship between the initial degradation rate and the initial concentration of metobromuron, indicates that adsorption plays a role in the photocatalytic reaction. However, the extent of adsorption of the compounds on TiO_2 is not necessarily decisive in the evolution of the photochemical process. This study demonstrates that a large extent of adsorption is not an indication of a highly efficient photodegradation of the herbicides or *vice versa*. This same statement is also valid for the photodegradation of *p*-halophenols.

Metobromuron adsorption constant on TiO_2 determined during a photocatalytic degradation experiment is about 280 times greater than that measured in the dark. This variability in the adsorption constant may be related to changes in the adsorptive sites on TiO_2 surface upon irradiation.

The photodegradation order found for the four phenylurea herbicides (IP ≥ CT >> MB ≥ CB) suggests that their photoreactivity is directly related to the donor or withdrawing effect induced by the different substituents of the aromatic ring. The influence of electron-donor or electron-withdrawing character of the groups on the herbicides molecules can be visualized using molecular electrostatic potentials of the aromatic ring. In this work, the magnitude of the

electronegative potential generated by the groups bound to the aromatic ring of the herbicide correlates directly with the molecule photoreactivity. A similar result is obtained when quantum molecular parameters obtained from molecular modelling are correlated with photoreactivity. The dipolar moment, a physicochemical parameter linked to charge separation within the molecule, is the best predictor of photoreactivity of such herbicides.

2.5 Bibliography

1. D'Oliveira, J.C., *et al.*, *Photodegradation of Dichlorophenols and Trichlorophenols in TiO2 Aqueous Suspensions - Kinetic Effects of the Positions of the Cl Atoms and Identification of the Intermediates.* J Photochem Photobiol A. Chem, 1993. 72(3): p. 261-267.

2. O'Shea, K.E. and C. Cardona, *Hammett study on the TiO2-catalyzed photooxidation of para-substituted phenols. A kinetic and mechanistic analysis.* J. Org. Chem., 1994. 59: p. 5005-5009.

3. Amalric, L., *et al.*, *Correlation Between the Photocatalytic Degradability over TiO2 in Water of Meta and Para-Substituted Methoxybenzenes and Their Electron-Density, Hydrophobicity and Polarizability Properties.* Water Res, 1996. 30(5): p. 1137-1142.

4. Sangchakr, B., T. Hisanaga, and K. Tanaka, *Photocatalytic degradation of sulfonated aromatics in aqueous TiO2 suspension.* Journal of Photochemistry and Photobiology A: Chemistry, 1995. 85(1-2): p. 187-190.

5. Tseng, J.M. and C.P. Huang, *Removal of chlorophenols from water by photocatalytic oxidation.* Water science and technology, 1991. 23: p. 377-387.

6. Assabane, A., *et al.*, *Photocatalytic degradation of polycarboxylic benzoic acids in UV-irradiated aqueous suspensions of titania. Identification of intermediates and reaction pathway of the photomineralization of trilellitic acid (1,2,4-benzene tricarboxylic acid).* Applied Catalysis B: Environmental, 2000. 24: p. 71-87.

7. Tang, W.Z. and H. An, *UV/TiO2 Photocatalytic oxidation of commercial dyes in aqueous solutions.* Chemosphere, 1995. 31(9): p. 4157-4170.

8. Tang, W.Z. and P.H. C., *Effect of Chlorine Content of Chlorinated Phenols on Their Oxidation Kinetics by Fenton's Reagent.* Chemosphere, 1996. 33(8): p. 1621-1635.

9. Tang, W.Z. and P.H. C., *The effect of chlorine position of chlorinated phenols on their dechlorination kinetics by Fenton's reagent.* Waste Management, 1995. 15(8): p. 615-622.

10. Miranda, M.A., *et al.*, *Pyrilium salt-photosensitized degradation of phenolic contaminants derived from cinnamic acid with solar light. Correlation of the observed reactivities with fluorescence quenching.* Applied Catalysis B: Environmental, 2000. 28: p. 127-133.

11. Dewar, M., *et al.*, *AM1: A new general purpose quantum mechanical molecular model.* J. Am. Chem. Soc., 1985. 107: p. 3902-3909.

12. Smith, M.B. and J. March, *Effect of Structure on reactivity*, in *Advanced Organic Chemistry. Reactions, Mechanisms, and Structure. 5th edition*. 2001, John Wiley & Sons, Inc.: New York.

13. Dean, J.A., *Handbook of organic chemistry*. 1987, New York: McGraw-Hill.

14. Rincon, A.G., *et al.*, *Interaction between E. coli inactivation and DBP-precursors-dihydroxybenzene isomers - in the photocatalytic process of drinking-water disinfection with TiO2*. Journal of Photochemistry and Photobiology A: Chemistry, 2001. 139: p. 233-241.

15. Walling, C., D.M. Camaioni, and S.S. Kim, *Aromatic hydroxylation by peroxydisulfate*. Journal of American Chemical Society, 1978. 100: p. 4814-4818.

16. Leo, A., C. Hanseh, and D. Elkins, *Partition coefficients and their uses*. Chem. Rev., 1971. 71(6): p. 555.

17. Cunningham, J., A.-S. G., and S. Srijaranai, *Adsorption of model pollutants onto TiO2 particles in relation to photoremediation of contaminated water.*, in *Aquatic and surface photochemistry*, G.R. Helz, R.G. Zepp, and D.G. Crosby, Editors. 1994, Lewis Publishiers: Boca Raton. p. 317-348.

18. Pitter, P. and J. Chudoba, *Biodegradability of organic substances in the aquatic environment*. 1990, Boca Raton, Florida: CRC Press, Inc.

19. Gimenez, J., D. Curco, and M.A. Queral, *Photocatalytic treatment of phenol and 2,4-dichlorophenol in a solar plant in the way to scaling-up*. Catalysis Today, 1999. 54(2-3): p. 229-243.

20. Chen, D. and A.K. Ray, *Photocatalytic kinetics of phenol and its derivates over UV irradiated TiO2*. Applied Catalysis B: Environmental, 1999. 23: p. 143-157.

21. Al-Sayyed, G., J.C. D'Oliveira, and P. Pichat, *Semiconductor-sensitized photodegradation of 4-chlorophenol in water*. Journal of Photochemistry and Photobiology A: Chemistry, 1991. 58: p. 99-114.

22. Percherancier, J.P., R. Chapelon, and B. Pouyet, *Semiconductor-sensitized photodegradation of pesticides in water: the case of carbetamide*. Journal of Photochemistry and Photobiology A: Chemistry, 1995. 87: p. 261-266.

23. Bandara, J., *et al.*, *Oxidative degradation and fluorescence of a non-biodegradable brightener via titania suspensions: Implacations for the natural cycle*. J. Adv. Oxid. Technol., 1996. 1(2): p. 126-137.

24. Le Campion, L., C. Giannotti, and J. Ouazzani, *Photocatalytic degradation of 5-nitro.1,2,4-triazol-3-one NTO in aqueous suspension of TiO2. Comparaison with Fenton oxidation*. Chemosphere, 1999. 38(7): p. 1561-1570.

25. Inel, Y. and A.N. Okte, *Photocatalytic degradation of malonic acid in aqueous suspension of titanium dioxide: an initial kinetic investigation of CO2 photogeneration*. Journal of Photochemistry and Photobiology A: Chemistry, 1996. 96: p. 175-180.

26. Arslan, I., I.A. Balcioglu, and D.W. Banheman, *Heterogeneous photocatalytic treatment of simulated dyehouse effluents using novel TiO2 photocatalysts*. Applied Catalysis B: Environmental, 2000. 26: p. 193-206.

27. Parra, S., J. Olivero, and C. Pulgarin, *Relationship between physicochemical properties and photoreactivity of four bioreaclcitrant phenylurea herbicides in aqueous TiO2 suspension*. Applied Catalysis B: Environmental, 2001. accepted.

28. Bhattacharjee, A.K., *et al.*, *Molecular similarity analysis between insect juvenile hormone and N, N-diethyl-m-toluamide (DEET) analogs may aid design of novel insect repellents.* J. Mol. Recognit., 2000. 13(4): p. 213-220.

29. Cunningham, J. and P. Sedlak, *Kinetic studies of depollution process in TiO2 slurries: interdependences of adsorption and UV-intensity.* Catalysis Today, 1996. 29: p. 309-315.

30. Bandara, J., J.A. Mielczarski, and J. Kiwi, *1. Molecular mechanism of surface recognition. Azo dyes degradation on Fe, Ti, and Al oxides through metal sulfonate complexes.* Langmuir, 1999. 15: p. 7670-7679.

31. Mills, A. and S. Morris, *Photomineralization of 4-chlorophenol sensitized by titanium dioxide: a study of the initial kinetics of carbon dioxide photogeneration.* Journal of Photochemistry and Photobiology A: Chemistry, 1993. 71: p. 75-83.

32. Cunningham, J. and G. Al-Sayyed, *Factors influencing efficiencies of TiO2-sensitised photodegradation. Part 1. Substituted benzoic acids: discrepancies with dark adsorption parameters.* J. Chem. Soc. Faraday Trans., 1990. 86(23): p. 3935-3941.

33. Xu, Y. and H. Langford, *Variation of Langmuir adsorption constant determined for TiO2-photocatalyzed degradation of acetophenone under different light intensity.* Journal of Photochemistry and Photobiology A: Chemistry, 2000. 133: p. 67-71.

34. Turchi, C.S. and D.F. Ollis, *Photocatalytic degradation of organic water contaminants: mechanisms involving hydroxyl radical attack.* J. Catal., 1990. 122: p. 178-192.

CHAPTER 3

INTEGRATED PHOTOCATALYTIC-BIOLOGICAL PROCESS

3.1 Introduction

As mentioned in chapter 1, Advanced Oxidation Processes are considered as very promising methods for the remediation of contaminated ground, surface, and waste waters containing non-biodegradable organic pollutants [1, 2]. Among these AOP, the combined systems UV/TiO_2/H_2O_2 and UV/Fe^{3+}/H_2O_2 are the most utilized for environmental applications since they use the UV component of solar light. A wide range of applications have been reported for different compounds using these systems [3, 4]. Even using natural sun light, the operational costs of these AOP for the total oxidation of hazardous organic compounds or non-biodegradable effluents remain relatively high compared to those of biological treatments, which are, at the present, the cheapest and the most compatible with the environment.

However, the use of AOP as a pre-treatment step to enhance the biodegradability of wastewater containing recalcitrant or inhibitory compounds can be justified if the resulting intermediates are easily degradable by microorganisms in a further biological treatment. There are currently a lot of investigations focused in the development of new chemical oxidation technologies that can be potentially applied in this field [5-7]. The chemical processes utilized are based on: ozone [8], ozone/hydrogen peroxide [9], hydrogen peroxide/UV [10], wet air oxidation [11], and artificial sunlight [12], among others. Some results obtained with such kind of methods, mainly at laboratory scale, suggest potential advantages for water treatment. The first coupled flow system was developed in our laboratory using Fenton reaction as pre-treatment step [13-15].

At present, there are not known reports of combined systems using TiO_2-photo-assisted reaction as pre-treatment process. The biggest problem of this approach is that the catalyst has to be recovered from the solution at the end of the photochemical process before coupling with the biological step. This problem could be solved by immobilizing the catalyst on an inert surface without activity losses. There are many works based on supported TiO_2 catalysts [16-18], in which a variety of supporting materials, coating methods, and reactor arrangements have been investigated from both engineering and fundamental points of view.

The present research aims to combine physicochemical and biological treatment processes to mineralize toxic and/or bio-recalcitrant compounds. Two kinds of combined systems are developed using in both cases immobilized biomass for the biological step and either photo-Fenton or TiO_2 supported on glass rings for the photocatalytic pre-treatment. The advantages of the latter system are that the catalyst can be re-used and that the pH of the solution remains at neutral values [19]. The photo-Fenton reaction instead, renders the phototreated solution acidic making neutralization necessary [15].

Both photochemical-biological flow systems are employed to completely mineralize an IP herbicide solution. Preliminary experiments concerning the chemical and biological characteristics of the phototreated solution are carried out to determine the moment at which it becomes biocompatible. Two operation modes (continuous or semi-continuous) of the photo-Fenton-biological coupled reactor are compared by studying the efficiency of the photochemical, biological, and overall treatments of a *p*-NTS solution.

3.1.1 General strategy for coupling photochemical and biological treatments

Coupling of photochemical and biological processes is a good alternative to minimize the treatment cost of wastewater containing biorecalcitrant, non-biodegradable and/or toxic pollutants. Due to the high cost of photochemical treatments, it must be first confirmed that target pollutants are definitively non-biodegradable since for biodegradable compounds, classical biological treatments are, at the present, the cheapest and most environmentally compatible.

In coupled systems, the physicochemical pretreatment is meant to modify the structure of pollutants by transforming them into less toxic and easily biodegradable intermediates, which allows the subsequent biological degradation to be achieved in a shorter time and in a less expensive way.

The solution resulting from the phototreatment stage is considered to be biologically compatible after the elimination of:

- the initial biorecalcitrant compound,

- the inhibitory and/or non-biodegradable intermediates, and

- the residual H_2O_2, or other inhibitory electron acceptors, whenever they are utilized for the phototreatment.

These requirements, together with information concerning the evolution of toxicity and biodegradability of the phototreated solutions, allow the determination of an optimal phototreatment time, which corresponds to the best cost-efficiency compromise. The phototreatment time must be as short as possible to avoid a high electricity consumption, which represents about 60% of the total operational cost when using electric light sources [13]. However, if the fixed pretreatment time is too short, the intermediates remaining in solution could still be structurally similar to initial biorecalcitrant compounds and therefore, non-biodegradable. Furthermore, at short phototreatment times, the residual H_2O_2 concentration may be high enough to inhibit the biological stage of the coupled reactor. This oxidant is not required for all the photochemical processes but, whenever utilized it has to be eliminated before the biological stage.

The strategy of coupling photochemical and biological systems, is not necessarily an universal solution. Chemical, biological, and kinetic studies must always be conducted to ensure that the photochemical pretreatment induces beneficial effects on the biocompatibility of the treated wastewater.

3.2 Experimental

3.2.1 Materials

All chemicals are used as received without further purification. Metobromuron (MB), isoproturon (IP), and *p*-nitro-*o*-toluenesulfonic acid (*p*-NTS) are obtained from Ciba (Monthey-Switzerland), $FeCl_3.6H_2O$ and H_2O_2 (30% w/w) analysis grade (p.a.) are Fluka, and TiO_2 is Degussa P-25, mainly anatase with a surface area of 50 m^2g^{-1}. The glass rings with supported TiO_2 are provided by the Laboratory of Renewable Resources of the University of Concepción, Chile. The chemicals for HPLC analysis are obtained from Fluka. Milli-Q water is used throughout for the preparation of aqueous solutions or as a component of the mobile phase, water-acetonitrile (HPLC grade) in HPLC analysis. The phototreated solutions are neutralised by means of NaOH. Neutral pH of the solutions is maintained during the biological treatment by adjusting with HCl or NaOH.

3.2.2 Coupled photochemical-biological flow reactor. Procedures

The coupled system used for the total mineralization of IP and *p*-NTS presented in this chapter has been designed and constructed in our laboratory. The coupled photochemical-biological flow reactor is presented in Figure 3.1 and described in detail below. The biological reactor shown at the right hand side of Figure 3.1, can be coupled with one of two possible photochemical reactors: the coaxial one or the coiled one as shown in the left hand side of Figure 3.1. The coaxial reactor is used for heterogeneous phase reactions using TiO_2 supported on glass rings, while the coiled reactor is used for experiments in homogeneous phase via photo-Fenton reaction.

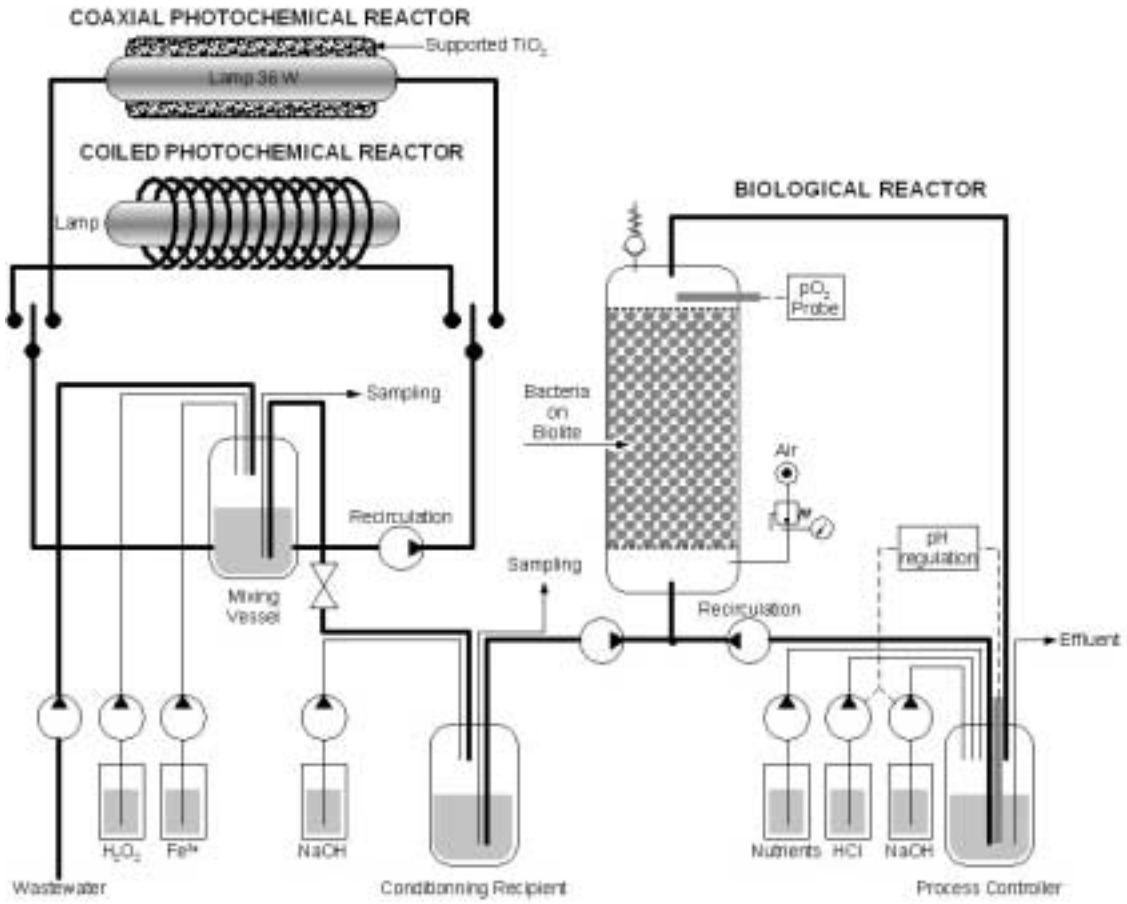

FIGURE 3.1 *Scheme of the coupled photochemical-biological flow reactor.*

3.2.2.1 Coiled photochemical reactor

In the coiled photochemical reactor shown in Figure 3.1, the contaminated water circulates through an 8 mm-diameter glass spiral of about 20 m long. A 400 W, 40 cm long, medium-pressure Hg-lamp (Applied Photophysics) is positioned in such a way that its center line passes through the axis of the coiled reactor. The predominant radiation is observed at 366 nm with 50% of the Hg-lamp output (equivalent to ~15 Watt). It has been taken care that all photons are absorbed in the optical thickness of the coiled reactor since the scattering effects are less significant in a reacting medium having a high optical absorption. The reactor was designed for different flow rates, organic loads, recirculation rates, and, oxidant addition rates. The

reactor mixing-vessel has a volume of 1 l. The runs are carried out at room temperature. The pollutant solution is fed into the system from a 20 l reservoir and H_2O_2 and Fe^{3+} solutions are automatically added by means of peristaltic pumps into the mixing-vessel. The solution is continuously or in batch mode recirculated at 22 l h^{-1} through the illuminated part of the reactor. In order to prepare the phototreated water for biological treatment, the solution is neutralized by means of NaOH at the photoreactor outlet, into the conditioning recipient.

3.2.2.2 Coaxial photocatalytic reactor

Titanium dioxide supported on glass rings (4 mm length, 4 mm internal diameter) is employed in the coaxial photocatalytic reactor shown in Figure 3.1. Immobilisation of the catalyst was performed by the Laboratory of Renewable Resources of the University of Concepción, Chile according to their previously reported procedure [20, 21]. A Philips 36 W (1.20 m long and 26 mm in diameter, TLD 36 W/08) black actinic light source is employed for irradiation in such a way that its centre passes through the axis of the reactor. The lamp radiation has a λ-distribution between 330 and 390 nm centred at 366 nm. The reactor has a total volume of 1.5 l where 0.8 l are illuminated. The runs are carried out at room temperature. The pollutant solution is fed into the system from a 20 l reservoir and is continuously recirculated at 90 l h^{-1} by means of a peristaltic pump through the illuminated part of the reactor. Samples are taken from a mixing-vessel sampling port. The glass rings impregnated of TiO_2 float freely in the space between the light source tube and the outer wall of the jacketed reactor. During the photocatalytic experiments, the coaxial reactor is covered with an aluminium-coated parabolic device to avoid loss of light by reflecting it through the bulk of the solution. To prepare the effluent for the biological treatment, a conditioning recipient is available between the photocatalytic and the biological reactor, in which, the pH of the phototreated solution can be automatically neutralised, if necessary, by means of NaOH.

3.2.2.3 Biological reactor

The Fixed Bed Reactor (FBR) shown on the right hand side of Figure 3.1 consists of a column of 1 l of capacity containing biolite colonized by activated sludge from a municipal

wastewater treatment plant (Vidy, Lausanne, Switzerland). The effluent of the photochemical step is circulated through the column, which operates as an up-flow reactor. To assure a good contact of the phototreated solution with the biomass, the water is recirculated at 6 l h^{-1} through the column. The pH is controlled by a probe and adjusted at 7 by means of HCl or NaOH, depending on the case. The required nutrients (N, P, K, and oligoelements) for the bacterial activity are also added. The aeration is about 150 l h^{-1} and the O_2 concentration is checked by means of an O_2 probe on the top of the column.

3.2.3 Chemical and biological analysis

3.2.3.1 Dissolved Organic Carbon (DOC)

A Shimadzu, model 5050A, TOC analyzer is used for DOC measurements. The instrument is equipped with an ASI automatic sample injector and it uses potassium phthalate solution as calibration standard. Acidification and stripping before analysis were sometimes necessary to keep the solutions free of atmospheric CO_2.

3.2.3.2 Chemical Oxygen Demand (COD)

The COD is used as a measure of the oxygen equivalent of the organic matter content of a sample that is susceptible to oxidation by a strong chemical oxidant. This analysis is carried out via a Hach-2000 spectrophotometer using dichromate solution as the oxidant in strong acid medium. Test solution (2 ml) is pipetted into the dichromate reagent and digested at 150^{o}C for two hours. Colour is developed during the oxidation and measured against a water blank using a Hach DR/890 colorimeter. The optical density for the change of colour of the dichromate solution was determined at λ = 430 nm.

3.2.3.3 High Performance Liquid Chromatography (HPLC)

The equipment used is a Varian 9065 unit provided with a Varian 9012 solvent delivery system, an automatic injector 9100, and a Varian Pro Star variable (200-400 nm) diode array detector 9065 Polychrom. All the modules are piloted with a PC computer with the Varian Star 5.3 software for liquid chromatography. A reverse phase Spherisorb silica column ODS-2 and acetonitrile/water as mobile phase are used to run the chromatography in gradient mode. The signals for IP, MB, and *p*-NTS are detected at 254, 246, and 275 nm respectively.

3.2.3.4 Biological Oxygen Demand (BOD)

The BOD measures the oxygen required for the biochemical degradation of organic material. This analysis is made by means of a Hg free WTW 2000 Oxytop unit thermostated at 20^{o}C. The pH of the samples are adjusted between 6.8 and 7.5 followed by addition (20% v/v) of decanted sludge (inoculum) from the biological plant of Vidy, Lausanne, Switzerland and of nutrients substances (solutions A, B, and C) and trace elements necessary for the bacterial activity.

Solution A: $FeCl_3.6H_2O$ (0.5 g), HCl 1N (1 ml) in 100 ml of distilled water.

Solution B: $MgSO_4.7H_2O$ (2.0 g), $CaCl_2$ (2.5 g), NH_4Cl (quantity depending of carbon concentration to degrade to have always a ratio C/N of 20) in 500 ml of distilled water.

Solution C: Na_2HPO_4 (6.8 g), KH_2PO_4 (2.8 g) in 1000 ml of distilled water.

Solution A+B: 50 ml of solution A, 500 ml solution B in 1000 ml of distilled water.

Solution trace elements: $FeSO_4.7H_2O$ (200 mg), $ZnSO_4.7H_2O$ (10 mg), $MnCl_2.4H_2O$ (3 mg), H_3BO_3 (30 mg), $CoCl_2.6H_2O$ (20 mg), $CuCl_2.2H_2O$ (1 mg), $NiCl_2.6H_2O$ (2 mg), $Na_2MoO_4.2H_2O$ (3 mg), in 1000 ml of distilled water.

For each BOD determination, 20 ml $l^{-1}$of solution A+B, 50 ml l^{-1} of C and 2 ml $l^{-1}$of trace elements are added for 400 mg C of the test solution. The BOD values are calculated according to Equation 3.1.

$$BOD = \frac{BOD_{sample} - 0.01(\%inoculum \times BOD_{inoculum})}{0.01 \times (100 - \%inoculum)} \quad \textbf{(Eq. 3.1)}$$

3.2.3.5 Zahn-Wellens biodegradability test

The Zahn-Wellens test was adapted in 1981 as OECD Guideline 302 B for determining inherent biodegradability [22]. A mixture containing the test substance, mineral nutrients (the same as for BOD determination), and a relatively large amount of activated sludge in aqueous medium is agitated and aerated at 20-25^{o}C in the dark or in diffuse light for up to 28 days. Blank controls, containing activated sludge and mineral nutrients but no test substance, are run in parallel. The biodegradation process is monitored by determination of DOC and by HPLC analysis of the test substance. The Zahn-Wellens Biodegradability test is applied with bacterial concentration of 1 g l^{-1}. The biomass from the biological activated sludge plant of Vidy, Lausanne, Switzerland, is previously aerated for 24 hours and subsequently centrifuged.

3.2.3.6 Microtox® rapid toxicity testing system

During the photochemical pretreatment, the toxicity is assessed using the Microtox® test system. The basic technology of this system is based upon the use of luminescent bacteria, specifically the strain *Vibrio fischeri* NRRL B-11177, to measure toxicity from environmental samples. When properly grown, luminescent bacteria produce light as a by-product of their cellular respiration. Cell respiration is fundamental to cellular metabolism and all associated life processes. Bacterial bioluminescence is tied directly to cell respiration, and any inhibition of cellular activity (toxicity) results in a decreased rate of respiration and a corresponding decrease in the rate of luminescence.

The tests are carried out using a Microtox Model 500 Analyzer, which is a laboratory-based temperature controlled photometer (15-27^{o}C) that maintains the luminescent bacteria

reagent and test samples at the appropriate test temperature. This self-calibrating instrument measures the light production from the luminescent bacteria reagent. The sample toxicity is determined by measuring the effective concentration at which 50% of the light is lost due to compound toxicity (EC_{50}).

3.2.3.7 Hydrogen peroxide analysis

Concentrations of H_2O_2 are determined by the Merk Merckoquant® peroxide analytical test strips and by permanganate titration. The latter method utilizes the reduction of potassium permanganate ($KMnO_4$) by hydrogen peroxide in sulfuric acid (see also: http://www.h2o2.com/intro/highrange.html).

3.3 Results and discussions

3.3.1 Biodegradability of metobromuron, isoproturon, and *p*-NTS initial solutions

The Zahn-Wellens biodegradability test shows that none of the herbicides can be biologically degraded, since the DOC of the solutions remains at its initial level (Figure 3.2). This test is carried out under similar conditions to those of a wastewater treatment plant using activated sludge. The DOC concentration does not change for these herbicides, even when continuing the test during a long period, which indicates that bacteria can not be adapted to degrade them. A parallel control experiment using diethylenglycol (0,5 g l^{-1}), is carried out to test if the sludge was otherwise active. Diethylenglycol is in fact degraded as much as 98% in 6 days.

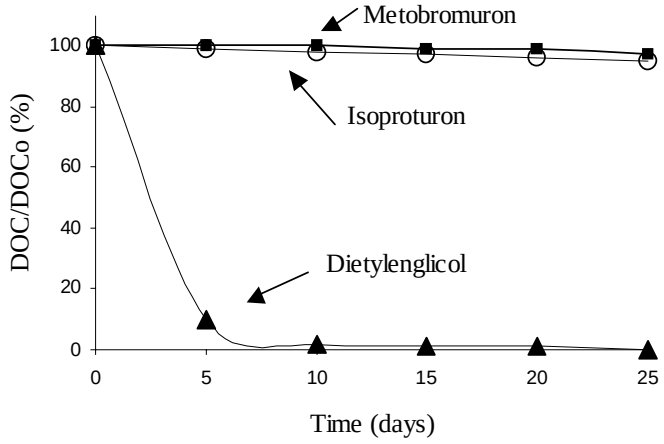

FIGURE 3.2 *Zahn-Wellens biodegradability test of MB and IP. Evolution of DOC as a function of time.*

A supplementary test to measure the biodegradation of the herbicides was carried out in batch mode with a FBR (section 3.2.2.3). Even under theoretically favourable conditions as presence of co-substrates and adapted bacteria, as well as a strict control of pH, temperature, and aeration, this test confirms that both herbicides are non-biodegradable in the tested conditions. The herbicide and the DOC concentration were measured during the test without any changes for any bacterial activity.

The non-biodegradability of *p*-NTS has also been proved. The same Zahn-Wellens biodegradability test was applied and the results are showed in Figure 3.3. As in the case of the herbicides, this test is carried out under conditions similar to those of a wastewater treatment plant using activated sludge. Two types of inoculum are tested. Samples 1 and 2 contain activated sludge from a wastewater treatment plant (Vidy, Lausanne, Switzerland). Sample 3 contains activated sludge, which had previously been in contact with *p*-NTS during 35 days. Two concentrations are tested in order to know if a toxicity effect is present. Sample 4 is a control experiment using diethylenglycol (0,5 g l^{-1}) to test the activity of the activated sludge. In fact, the diethylenglycol is degraded up to 98% in 6 days under the same conditions used to test the biodegradability of the *p*-NTS.

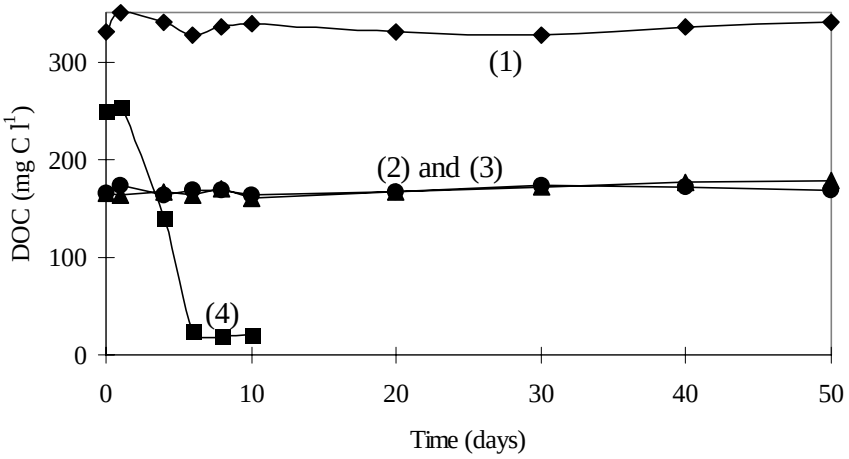

FIGURE 3.3 *Zahn-Wellens biodegradability test of p-NTS. Evolution of DOC as a function of time: (1) non-adapted biomass; (2) non-adapted biomass and lower concentration of p-NTS; (3) adapted biomass; (4) control with diethylenglycol.*

To conclude this biodegradability study, a large number of supplementary experiments attempting biodegradation of *p*-NTS are carried out in batch mode with the FBR. In this biological reactor, urban and industrial activated sludge are used in different aerobic culture media. The results summarised in Table 3.1 show no-biodegradation of *p*-NTS under several theoretically favourable conditions. Three methods are used to follow the test: (a) respirometric measurements with an O_2 probe in the inlet and outlet of the FBR, (b) determination of *p*-NTS concentration by HPLC, and (c) measurements of DOC as a function of time.

TABLE 3.1 *Attempts of biodegradation of a p-NTS solution in a fixed bed biological reactor.*

Test	Media used	Biodegradation
1	Standard nutrient, *p*-NTS as the sole source of carbon	Negative
2	Standard nutrient, glucose added as co-substrate	Negative
3	Standard nutrient, yeast extract added as co-substrate	Negative
4	Standard nutrient, *p*-NTS as the sole source of nitrogen	Negative
5	Standard nutrient as in 4, but glucose added as co-substrate	Negative

TABLE 3.1 *(Continued)... Attempts of biodegradation of a p-NTS solution in a fixed bed biological reactor.*

Test	Media used	Biodegradation
6	Standard nutrient, *p*-NTS as the sole source of sulphur	Negative
7	Standard nutrient as in 6, but glucose added as co-substrate	Negative
8	Sewage bacteria only, with the standard nutrient without a carbon source	Control
9	Standard nutrient, *p*-NTS with glucose as the source of carbon. The concentration of *p*-NTS was progressively increased in order to attempt the adaptation of bacteria	Negative

3.3.2 Photochemical-biological flow system for *p*-nitro-*o*-toluenesulfonic acid treatment

The photochemical-biological coupled flow system, using the coiled reactor, is employed to mineralize a *p*-NTS solution. The efficiency of the photo-Fenton process is first studied in continuous and batch operation modes. Afterwards, the functioning of the coupled reactor is compared in two operation modes (continuous and semi-continuous) studying the efficiency of the photochemical, biological, and overall treatments.

3.3.2.1 Continuous *versus* batch photo-Fenton process

3.3.2.1.1 Continuous mode

The coiled photoreactor shown in Figure 3.1 was first operated in continuous mode to attempt the mineralisation of *p*-NTS solutions. Figure 3.4 shows the DOC of the water going out of the photoreactor (into conditioning recipient) as a function of time when the system is operated at different feeding flow rates: 0.90, 0.60, 0.18, and 0.06 l h^{-1} (or 15, 10, 3 and 1 ml min^{-1}). The *p*-NTS input concentration is in all cases, of 1 g l^{-1} (330 mg C l^{-1}). The *p*-NTS solution is simultaneously recirculated at 22 l h^{-1} through the 0,4 l illuminated part of the photoreactor. The *p*-NTS photodegradation in this continuous mode starts when H_2O_2 (30%) is

added (1 ml every 10 minutes) to the mixing-vessel. The photodegradation is followed at least during 3 days after reaching the steady state and the photoreactor exhibits a very high stability.

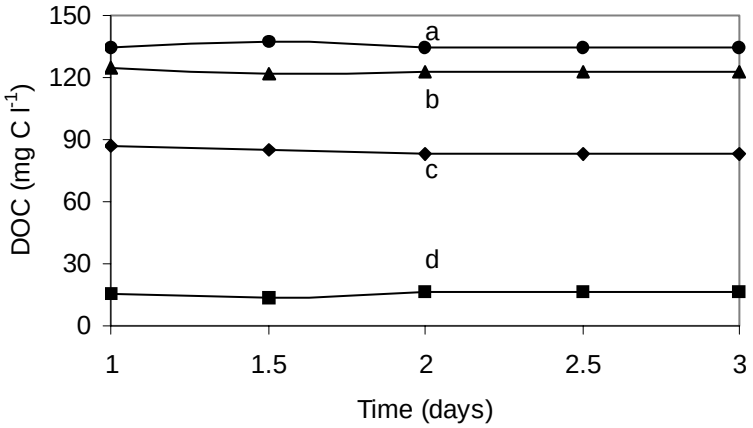

FIGURE 3.4 *DOC evolution as a function of time at different flow rates. The photoreactor is operated in continuous mode: (a) 0.90, (b) 0.60, (c) 0.18, and (d) 0.06 l h^{-1}. The input carbon and iron concentrations are of 330 and 75 mg l^{-1}, respectively. One ml of H_2O_2 (30%) is automatically added every 10 minutes.*

Table 3.2 summarises the characteristics and performance of the system at the four mentioned flow rates for the degradation of a *p*-NTS solution. The primary degradation efficiency expressed as % of removed *p*-NTS (followed by HPLC analysis) is of 100% for all tested flow rates. In contrast, ultimate degradation efficiencies (mineralisation followed by DOC analysis) are very different: 59, 63, 74 and 95% for 0.9, 0.6, 0.18 and 0.06 l h^{-1}, respectively. Table 3.2 shows that both DOC degradation and flow rates decrease while the residence time, the energy consumption, and the subsequent phototreatment cost, increase. The energy consumption values are calculated knowing that the light source is a 400 W lamp (energy consumption = 0.4 kW x t_r / 0.4 l). These values are useful only for comparisons purposes and can not be used to calculate the real energy consumption for industrial photochemical processes because commercial lamps used in those cases are far more efficient than the lamp used in this study.

TABLE 3.2 *Performance of the coiled photochemical reactor operated in continuous mode at four different flow rates for degradation of a p-NTS solution (330 mg C l^{-1}).*

	Flow rate (l h^{-1})			
	0.9	0.6	0.18	0.06
Dilution rate, D (h^{-1})	2.25	1.5	0.45	0.15
Residence time, t_r (h)	0.44	0.67	2.22	6.67
Input concentration (mg C l^{-1})	330	330	330	330
Output concentration (mg C l^{-1})	136	124	85	15
Removed *p*-NTS (%)	100	100	100	100
Removed DOC (%)	59	63	74	95
DOC degradation rate (mg C h^{-1})	175	124	44	19
Specific DOC degradation rate (mg C $h^{-1}l^{-1}$)	434	310	110	47
Energy consumption using a 0.4 kW lamp (kW h l^{-1})	0.44	0.67	2.22	6.67
Normalized energy consumption (%)	6.7	10	33.3	100

Figure 3.5 shows the energy consumption as a function of DOC removed at different flow rates. Decreasing the flow rate from 0.90 to 0.18 l h^{-1} does not meaningfully enhance the mineralisation efficiency (from 59 to 74%). The energy required to eliminate the additional 36% of DOC (with respect to the 59% removed at 0.9 l h^{-1}) is dramatically increased representing 90% of the total energy required to mineralise 95% of the DOC. The quasi-total mineralisation of the *p*-NTS solution is attained only at a very low flow rate (0.06 l h^{-1}), which implies a long residence time (6.67 h) and a high energy consumption (6.67 kW h l^{-1}).

From the observations presented above, one can conclude that the intermediates formed during the initial stage of the photo-Fenton treatment are very photorecalcitrant and that the decrease of the flow rate (or the increase of the retention time) is not a cost-efficient strategy to reach mineralisation of *p*-NTS solution in a continuous flow photoreactor.

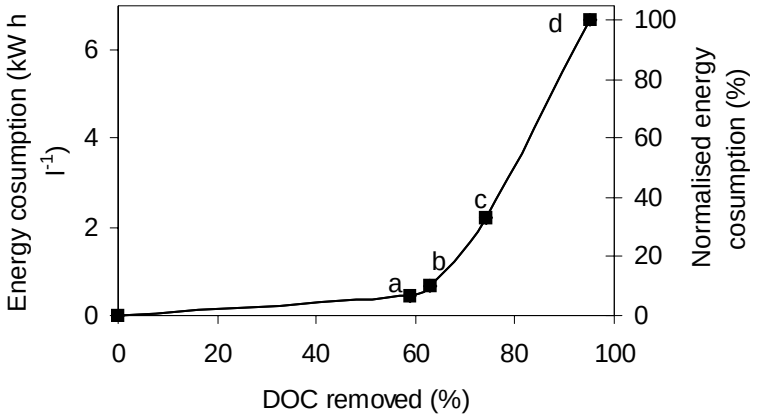

FIGURE 3.5 *Energy consumption in kW h l^{-1} for the treatment of a p-NTS solution as a function of DOC removed. at different flow rates: (a) 0.90, (b) 0.60, (c) 0.18, and (d) 0.06 l h^{-1}. Right-side axis shows the normalised energy consumption with 6.67 kW h l^{-1} corresponding to 100%.*

3.3.2.1.2 Batch Mode

The coiled photoreactor shown in Figure 3.1 was also operated in batch mode to attempt the mineralization of a *p*-NTS solution via photo-Fenton reaction. The *p*-NTS solution (1 g p-NTS l^{-1}) is recirculated from the mixing-vessel into the reactor at 22 l h^{-1}. Hydrogen peroxide (300 µl, 30%) is added every 5 minutes and different Fe^{3+} concentrations were tested.

Figure 3.6 shows that the best degradation rate was obtained with a Fe^{3+} concentration of 75 mg l^{-1}. This concentration was selected to continue the phototreatment up to 220 min, as shown in Figure 3.7, to reach almost total mineralization of the *p*-NTS solution. In this case, the residence time (t_r) in the illuminated part of the photoreactor is 1.22 hours, which is obtained by Equation 3.2.

$$t_r = V_i \times t / V_t \qquad \textbf{(EQ. 3.2)}$$

In Equation 3.2, V_t is the total volume of the *p*-NTS solution (1.2 l), t is the time necessary for its mineralization (220 min = 3.66 h), and Vi is the volume exposed to light into the photoreactor (0.4 l). .

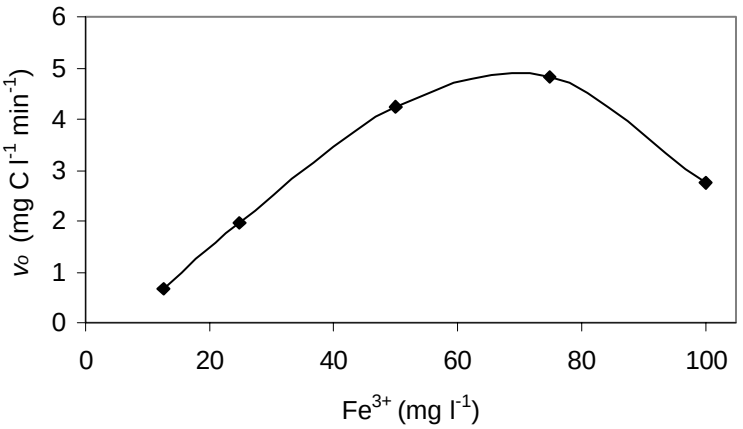

FIGURE 3.6 *Photo-Fenton batch degradation of a p-NTS solution at different Fe^{3+} concentrations.*
Hydrogen peroxide (300 µl, 30%) is added every 5 minutes.

This system mineralises 1.2 l of the *p*-NTS solution (containing 400 mg of DOC) in 3.66 h that corresponds to a degradation rate of approximately 0.33 l h^{-1} or 109 mg C h^{-1}. Since the illuminated part of the reactor has a volume of 0.4 l, the specific degradation rate attained is 0.82 l h^{-1} (273 mg C l^{-1}) per litre of photoreactor. In this batch mode, the energy required for the total mineralization is of about 1.22 kW h l^{-1} while using the continuous mode discussed above, it is 6.67 kW h l^{-1}. The treatment time, the energy consumption, and consequently the cost of the phototreatment, increases in 5.4 times in continuous compared to, batch mode (see Table 3.2). From the economical point of view, the batch operation mode seems to be more attractive than the continuous one, however, the complete mineralization obtained by this way is still too expensive and is not a convenient strategy.

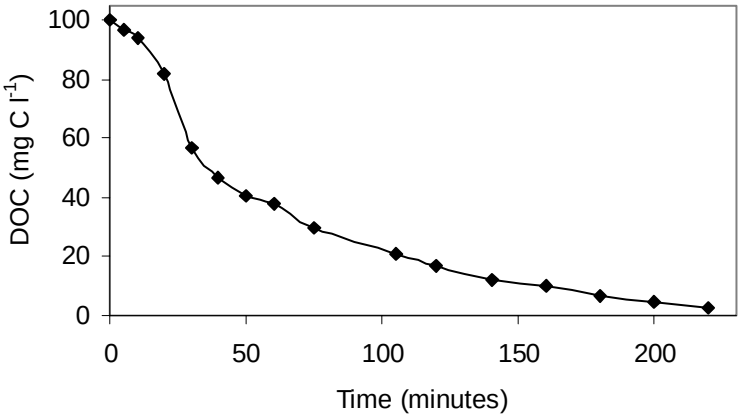

FIGURE 3.7 *DOC evolution during the photo-Fenton treatment of a p-NTS solution.*

3.3.2.2 Chemical and biological characteristics of the phototreated *p*-NTS solution

To ensure that the photochemical process can be used as a pre-treatment for a biological process, it is very important to gather information concerning the chemical nature of the intermediates formed during the photo-pre-treatment, and so is the following of the toxicity and biodegradability evolution. Figure 3.8 shows the evolution of these parameters for *p*-NTS degradation in batch mode in the presence of H_2O_2 (300 μl each 5 minutes) and Fe^{3+} (75 mg l^{-1}).

Figure 3.8a shows that before 5 min of photochemical treatment the initial *p*-NTS disappears from the solution. Scanning by a diode array detector revealed the presence of aromatic and aliphatic degradation by-products that could not be identified against commercial standards. The single aromatic intermediate detected attained a maximum concentration within 5 minutes and was totally degraded within 20 minutes.

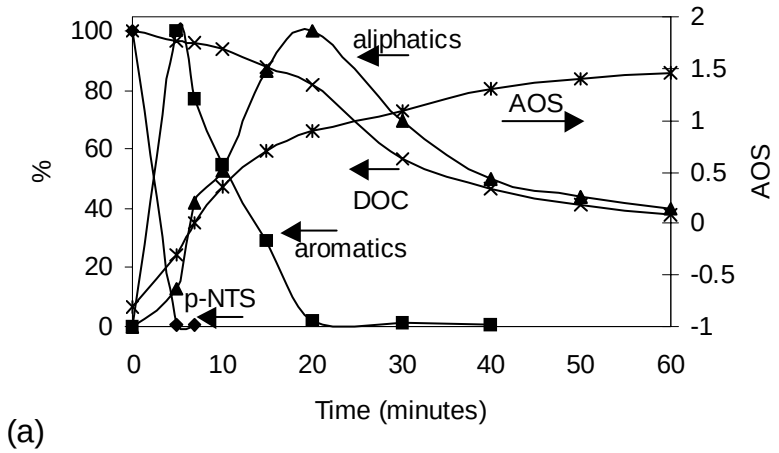

(a)

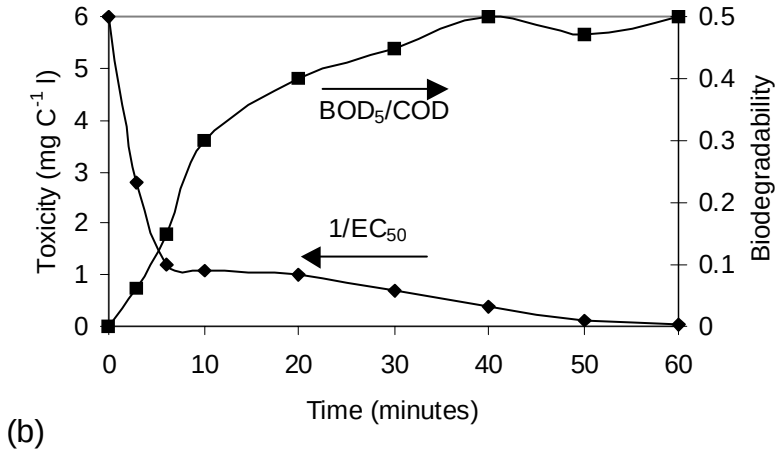

(b)

FIGURE 3.8 *Phototreatment of a p-NTS solution by Fenton reaction. (a) relative concentration of p-NTS, aliphatics, and aromatics intermediates. p-NTS (330 mg C l^{-1}), H_2O_2 (300 μl every 5 minutes), and Fe^{3+} (75 mg l^{-1}). The AOS evolution is shown using the left hand side axis. (b) Evolution of toxicity and biodegradability of the phototreated solution of p-NTS as a function of time.*

The Average Oxidation State (AOS) of the solution is shown at the right hand side axis of Figure 3.8a as a function of the photo-pre-treatment time. These values were estimated according to the following Equation [6]:

$$AOS = \frac{4(DOC - COD)}{DOC}, \qquad \textbf{(EQ. 3.3)}$$

where DOC and COD are respectively expressed in moles of C l^{-1} and moles of O_2 l^{-1}. Average oxidation state takes values between +4 for CO_2, the most oxidised state of C and -4 for CH_4, the most reduced state of C. In Figure 3.8a a plateau is observed for this parameter after 20 min of photo-treatment, suggesting that the chemical nature of intermediates does not vary significantly after 20 min of reaction. Furthermore, the AOS value at the plateau after 50 minutes (average 1.5) is characteristic of very oxidised and biocompatible aliphatic compounds like oxalic acid.

Chemical features described above are validated by the concomitant decrease of the toxicity and increase of biodegradability of the photo-treated *p*-NTS solution. As shown in Figure 3.8b, the reduction of toxicity reflects the abatement of *p*-NTS in 6 min. A slower decrease was subsequently observed until complete disappearance of toxicity (50 min). The *p*-NTS toxicity can be considered as weak given its EC_{50} value, however toxicity evolution was followed in this study to know the toxicity of the formed intermediates during the photo-treatment. The results show that intermediates more toxic than *p*-NTS did not develop during the photo-assisted pre-treatment process.

The most undesirable property of the *p*-NTS is its recalcitrance to biodegradation leading to potential chronic effects in natural environment. The beneficial effect of a short photo-treatment, on the *p*-NTS solution biodegradability is shown in Figure 3.8b. After 20 minutes (20% of mineralization) of phototreatment, the BOD_5/COD ratio, representative of biodegradability, surpasses the value 0.4, which is the threshold for a wastewater to be considered easily biodegradable.

3.3.2.3 Mineralization with the coupled reactor

If the photochemical treatment is stopped when 60% of the initial DOC value has been removed, the energy consumption and cost of the photoprocess is dramatically reduced. This is the case for both, continuous and batch operation modes. In batch mode, the energy consumption is 0.28 kW h l^{-1} which represents 23% of the energy required for total mineralization (1.22 kW h l^{-1}). In continuous mode, the energy required to remove 60% of DOC

is 0.44 kW h l^{-1} representing 6.5% of the 6.67 kW h l^{-1} required for total mineralization (Figure 3.5 and Table 3.2).

The sole way to render photo-Fenton treatment economically attractive for the complete mineralization of non-biodegradable and/or toxic compounds like *p*-NTS is to apply the photochemical reaction as a pretreatment preceding the biological treatment. The pretreatment to modify the chemical structure of the biorecalcitrant *p*-NTS should be short enough and efficient to render a cost-effective process. In this sense, the chemical and biological characteristics of phototreated solutions studied allow the determination of the earliest moment when the photochemical pretreatment (expensive) reduces the antiphysiological properties of *p*-NTS. This would permit the transfer of phototreated water to a biological treatment (low cost).

3.3.2.3.1 Coupled reactor in continuous mode

The coupled reactor shown in Figure 3.1 is operated in continuous flow mode searching for the best conditions leading to good performance of both photochemical and biological reactors. A molar H_2O_2/DOC ratio between 15 and 30 is considered optimal for the photo-Fenton process. Unfortunately, H_2O_2 is known to induce detrimental physiological effects on bacteria and therefore, at high concentrations, it affects the performance of the biological reactor [13].

In the coupled reactor, the feeding solution containing 330 mg C l^{-1} (1 g $l^{-1}$of *p*-NTS) and 75 mg l^{-1} of Fe^{3+} was introduced from the feeding tank (named wastewater in Figure 3.1) to the mixing vessel. The mixing vessel also received 1 ml of H_2O_2 every 10 minutes (6 ml h^{-1}) in order to maintain a favourable H_2O_2/DOC ratio in the photoreactor. The solution was continually recirculated at 22 l h^{-1} through the illuminated part of the reactor. In the conditioning recipient the pH was neutralised, going from average 3 (optimal to Fenton reaction) to 7 (optimal to biological work) by means of NaOH solution. After this, the pretreated solution was brought to the bottom of the FBR previously colonised by activated sludge from the aerobic municipal treatment plant of Vidy, Lausanne, Switzerland.

Table 3.3 shows the results obtained when the coupled photochemical-biological reactor is operated in continuous mode at feeding flow rates of 0.60 and 0.18 l h^{-1}. At 0.60 l h^{-1} (residence time of 0.67 h), the DOC removal efficiencies of the photochemical and biological processes are 53 and 29%, respectively. The removed carbon in the biological step is low, which could be explained either because the intermediates formed during the photochemical step are still structurally similar to *p*-NTS and thus non-biodegradable or because the residual concentration of H_2O_2 induces an inhibitory effect on the bacterial consortium in the biological reactor.

In order to eliminate the biorecalcitrant intermediates possibly formed, the residence time of the solution in the photoreactor was increased from 0.67 to 2.2 h by changing the flow rate to 0.18 l h^{-1}. Under these conditions, the DOC removal efficiency of the biological step is increased but still low, leading to the conclusion that the residual H_2O_2 is responsible for the poor performance of the biological treatment.

In continuous mode, the inertia of the system renders difficult the regulation of the residual H_2O_2 concentration and consequently, the phototreated solutions arriving to the biological part of the coupled system contain high H_2O_2 amounts. In order to maintain a good H_2O_2/DOC ratio and consequently, a good performance of the photochemical step, the initial H_2O_2 concentration should not be reduced. However, trying to improve the overall efficiency of the coupled system, the H_2O_2 addition was diminished from 6 ml h^{-1} to 0.6 ml h^{-1} and the flow rate was changed to 0.12 l h^{-1} obtaining a phototreated solution with a residual H_2O_2 concentration lower than 10 mg l^{-1}, which is tolerated by bacteria. As shown in Table 3.3, the photochemical efficiency diminishes while the biological DOC degradation efficiency notably increases. The overall efficiency of the coupled reactor under the latter conditions is high (91%), but given the long required residence time in the photochemical reactor, this coupled system is not convenient from an economical point of view.

Since the photochemical treatment is more efficient in batch mode than in continuous mode (section 3.3.2.1.), a last attempt of coupling the photochemical and biological processes is done applying the photochemical treatment in batch mode.

TABLE 3.3 *Performances for p-NTS degradation by the coupled photochemical (coiled) - biological reactor in continuous mode at three different flow rates.*

	Photochemical treatment			**Biological treatment**			**Coupled treatment**		
	Input flow rate $l\ h^{-1}$			Input flow rate $l\ h^{-1}$			Input flow rate $l\ h^{-1}$		
	0.60[a]	0.18[a]	0.12[b]	0.60[a]	0.18[a]	0.12[b]	0.60[a]	0.18[a]	0.12[b]
Residence time, tr (h)	0.67	2.22	3.33	1.67	5.55	8.3			
Input concentration (mg C l^{-1})	330	330	330	155	110	135	330	330	330
Output concentration (mg C l^{-1})	155	110	135	110	60	30	110	60	30
Removed p-NTS (%)	100	100	100				100	100	100
Removed DOC (%)	53	67	59	29	45	78	67	82	91

[a]Addition of 6 ml h^{-1} of H_2O_2 at the inlet of the photochemical reactor.
[b]Addition of 0.6 ml h^{-1} of H_2O_2 at the inlet of the photochemical reactor.

3.3.2.3.2 Coupled reactor in semi-continuous mode

The coupled reactor operates in semi-continuous mode when the photochemical step treats the *p*-NTS solution in short-duration batch cycles providing phototreated water to continuously feed the biological reactor. The photochemical reactor is operated under the conditions described in section 3.3.2.1.2. Up to now, the two main parameter affecting the performance of the photo-assisted reactor in continuous mode are related to the very low pollutant concentration that characterise this kind of operation mode and to the high residual H_2O_2 concentration after the pretreatment. The operation of the system in semi-continuous mode allows to overcome this inconvenience.

As indicated in section 3.3.2.2, the *p*-NTS solution becomes biocompatible after 30 minutes of phototreatment in batch mode when the *p*-NTS is completely degraded and the average oxidation state of the intermediates does not change any longer. In this sense, the coupled system can be better used to attain the total mineralization of the solution since the high

energy consumption required to reach good levels of mineralization with single photochemical reactor makes it not attractive from an economical point of view.

The coupled photochemical-biological reactor is operated at five different phototreatment times: 50, 70, 95, 110, and 125 min (corresponding respectively to the following flow rates: 0.96, 0.68, 0.50, 0.44, and 0.38 l h^{-1}). Even though the phototreated solution becomes biocompatible at 30 minutes, the phototreatment time in these experiments are higher looking for low enough residual H_2O_2 concentrations to avoid bacterial inhibition.

The *p*-NTS solution (800 ml) is phototreated in a classical batch mode, as explained before, and when the chosen time is attained, the solution passes to the conditioning recipient, where it is neutralised by addition of NaOH. The phototreated water is then led to the biological reactor in a classical continuous mode.

Table 3.4 summarises the performance of the coupled system and Figure 3.9 shows the energy consumption and the percentage of DOC removed in the photochemical, the biological, and the whole coupled process as a function of phototreatment time.

TABLE 3.4 *Performances for p-NTS degradation by the coupled photochemical (coiled) - biological reactor in semi-continuous mode at five different flow rates.*

	Photochemical treatment					**Biological treatment**				
	Input flow rate l h^{-1}					Input flow rate l h^{-1}				
	0.96	0.68	0.50	0.44	0.38	0.96	0.68	0.50	0.44	0.38
Treatment time (min)	50	70	95	110	125					
Dilution rate, D (h^{-1})	2.4	1.7	1.25	1.1	0.95	0.96	0.68	0.50	0.44	0.38
Residence time, tr (h)	0.42	0.59	0.80	0.91	1.05	1.04	1.47	2.00	2.27	2.63
Input concentration (mg C l^{-1})	330	330	330	330	330	200	136	100	80	76
Output concentration (mg C l^{-1})	200	136	100	80	76	78	28	24	19	17
Removed p-NTS (%)	100	100	100	100	100					
Removed DOC (%)	40	59	70	76	77	61	80	76	76	77

TABLE 3.4 *(Continued)... Performances for p-NTS degradation by the coupled photochemical (coiled) - biological reactor in semi-continuous mode at five different flow rates.*

	Photochemical treatment					Biological treatment				
DOC degradation rate (mg C h^{-1})	125	132	115	110	96	141	64	24	12	11
Specific DOC degradation rate (mg C h^{-1} l^{-1})	312	330	288	275	240	141	64	24	12	11
Energy consumption using a 0.4 W lamp (Kw h l^{-1})	0.42	0.59	0.80	0.91	1.05					

	Coupled treatment				
	Input flow rate l h^{-1}				
	0.96	0.68	0.50	0.44	0.38
Input concentration (mg C l^{-1})	330	330	330	330	330
Output concentration (mg C l^{-1})	78	28	24	19	17
Overall efficiency (removed DOC, %)	76	92	93	94	95

From results presented in Table 3.4 and Figure 3.9, it can be concluded that the most suitable conditions for the coupled treatment are obtained when the phototreatment time is short enough to achieve a cost-effective process together with high biological and overall efficiencies. However, if the pretreatment time is too short (e.g., 50 minutes), the intermediates formed during the photochemical step are still structurally similar to *p*-NTS and thus non-biodegradable and maybe a high residual H_2O_2 concentration remains in the phototreated solution affecting the performance of the biological reactor and consequently, the overall efficiency of the coupled system. At 70 minutes, the residual H_2O_2 becomes tolerated by bacteria (i.e., is lower than 10 mg l^{-1}), which is reflected in an increased biological DOC removal efficiency. At longer phototreatment times, the photochemical efficiency is improved by the unnecessary photodegradation of substances biologically degradable while the biological and the overall efficiencies remain almost invariable, which implies higher energy consumption without beneficial effects. In this sense, the optimal time to stop the photochemical treatment before leading the treated water to the biological reactor was found to be 70 minutes.

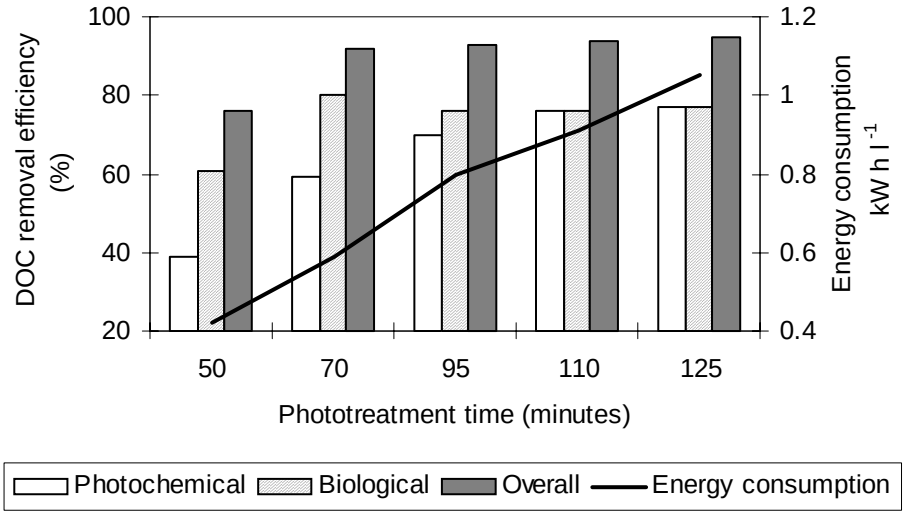

FIGURE 3.9 *DOC remotion by photochemical, biological, and coupled (overall) treatment of p-NTS.*
The consumed energy for the photochemical step is represented on the right-side axis.

3.3.3 Photochemical-biological flow system for metobromuron and isoproturon herbicides treatment

A coupled photochemical-biological flow reactor, operating in semi-continuous mode, is used to attain the complete mineralization of the IP solution. Concentrations of Fe^{3+} and H_2O_2 are optimized to obtain the best MB and IP degradation efficiencies *via* photo-Fenton reaction. The biocompatibility of the treated solutions is then determined as a function of the phototreatment time.

3.3.3.1 Optimal photodegradation conditions

Herbicides degradation rate constant (k) is determined and evaluated at different Fe^{3+} and H_2O_2 concentrations to find out the values at which maximum efficiency (k_{max}) is obtained.

In all the following experiments the transformation of herbicides is described assuming a pseudo-first order reaction. Then, an approximation of a Langmuir-Hinsheldwood expression can be used:

$$-\frac{d(DOC)}{dt} = k(DOC) \qquad \textbf{(EQ. 3.4)}$$

where k is the pseudo-first order reaction rate constant. Integration of Equation 3.4 leads to:

$$\frac{\ln(DOC)}{DOC_o} = -kt \qquad \textbf{(EQ. 3.5)}$$

From where the slope of the plot $\ln(DOC)/(DOC_o)$ vs. *t* (time of irradiation) renders the reaction rate constant (k).

3.3.3.1.1 Effect of the iron salt concentration

Figure 3.10 shows a plot of k as a function of the catalyst concentration. Keeping a fixed $[H_2O_2]$, the optimal Fe^{3+} concentration is found to be 1.0 mmol l^{-1} for the photodegradation of MB ($[MB]_0$ 0.93 mmol l^{-1}) and IP ($[IP]_0$ 0.21 mmol l^{-1}). The Fe^{3+}:substrate ratio is approximately 1:1 for MB and 1:5 for IP.

It can be observed that the efficiency of the degradation attains a plateau when the concentrations of Fe^{3+} are between 0.5 and 1 mmol l^{-1} while at higher concentrations the efficiency decreases. This may be due to: (a) The increase of a brown turbidity in the solutions during the phototreatment, which hinders the absorption of the UV light required for the photo-Fenton process. (b) Excessive formation of Fe^{2+} (Equations 3.6 and 3.7), which can compete with herbicides in solution for $^{\bullet}OH$ radicals (Equation 3.8). (c) The fixed H_2O_2 concentration, can become the limiting factor of the oxide-reductive reaction (Equation 3.7) when high concentrations of Fe^{3+} are used.

$$Fe^{3+} + h\upsilon \rightarrow Fe^{2+} + {}^{\bullet}OH \qquad \textbf{(EQ. 3.6)}$$

$$Fe^{3+} + H_2O_2 \rightarrow Fe^{2+} + HO_2^{\bullet} + H^+ \qquad \textbf{(EQ. 3.7)}$$

$$Fe^{2+} + {}^{\bullet}OH \rightarrow Fe^{3+} + {}^{-}OH \qquad \textbf{(EQ. 3.8)}$$

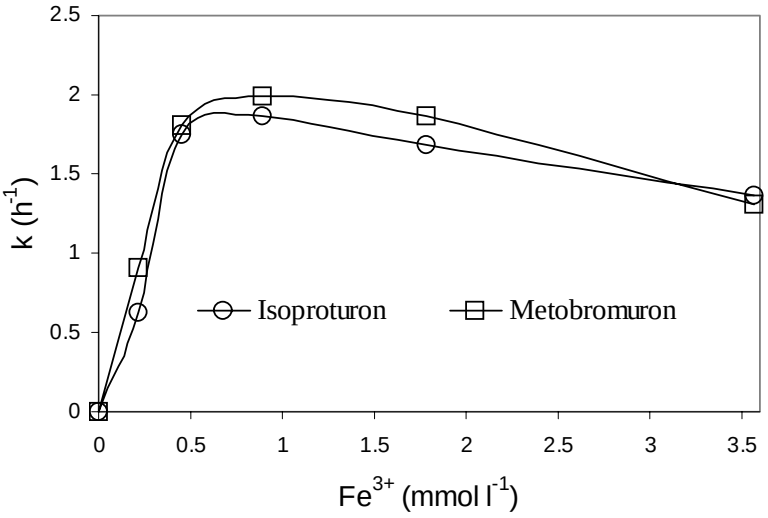

FIGURE 3.10 *Rate constant of IP and MB oxidation at different Fe^{3+} concentrations.*

3.3.3.1.2 Effect of hydrogen peroxide concentration

To further elucidate the role of H_2O_2 concentration on the photodegradation of these herbicides in the UV/H_2O_2/Fe^{3+} system, some experiments are carried out. As shown in Figure 3.11, a significant enhancement of degradation efficiency is demonstrated when H_2O_2 concentrations are increased from 0 to 25 mmol l^{-1}. Above this concentration, the rate of MB degradation is negatively affected by the progressive increase of H_2O_2. This is probably due to both, auto-decomposition of H_2O_2 into oxygen and water (Equation 3.9) and the recombination of $^{\bullet}OH$ (Equation 3.10) as follows:

$$2H_2O_2 \rightarrow 2H_2O + O_2 \qquad \textbf{(EQ. 3.9)}$$

$$OH + H_2O_2 \rightarrow HO_2^{\bullet} + H_2O \qquad \textbf{(EQ. 3.10)}$$

Excess of H_2O_2 will react with $^{\bullet}OH$ (Equation 3.10) competing with organic pollutants and consequently reducing the efficiency of the treatment. It is found that the optimal H_2O_2 concentration is 25 mmol l^{-1} for the degradation of both herbicides as shown in Figure 3.11.

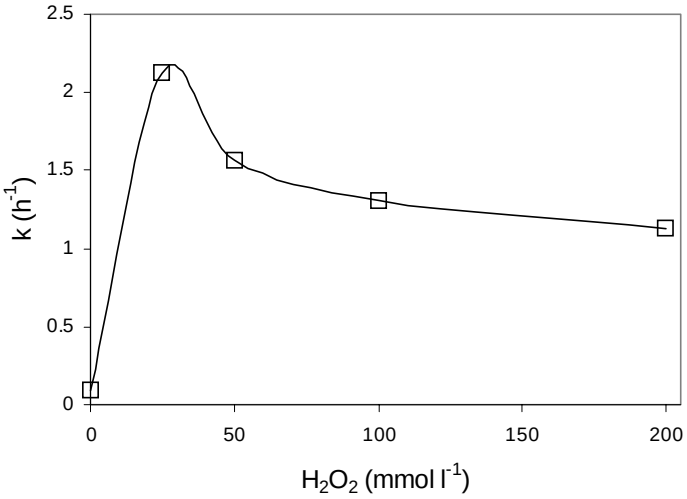

FIGURE 3.11 *Rate constant of MB oxidation at different H_2O_2 concentrations. Fe^{3+} concentration: 1.0 mmol l^{-1}.*

3.3.3.2 Chemical and biological characteristics of the phototreated solutions

As mentioned before, to ensure that the photochemical process can be used as a pretreatment for a biological process, it is very important to gather information concerning the chemical nature of the intermediates formed during the phototreatment, and so is the following of ions, toxicity, and biodegradability evolution. Figure 3.12 shows the evolution of these parameters for MB degradation in batch mode in the presence of H_2O_2 (25.0 mmol l^{-1}) and Fe^{3+} (1.0 mmol l^{-1}).

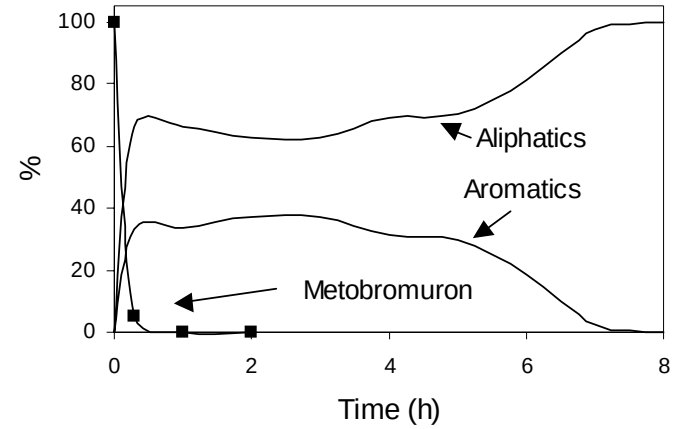

(a)

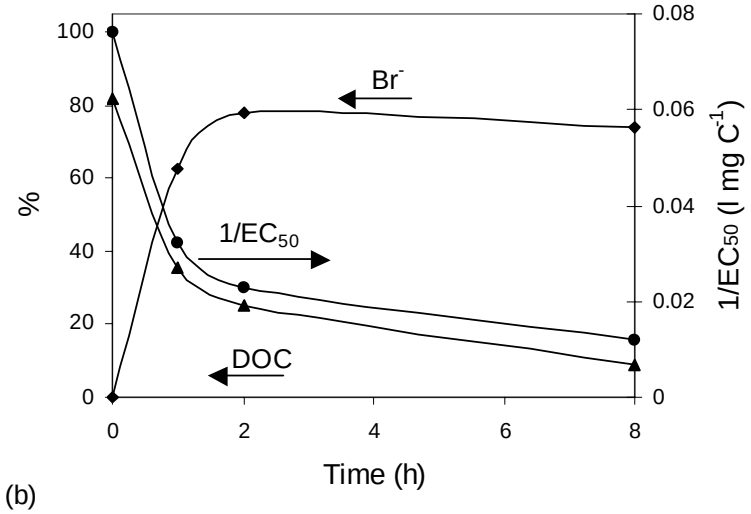

(b)

FIGURE 3.12 *Phototreatment of a MB solution using suspended TiO_2 catalyst. (a) Relative concentration of the initial compound, aromatic, and aliphatic intermediates. MB (0.93 mmol l^{-1}), 25 mmol l^{-1} of H_2O_2 and 1 mmol Fe^{3+}. (b) Evolution of DOC, Br^-, and toxicity (expressed as $1/EC_{50}$) during the same phototreatment as a function of time.*

Figure 3.12a shows the results obtained by HPLC analysis of MB degradation, where it can be seen that in less than 20 minutes of photochemical treatment the initial compound disappears from the solution. The scanning by a diode array detector revealed the existence of aromatic and aliphatic degradation by-products. The aromatic intermediates attained a

maximum concentration within 1 hour, remaining constant for about 6 hours after which it started to decay, coinciding with an increase of aliphatic intermediates. Analysis of Br^- in solution (Figure 3.12b) shows that approximately 80% of the bromo bound to organic carbon has been liberated after 1 hour and remains constant during the phototreatment. The Br^- evolution is consistent with the MB degradation, but its final concentration (~54.0 mg Br^- l^{-1}) does not correspond to the theoretical stoichiometric value (73.98). Thus, the degradation of MB should be leading to the formation of bromide intermediates, which are photo-recalcitrant in the tested conditions. The DOC evolution, indicates a very slow mineralization rate after 2 hours of treatment (Figure 3.12b).

A biocompatibility study (toxicity and biodegradability tests) shows that, the solution resulting from the MB photodegradation is not appropriate for a biological treatment. During the photodegradation, even if the toxicity (expressed as $1/EC_{50}$ in Figure 3.12b) is reduced together with the reduction of DOC, the ratio BOD_5/COD (representative of the biodegradability) does not vary significantly, having values of 0.0 and 0.1 before and after the treatment. As a reference, this parameter for municipal biodegradable wastewater is of around 0.4. The FBR (Fixed Bed Reactor) presented in section 3.2.2.3 is also used to evaluate the biodegradability of the solution resulting from the MB phototreatment with no biodegradation observed. From these results it can be conclude that, even if the bromo-aliphatic compounds remaining in the solution after 8 hours of phototreatment are non toxic, they remain highly bio-recalcitrant.

The same analyses are made for the IP degradation. In this case, the ratio BOD_5/COD was found to be 0.0 without phototreatment and it increases up to 0.65 after pretreatment. Figure 3.13 shows the results obtained by HPLC analysis as well as the evolution of NO_3^-, DOC, and toxicity.

A very high toxicity increase is observed at the beginning of the treatment, followed by a sharp decrease (Figure 3.13b). This indicates that at the beginning of the photo-assisted process there is formation of intermediates, which are more toxic than the initial compound. Toxicity evolution is related to the appearance and disappearance of intermediates. Figure 3.13a shows firstly that the occurrence of aliphatic intermediates goes together with the abatement of IP and secondly, that the aromatic compounds are rapidly degraded coinciding with the decrease of

toxicity. The NO_3^- ion (Figure 3.13b) reaches the stoichiometric value (25.8 mg $NO_3^- l^{-1}$, corresponding to 100% in the Figure.) in about 2 hours of treatment after which there will no be nitro-compounds in solution. The evolution of DOC shows that the mineralization is of about 90% after 8 hours of treatment.

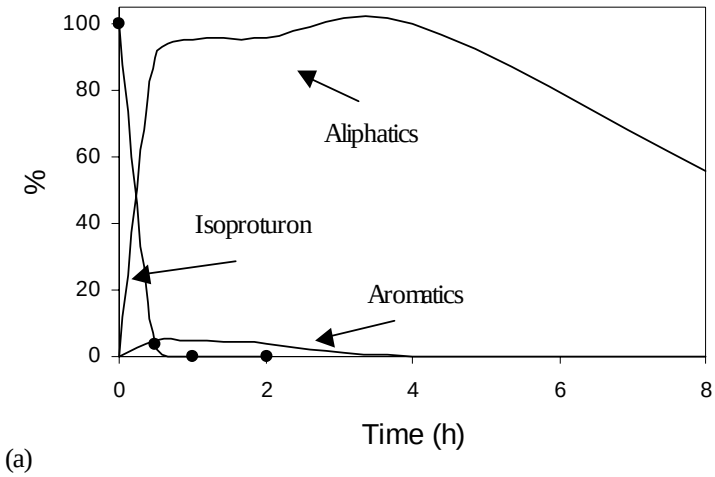

(a)

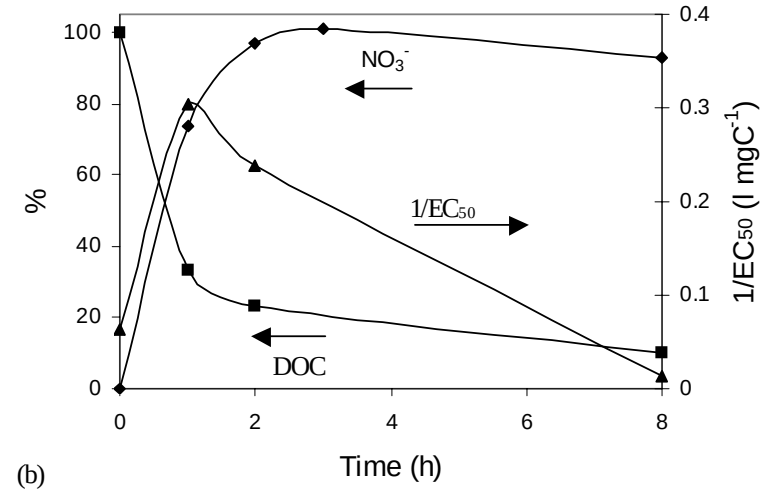

(b)

FIGURE 3.13 *Phototreatment of a IP solution using suspended TiO_2 catalyst.*
(a) Relative concentration of the initial compound, aromatic and aliphatic intermediates. IP (0.21 mmol l^{-1}), 25 mmol l^{-1} of H_2O_2, and 1 mmol Fe^{3+}.
(b) Evolution of DOC, NO_3^-, and toxicity (expressed as $1/EC_{50}$) during the same phototreatment as a function of time.

The chemical features described above, validated by the concomitant toxicity decrease and biodegradability increase of the treated IP solution, suggest that the photo-Fenton process is a promising pretreatment method. Therefore, a photochemical-biological coupled flow treatment can be applied for the complete mineralization of this compound.

3.3.3.3 Isoproturon mineralization by the coupled reactor in semi-continuous mode

The coupled system, using the coiled photoreactor described in section 3.2.2.1 was tested for the degradation of an IP solution (0.8 l). This herbicide was chosen because in contrast to MB, the biocompatibility of its photodegraded solution had been demonstrated. As in the case of *p*-NTS, the coupled system developed here is operated in semi-continuous mode using a photo-Fenton reaction as pretreatment.

During the phototreatment, the AOS of the treated solution was calculated and its evolution is shown in the Figure 3.14. The AOS was estimated according to Equation 3.3. As shown in Figure 3.14, the AOS attains a plateau after approximately 30 minutes of treatment reaching a value close to 2.

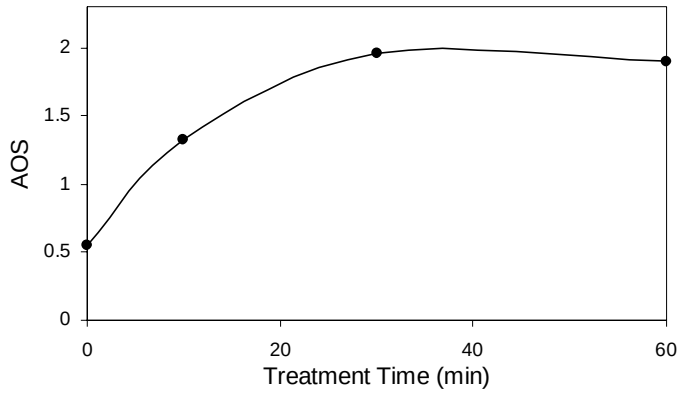

FIGURE 3.14 *Average Oxidation State evolution as a function of time for the photodegradation of IP.*

These results suggest that after 30 minutes of phototreatment the chemical nature of the intermediates does not vary any more. Biodegradability and toxicity tests performed during a photodegradation run in batch mode show that the resulting solution becomes biocompatible when the DOC gets constant (Figure 3.13b) and after the total depletion of H_2O_2. The DOC evolution in this batch system seems to be directly correlated with AOS evolution shown in Figure 3.14. Consequently, when the stabilization of these parameters is reached, the phototreated solution may be considered as biocompatible if only the chemical nature of intermediates is considered. The AOS stabilization is reached after 30 minutes of the phototreatment when between 50-65% of DOC is mineralized.

Unfortunately, at 30 minutes of phototreatment, a high residual H_2O_2 concentration is still present in the solution. In these conditions the phototreated water should not be fed to the biological stage. The fate of H_2O_2 concentration is monitored and it is found that after 60 minutes of treatment, the concentration of this oxidant becomes negligible (around of 0.5 mg l^{-1}). Consequently, the optimal time to stop the phototreatment before feeding the treated water to the biological reactor is 60 minutes. In addition, at this time the oxidation degree of the substances in solution reaches a value that is characteristic of very oxidized, hence, biocompatible compounds. In this stage of the treatment the pH of the solution is around 3.0 which is automatically neutralized with NaOH at the outlet of the photoreactor in order to prepare the solution for the biological treatment. During the biological process the pH is maintained between 6.5 and 7.5.

The evolution of the initial compound and its degradation intermediates is followed by HPLC during the whole degradation process. It is observed that at 30 minutes, the phototreatment depleted IP up to 97% producing aromatic and aliphatic by-products. After 60 minutes of phototreatment, the IP concentration is below HPLC quantification limits, while aromatic and aliphatic by-products are detected. After the biological process there are no substances detected by HPLC. The effective total solution mineralization is verified by the absence of carbonated substances (DOC measurements).

To start the coupled photochemical-biological flow process, sequential batches of the phototreatment were carried out every 60 minutes which corresponds to an input flow rate of

0.8 l h^{-1}. This flow rate was maintained during at least 3 days after reaching steady state to check-up the stability of the system during a long time period.

The photoreactor characteristics and the performance of the coupled system are summarised in Table 3.5. In this coupled system, 100% of the initial concentration of isoproturon and 95% of DOC were removed.

Table 3.5 suggests that the coupled process has a potential practical application. Putting the input flow rate (F_o) and the dilution rate (D) values in Equation 3.11 it is obtained a reasonable photoreactor volume (V) of 0.2 m^3, which can treat 10 m^3 of wastewater per day.

$$V = \frac{F_o}{D} = \frac{10 m^3}{2 h^{-1} \times 24 h} = 0.2 m^3 \qquad \textbf{(EQ. 3.11)}$$

TABLE 3.5 *Performances for IP degradation by the coupled photochemical (coiled) - biological reactor in semi-continuous mode.*

Parameter	**Photochemical coiled reactor**	**Biological reactor**
Volume of reactor (l)	0.4	1.0
Input flow rate (l h^{-1})	0.8	0.8
Dilution rate, D (h^{-1})	2.0	0.8
Residence time (h)	0.5	1.25
Input concentration (mg C l^{-1})	60.0	30.0
Output concentration (mg C l^{-1})	30.0	3.0
Isoproturon removed (%)	100.0	
DOC removed (%)	50.0	90.0
DOC degradation rate (mg C h^{-1})	24.0	22.0
Specific DOC degradation rate (mg C h^{-1} l^{-1})	60.0	22.0
Overall efficiency related to DOC degradation (%)	**95**	

3.3.4 Mineralization of isoproturon using supported TiO_2 for the photochemical stage

The advantages of using supported TiO_2 for the photochemical stage of the coupled process are that the catalyst can be reused, the pH of the solutions remains neutral, and H_2O_2 is not necessarily required for the reaction. In this way, the phototreated solution is ready to be biologically treated when it is biocompatible. This process is illustrated in the present section by mineralizing an IP solution. Supported TiO_2 activity and its catalytic durability are also studied.

3.3.4.1 Supported *versus* suspended TiO_2

Employing the coaxial reactor described in section 3.2.2.2, the photocatalytic degradation of IP with TiO_2 supported on glass rings is compared with the one using the catalyst suspended in solution. For this comparison, 0.2 g l^{-1} of TiO_2 in suspension is used which is equivalent to the amount of catalyst deposited on the ~3000 glass rings used to fill out the coaxial reactor treating 1.5 l of solution.

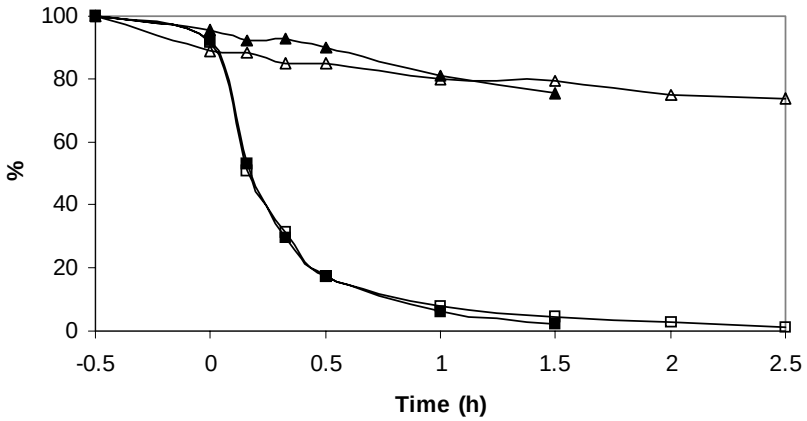

FIGURE 3.15 *Photocatalytic degradation of IP by supported (open points) and suspended (full points) TiO_2.*
Evolution of DOC (triangle points) and initial compound (square points).

As shown in Figure 3.15, the kinetic curves of IP degradation behave as a first order process. In both systems, the total elimination of IP is reached in approximately 120 minutes of phototreatment whereas the mineralization reached in the same time is only of about 20%. The degradation kinetics of IP and the DOC evolution in both supported and suspended TiO_2 systems are very similar. These results clearly indicate that the catalytic activity of the TiO_2 is not reduced when it is immobilized on the inert surface. In addition, supported photocatalyst is rather advantageous for systems under continuous flow, since usual recovering steps such as filtration and decantation can be avoided. Encouraging results are also obtained by Yeber, *et. al.* [20] using the same TiO_2 impregnated on glass rings for the degradation of cellulose bleaching effluents.

3.3.4.2 Supported TiO_2 durability

The durability of the catalyst activity was investigated by using the TiO_2-impregnated glass rings for the photocatalytic degradation of several compounds. A single batch of glass rings was regularly utilized during 5 months cumulating approximately 300 h of photodegradation experiments on 5 different compounds. After that, it is observed that the photocatalytic activity of the supported TiO_2 for the IP degradation remains as high as at the beginning of its use. The catalytic activity retention is quite high and renders the supported TiO_2 very interesting as it does not need to be separated from the treated solution and can be easily held in a technical system and reused many times.

3.3.4.3 Chemical and biological characteristics of the phototreated isoproturon solution

Biocompatibility of the photochemically treated solution was studied to be sure that this process can be used as a pretreatment, preceding the biological stage. Figure 3.16 shows the evolution of IP, DOC, NO_3^-, and the toxicity for the IP photodegradation.

The system presents the same kind of toxicity profile as in the case of photo-Fenton treatment (Section 3.3.3.2) with a high toxicity increase at the beginning of the treatment,

followed by a sharp decrease. After 2 h of phototreatment, solution toxicity is as low as that of the initial compound and NO_3^- ion stoichiometric value (24.8 mg NO_3^- l^{-1}, corresponding to 100% in Figure 3.16) is reached. The DOC evolution shows that the mineralization is only of about 20% when IP is completely eliminated.

The ratio BOD_5/COD (representative of the biodegradability) is found to be 0.0 before phototreatment and it increases up to 0.65 after 1 h of pretreatment. As indicated before, this parameter for biodegradable municipal wastewater is of around 0.4.

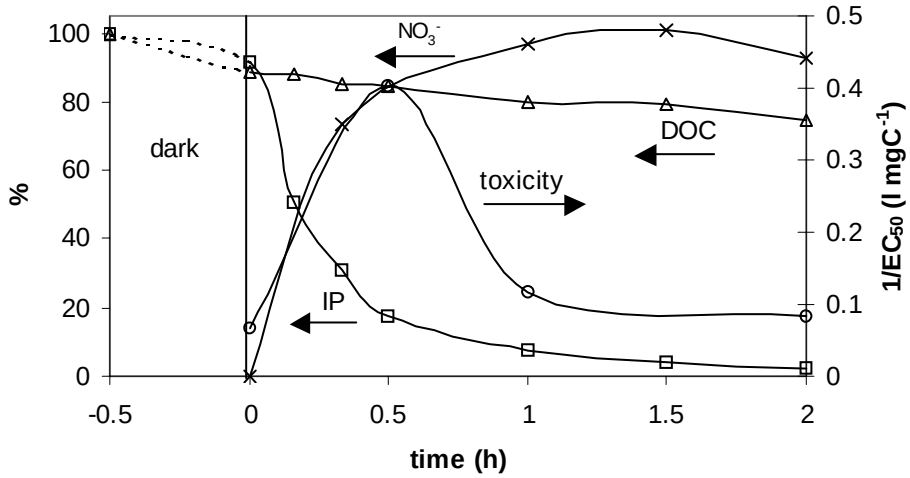

FIGURE 3.16 *Phototreatment of an IP solution using supported TiO_2 catalyst. Evolution of initial compound, DOC, NO_3^-, and toxicity (expressed as 1/ EC_{50}). IP (0.2 mmol l^{-1}).*

Based on these results photochemical-biological coupled flow treatment can be considered for the complete mineralization of this compound since supported TiO_2 looks like a promising pretreatment method.

3.3.4.4 Photochemical-biological coupled flow treatment

The coupled photochemical (coaxial) - biological flow reactor, described in the experimental section (Section 3.2.2.2) is used operating it in semi-continuous mode for the mineralisation of an IP aqueous solution (1.5 l).

Figure 3.17 shows the evolution of the initial compound during the pretreatment process and the evolution of DOC in both photochemical and biological treatments. At 60 minutes of phototreatment, when IP is completely eliminated, about 80% of DOC remains in solution. The slow decrease of DOC compared with IP evolution indicates an accumulation of intermediates. The biodegradability and toxicity tests performed during a photodegradation run in batch mode show that the resulting solution becomes biocompatible when the DOC becomes almost stable and after the quasi-total elimination of IP. Consequently, the optimal time to stop the phototreatment before feeding the treated water to the biological reactor was found to be 1 hour. At this stage of the phototreatment, the pH of the solution was around 6.5 with no need of neutralisation. Normally, employing photo-Fenton process, neutralisation of the solution is necessary because after reaction the acidity of the solution becomes very high. During the biological process the pH must be maintained between 6.5 and 7.5.

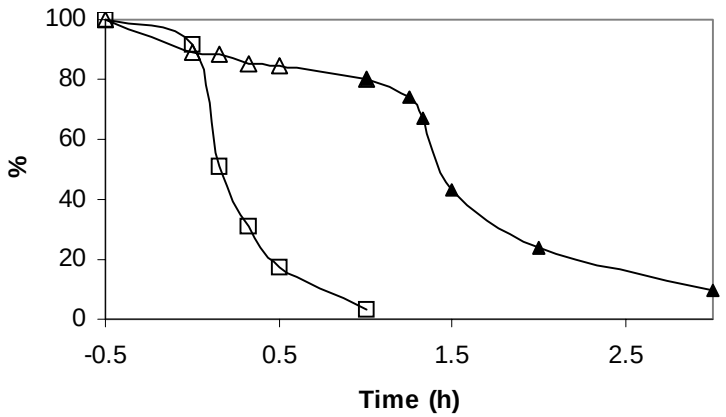

FIGURE 3.17 *Coupled photocatalytic and biological process for the mineralization of IP. Evolution of IP (square points) and DOC (triangle points). The open and full points correspond to the photocatalytical and biological treatment, respectively.*

Isoproturon and its degradation intermediates are followed by HPLC analysis and UV spectrophotometry during the photochemical and biological degradation processes. It is observed that at 1 hour, the phototreatment depleted IP up to 97% producing aromatic and aliphatic by-products, which were not identified. The Figure 3.18 shows the UV spectra of samples taken before the biological treatment and 10 and 120 minutes, afterwards. These results confirm the presence of photochemically resulting aromatic and aliphatic intermediates and its decay during the biological stage. The effective mineralisation of the solution during the biological stage was proved by the DOC evolution shown in Figure 3.17. Total mineralisation could also be obtained via a single photocatalytic process but this approach is rather expensive due to the high electricity consumption over long irradiation periods.

In the coupled reactor, sequential batches of the phototreatment process were carried out every 60 min that corresponds to an input flow rate of 1.5 l h^{-1}. This flow rate was maintained during at least 3 days after reaching the steady state to assure the stability of the system during a long time period.

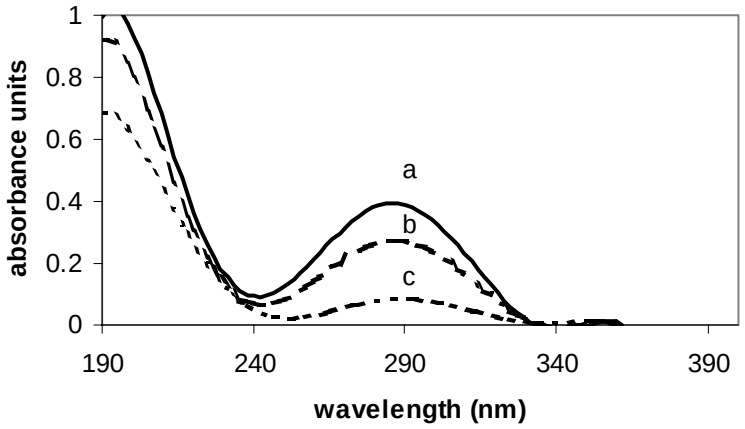

FIGURE 3.18 *UV spectra between 190 and 400 nm of a phototreated solution of IP. (a) Before the biological treatment and after (b) 10 and (c) 120 minutes of biological treatment.*

The photoreactor characteristics and the performance of the coupled system are summarized in Table 3.6. In this case, 100% of the initial concentration of IP and 95% of DOC were removed.

TABLE 3.6 *Performances for IP degradation by the coupled photochemical (coaxial)- biological reactor using supported TiO_2 and fixed bacteria.*

Parameter	**Photochemical coaxial reactor**	**Biological reactor**
Volume of reactor (l)	0.8	1.0
Input flow rate (l h^{-1})	1.5	0.75
Dilution rate, D (h^{-1})	1.0	0.75
Residence time (h)	0.5	1.0
Input concentration (mg C l^{-1})	35.0	28.0
Output concentration (mg C l^{-1})	28.0	2.0
Isoproturon removed (%)	100.0	
DOC removed (%)	20.0	93.0
Overall efficiency related to DOC degradation (%)	**95**	

3.4 Conclusions

The pollutants *p*-NTS, MB and IP were determined to be non-biodegradable by the Zahn-Wellens biodegradability test and in a fixed bed reactor under theoretically favourable conditions such as the presence of co-substrates and adapted bacteria justifying the utilisation of photochemical process.

The photodegradation kinetics of IP employing either suspended or supported TiO_2 are very similar indicating that the activity of the TiO_2 is not reduced when it is immobilized on an inert surface like the glass rings used in this work. After 300 hours of photodegradation experiments using the same single batch of impregnated glass rings, it was verified that the activity of the supported TiO_2 was not affected. The level of catalytic activity retention is quite

high and shows that besides supported TiO_2 does not need to be separated from the treated solution, it can be widely reused, which represents an added advantage in favour of its use.

The coupling of a photochemical and biological flow reactor was operated in continuous and semi-continuous mode for the total mineralisation of a *p*-NTS solution. The main parameter affecting the performance of the photo-assisted reactor in continuous mode is related to the high residual H_2O_2 concentration after the pretreatment. The semi-continuous mode was applied to try to overcome this inconvenience.

Toxicity and biodegradability analysis of the phototreated solutions of *p*-NTS, MB, and IP show that, the solution resulting from the photodegradation of MB is not biocompatible while the photodegraded solution of *p*-NTS and IP are biologically compatible and their complete mineralisation can be performed by biological means.

This study demonstrates the usefulness of the photo-Fenton reaction and of the photo-assisted TiO_2 process as pretreatment methods preceding a biological treatment for the complete mineralisation of non-biodegradable organic substances. However, the strategy of coupling photochemical and biological systems is not necessarily an universal solution. Chemical, biological, and kinetic studies must always be carried out for all kind of compounds and wastewaters in order to be sure that the photochemical pretreatment induces a beneficial effect on the biocompatibility of the treated effluent.

The coupled photochemical (annular or coaxial using respectively Fenton reaction or TiO_2 as catalyst) and biological flow reactor operated in semi-continuous mode seems to be an efficient system for the mineralisation of *p*-NTS and IP solutions. The primary degradation efficiency expressed as percentage of IP and *p*-NTS removed (followed by HPLC analysis) was 100% and the mineralisation efficiency (followed by TOC analysis) was 95%.

The coupled system developed in the last part of this work employs TiO_2 supported on glass rings in the photocatalytic coaxial reactor and fixed bacteria on biolite. These fixed components renders this coupled technology for the treatment of wastewater more economic and simpler.

3.5 Bibliography

1. Ollis, D.F.a.A.-E., H, *Photocatalytic Purification and Treatment of Water and Air*. 1993, Amsterdam: Elsevier.

2. Blake, D., *Bibliography of work on the heterogeneous photocatalytic removal of hazardous compounds from water and air. Update number 3 to january 1999, NREL/TP-570-26797. National Technical Information Service (NTIS), U.S. Department of comerce, Springfield, VA 22161*. 1999.

3. Huston, P.L. and J.J. Pignatello, *Degradation of Selected Pesticide Active Ingredients and Commercial Formulations in Water by the Photo-Assisted Fenton Reaction.* Water Res, 1999. 33(5): p. 1238-1246.

4. Bahnemann, D., *et al.*, *Photocatalytic Treatment of Waters*, in *Aquatic and Surface Photochemistry*, G.R. Helz, R.G. Zepp, and D.G. Crosby, Editors. 1994, Lewis Publishiers: Boca Raton. p. 261-316.

5. Marco, A., S. Esplugas, and G. Saum, *How and Why to Combine Chemical and Biological Processes for Waste-Water Treatment.* Water Sci Technol, 1997. 35(4): p. 321-327.

6. Scott, J.P. and D.F. Ollis, *Integration of chemical and biological oxidation processes for water treatment: review and recommendations.* Environmental Progress, 1995. 14(2): p. 88-103.

7. Scott, J.P. and D.F. Ollis, *Integration of chemical and biological oxidation processes for water treatment: II. Recent illustrations and experiences.* J. Adv. Oxid. Technol., 1997. 2(3): p. 374-381.

8. Stern, M., *et al., Removal of Substituted Pyridines by Combined Ozonation/ Fluidized Bed Biofilm Treatment.* Water Sci Technol, 1997. 35(4): p. 329-335.

9. Kitis, M., *et al., Effects of Ozone/Hydrogen peroxide pretreatment on aerobic biodegradability of nonionic surfactants and polipropylene glycol.* Environmental Science and Technology, 2000. 34(11): p. 2305-2310.

10. Adams, C.D. and J.J. Kuzhikannil, *Effects of UV/H2O2 preoxidation on the aerobic biodegradability of quaternary amine surfactants.* Water Research, 2000. 34(2): p. 668-672.

11. Mantzavinos, D., *et al., Wastewater treatment: wet air oxidation as a precursor to biological treatment.* Catalysis Today, 1999. 53(1): p. 93-106.

12. Dutta, T.K. and S. Harayama, *fate of crude oil by the combination of photooxidation and biodegradation*. Environmental Science and Technology, 2000. 34(8): p. 1500-1505.

13. Bandara, J., *et al., Chemical (Photo-Activated) Coupled Biological Homogeneous Degradation of P-Nitro-O-Toluene-Sulfonic Acid in a Flow Reactor.* J Photochem Photobiol A. Chem, 1997. 111(1-3): p. 253-263.

14. Pulgarin, C., *et al., Strategy for the coupling of photochemical and biological flow reactors useful in mineralization of biorecalcitrant industrial pollutants.* Catalysis Today, 1999. 54(2-3): p. 341-352.

15. Parra, S., *et al., Photochemical versus coupled photochemical-biological flow system for the treatment of two biorecalcitrant herbicides: metobromuron and isoproturon.* Applied Catalysis B: Environmental, 2000. 27: p. 153-168.

16. Pozzo, R.L., M.A. Baltanas, and A.E. Cassano, *Supported titanium oxide as photocatalyst in water decontamination: State of the art.* Catalysis Today, 1997. 39(3): p. 219-231.

17. Dionysiou, D.D., *et al.*, *Continous mode photocatalytic degradation of chlorinated phenols and pesticides in water using a bench-scale TiO2 rotating disk reactor.* Applied Catalysis B: Environmental, 2000. 24: p. 139-155.

18. Chen, D. and A.K. Ray, *Photocatalytic kinetics of phenol and its derivates over UV irradiated TiO2.* Applied Catalysis B: Environmental, 1999. 23: p. 143-157.

19. Parra, S., S. Malato, and C. Pulgarin, *New integrated photocatalitic-biological flow system using supported TiO2 and fixed bacteria for the mineralization of isoproturon.* Applied Catalysis B: Environmental, 2001. accepted.

20. Yeber, M.C., *et al.*, *Photocatalytic degradation of cellulose bleaching effluent by supported TiO2 and ZnO*. Chemosphere, 2000. 41: p. 1193-1197.

21. Yeber, M.C., *et al. TiO2 and ZnO thin film formation on glass*. in *Second International conference on Advanced Wastewater Treatment Recycling and Reuse.* 1998. Milano, Italy.

22. OECD, *Guidelines for testing of Chemicals, Vol 2, test 302B.* 1996.

CHAPTER 4

APPLICATION OF THE SOLAR FIELD SCALE TECHNOLOGY

4.1 Introduction

Solar photochemistry technology can be defined as the one that efficiently collects solar photons and introduces them in a volume reactor to promote specific chemical reactions [1]. This section describes the power of light as a source of energy as well as the basic factors related to the solar photocatalytic technology [2] and its applications [3]. It outlines the basic principles related to the solar spectrum and specifically to the solar UV radiation since this part of the solar spectrum is the most important for driving chemical processes, the application of the solar photocatalysis, and the main features of the collectors used for wastewater decontamination.

4.1.1 Solar radiation

Solar radiation is all the energy coming from that huge reactor, the sun, from which the earth receives 1.7×10^{14} kW, meaning 1.5×10^{18} kWh per year, or approximately 28000 times the world energy consumption per year. The wavelength of the radiation beyond the atmosphere ranges between 0.2μm and 50μm. This range is reduced to 0.3 μm and 3.0 μm when reaching the earth surface due to the absorption of part of the radiation by different atmospheric components (e.g., ozone, oxygen, carbon dioxide, aerosols, steam, clouds). The solar radiation that reaches the ground without had being absorbed or scattered is called direct radiation, the radiation that reaches the ground but has been dispersed is called diffuse radiation, and the sum of both is called global radiation. In other words, direct radiation is the one that produces shadow when an opaque object blocks it, while diffuse radiation does not. In general, the direct

component of global radiation on cloudy days is minimum and the diffuse component is maximum. The opposite is verified on clear days.

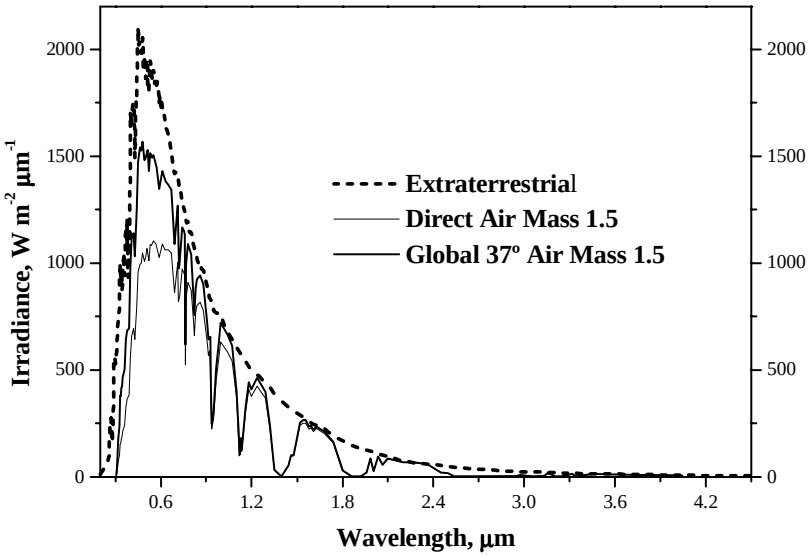

FIGURE 4.1 *Solar radiation spectrum plotted from 0.2 to 4.5 μm.*

Figure 4.1 shows the standard solar radiation spectrum [4] at ground level on a clear day. The dotted line corresponds to the extraterrestrial radiation in the same wavelength interval. When this radiation enters the atmosphere, it is absorbed and scattered by atmospheric components, such as air molecules, aerosols, water vapour, liquid water droplets, and clouds.

The spectral irradiance data are given at a solar zenith angle of 48.19º. This zenith angle corresponds to an Air Mass (AM) of 1.5 (Figure 4.2), which is the ratio of the direct-beam solar-irradiance path length through the atmosphere at a solar zenith angle of 48.19º to the path length when the sun is in a vertical position. Air mass is equal to unit when the sun is directly overhead (zenith). As air mass increases, the direct beam traverses longer path lengths in the atmosphere, which results in higher scattering and absorption of the direct beam and a lower percentage of direct total radiation (for the same atmospheric conditions).

The AM 1.5 global irradiance is shown in Figure 4.1 for a flat surface facing the sun and 37º tilted from the horizontal. The 37º tilting angle is used because that is the latitude of the Plataforma Solar de Almería, where the research presented here was done.

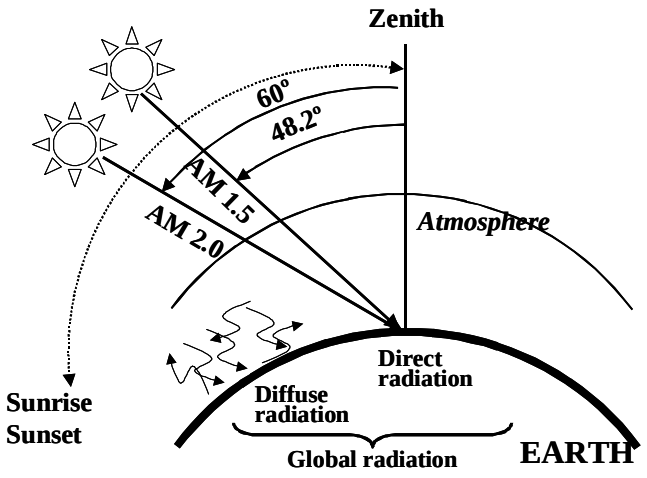

FIGURE 4.2 *Air mass and solar components.*

Solar ultraviolet radiation is only a very small part of the total solar spectrum, going between 3.5% and 8%, as demonstrated by measurement, although this percentage may vary for a given location on cloudy and clear days. The percentage of global UV radiation (direct + diffuse) generally increases with respect to the total global radiation when atmospheric transmissivity decreases mainly because of clouds, but also because of aerosols and dust. In fact, the average percentage of UV with respect to total radiation on cloudy days is up to two percent points higher than values on clear days.

The two spectra shown in Figure 4.3 correspond to the solar UV spectra at ground level. The direct radiation spectrum (UV_D) and the global radiation spectrum (UV_G) cumulate 22 and 46 Wm^{-2}, respectively, between 300 and 400 nm. These two values give an idea of the energy coming from the sun that is available for photocatalytic reactions with TiO_2 that uses UV solar radiation just up to 387 nm. In any case, the UV radiation values vary from one location to another, and obviously, at different hours of the day and in different seasons, making necessary to know these data for any particular location in real time.

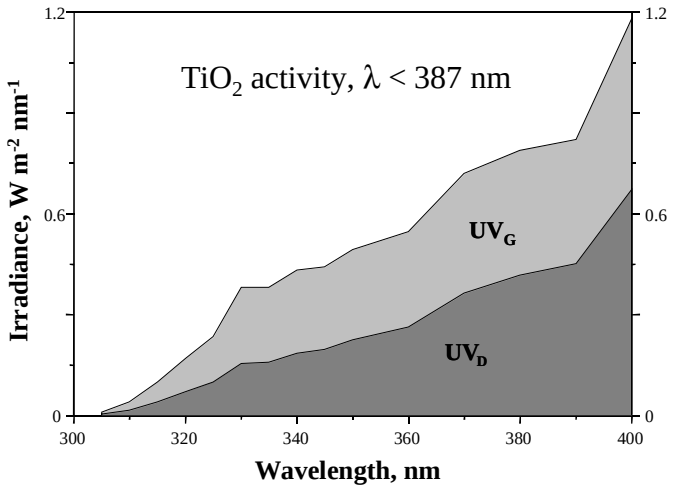

FIGURE 4.3 *Ultraviolet spectrum on the earth surface (standard ASTM).*

4.1.2 Solar collector technology

Traditionally, different solar collector systems have been classified depending on the level of concentration they attain. The Concentration Ratio (CR) can be defined as the ratio of collector aperture to absorber areas. The aperture area intercepts radiation, while the absorber area receives concentrated solar radiation (either fully illuminated or not). The CR is directly related to the system working temperature. According to this criterion, there are three types of collectors:

- non-concentrating or low-temperature, up to 150º C;

- medium-concentrating or medium temperature, from 150º C to 400º C;

- high-concentrating or high temperature, over 400º C.

This traditional classification considers only the thermal efficiency of the solar collectors. However, in photocatalytic applications, the thermal factor is secondary whereas the amount of

useful radiation collected (in the case of the TiO_2 catalyst, with a wavelength shorter than 387 nm) is very important.

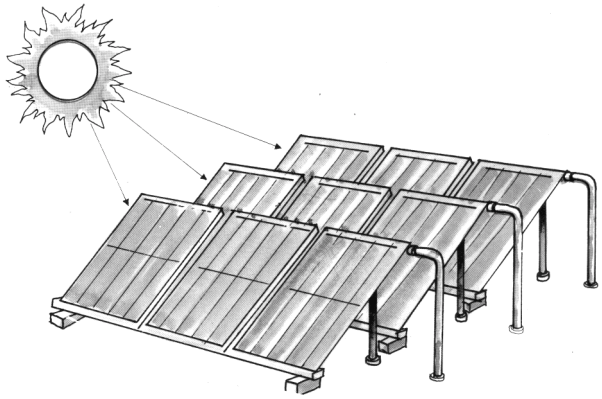

FIGURE 4.4 *Non-concentrating solar collectors for domestic heat water application.*

Non-concentrating solar collectors (Figure 4.4) are static and non-solar-tracking. Usually, they are flat plates, often aimed at the sun at a specific tilt, depending on the geographic location. Their main advantage is their simplicity and low cost.

Medium-concentrating solar collectors concentrate sunlight between 5 and 50 times and usually require continuous tracking of the sun. Parabolic Trough Collectors (PTC) and holographic collectors (Fresnel lenses) are in this group. Parabolic trough collectors have a parabolic reflecting surface (Figure 4.5) which concentrates the radiation on a tubular receiver located in the focus of the parabola. These collectors may be one-axis tracking, either azimuthal (east-west movement around a north-south-oriented axis) or elevation (north-south movement around an east-west-oriented axis), or two-axis tracking (azimuth + elevation) as the Helioman collector presented in section 4.2.2.1. Fresnel lens collectors consist of refracting surfaces (similar to convex lenses) which deviate the radiation at the same time they concentrate it onto a focus.

High concentrating collectors have a focal point instead of a linear focus and are based on a paraboloid with solar tracking. Typical concentration ratios are in the range of 100 to 10000 requiring optical precision elements. They include parabolic dishes and solar furnaces (Figure 4.6).

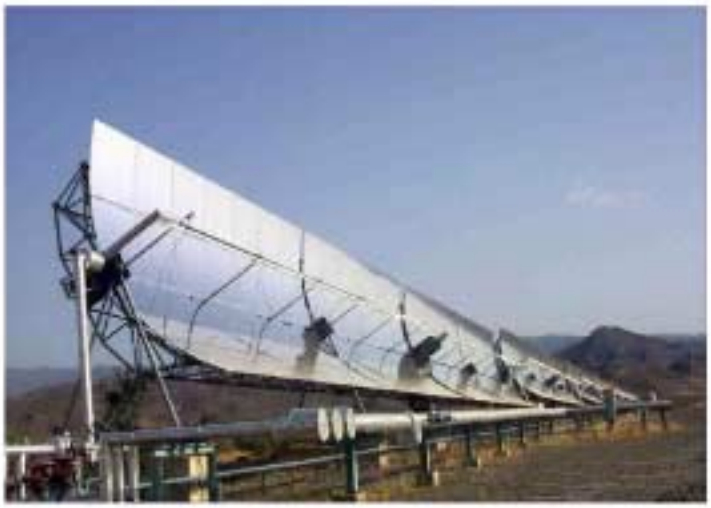

FIGURE 4.5 *Medium-concentrating solar collectors. PTC type (PSA, Spain).*

Up to now, most of the solar collectors used for photocatalysis belong to non-concentrating and medium-concentrating categories.

FIGURE 4.6 *High concentrating solar collector. Parabolic dish solar collector (PSA, Spain).*

4.1.3 Solar water detoxification collectors

The specific hardware needed for solar photocatalytic applications have a lot in common with those used for thermal applications. As a result, photocatalytic systems and reactors have followed conventional solar thermal collector designs, such as parabolic troughs and non-concentrating collectors. At this point, their designs begin to diverge, since:

- The fluid is exposed to ultraviolet solar radiation, and therefore, the absorber must be UV-transparent.

- The temperature does not play a significant role in the photocatalytic process, so no insulation is required.

The first engineering-scale outdoor reactor for solar detoxification was developed by Sandia National Laboratories (USA) at the end of the eighties. A parabolic-trough solar thermal collector was simply modified by replacing the absorber/glazing-tube combination with a Pyrex tube through which contaminated water could flow. Since then, many different concepts with a wide variety of designs have been proposed and developed all over the world, in a continuous effort to improve performance and to reduce the cost of solar detoxification systems. The most important concepts to be considered are those related to whether or no radiation must be concentrated, the type of reflective surface, the way the water circulates through the reactor (e.g., tube, falling film, or stirred vessel), and how the catalyst is employed.

One of the most important reactor-design issues is the decision between concentrating or non-concentrating collector systems. Concentrating systems have the advantage of a much smaller reactor-tube area, which could mean a shorter circuit in which to confine, control and handle the contaminated water to be treated. If concentrating collector systems have to be used, an improving alternative, from both economical and engineering points of view, would be the use of high-quality ultraviolet-light-transmitting reactors and supported-catalyst devices.

Nevertheless, concentrating reactors have two important disadvantages compared to non-concentrating ones. The first one is that they cannot concentrate (i.e., use) diffuse solar radiation. This fact is irrelevant for solar thermal applications because diffuse radiation is just a

small fraction of the total solar radiation. However, this disadvantage becomes important in solar TiO_2-photocatalytic detoxification as it uses only the UV fraction of the solar spectrum from which as much as 50 percent can be diffuse, since it is not absorbed by water vapour. This percentage can be even higher in very humid locations or during cloudy or partly cloudy periods. In this sense, efficiency of non-concentrating solar collectors can be noticeably higher, as they can take advantage of both direct and diffuse UV radiation. The second disadvantage of concentrating collectors is their complexity, cost and maintenance requirements. As a consequence of these disadvantages, the present state-of-the-art favours the use of non-concentrating reactors for solar photocatalytic applications [5].

An additional disadvantage of concentrating reactors is the low degradation-rate dependence on light intensity. It has been demonstrated [6, 7] that the ratio of photocatalytic reaction rate to radiation intensity, changes with the radiation power as shown in Figure 4.7. This variation does not seem to occur at a particular radiation intensity, as different researchers obtain different results, but presumably is significantly affected by experimental conditions.

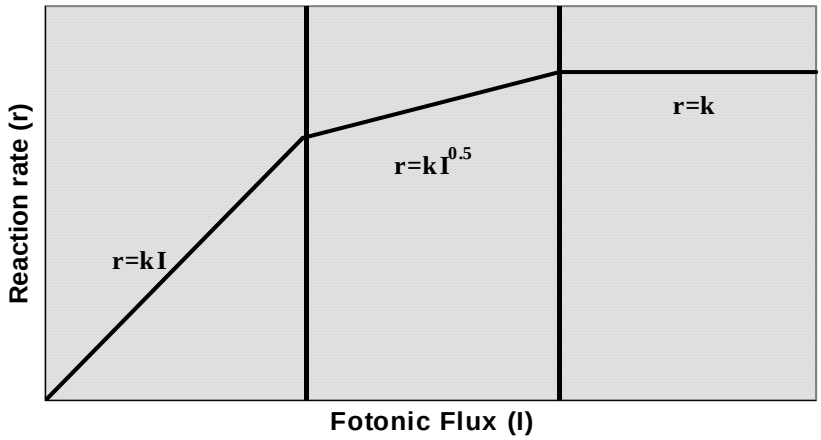

FIGURE 4.7 *Relation between the photocatalytic reaction rate and the intensity of the radiation received.*

Some authors [8, 9] impute the transition of $I^{1.0}$ to $I^{0.5}$, to the excess of photogenerated species (e^-, h^+ and $^{\bullet}OH$). At higher radiation intensity, another transition from $I^{0.5}$ to I^{0} is produced and from this point, the photocatalytic reaction rate is no longer dependent on the radiation received, but just on mass transfer within the reaction. This effect may be due to

different causes, such as a lack of electron scavengers (e.g., O_2) or organic molecules in the proximity of the TiO_2 surface, and/or excess of products occupying active centre of the catalyst. Currently, these phenomena appear more frequently when working with supported-catalyst and/ or at slow agitation speed, which implies less catalyst surface in contact with the liquid and less turbulence.

Many papers provide information of the light intensity at which the change of light intensity (I) exponent is produced, but the values found are very dissimilar [3]. It may be intuited that at an intensity of several suns (1 sun UV = 22 W_{UV} m^{-2}), quantum yield diminishes. This effect should be experimentally measured in each device, but a limit of several suns is usually accepted as a general rule.

Construction materials for many of the solar detoxification systems are commercially available. Most piping may be made of polyvinylidene fluoride (PVDF), chlorinated polyvinyl chloride (CPVC), or simply polyethylene. In any case, piping, as well as the rest of the materials, must be resistant to corrosion by the original contaminants and their possible degradation by-products in the destruction process. Construction materials must be non-reacting so they will not interfere with the photocatalytic process. All materials used must be inert to UV solar light degradation.

Photocatalytic-reactor optical material must efficiently transmit UV light because of the process requirements. However, in some cases, when vapour pressure of contaminants in water is sufficiently low, system does not need to be closed and consequently an UV transmissive container is not required.

All pipes, reactor, and connection devices must be strong enough to withstand the water-flow pressure. Typical parameters are 2 to 4 bar for nominal system pressure drop and a maximum of 5 to 7 bar. Concentrating-system materials must also be able to withstand possible high temperatures that could result from absorption of concentrated visible and infrared light in the reactor.

With regard to the reflecting/concentrating materials, aluminium is the best option given its low cost and high reflectivity in the UV spectrum. Commercially available films consists of a thin aluminium foil with an acrylic coating.

4.1.3.1 Parabolic trough collectors

Solar reactors for photochemical applications were originally designed using Parabolic Trough Collectors (PTC). This was, in part, because of the historical emphasis on trough units for solar thermal applications. Furthermore, PTC technology was relatively mature and existing hardware could be easily modified for photochemical processes. As mentioned before, there are two types of PTC:

- One-axis parabolic trough (Figure 4.5).

- Two-axis parabolic trough (Figure 4.9).

The first engineering-scale solar photochemical facility for water detoxification was developed in 1989 by Sandia National Laboratories (USA) using one-axis PTC. The second one was developed by CIEMAT (Spain) in 1990 using two-axis PTC. Both facilities are considerably large pilot plants (hundreds of square meters of collecting surface) and can be considered the first steps toward the industrialization of photochemical processes.

One-axis tracking PTC has been demonstrated to be the most economically advantageous for solar thermal applications. However, Two-axis tracking PTC are better suited for photocatalysis research purposes since they allow the exact calculation of the radiation hitting the photoreactor. This feature permits comparison of experiments carried out in such large photoreactors with those performed at laboratory-scale, where the calculation of incident radiation is simple.

The basic components of a PTC for photocatalytic applications are: the reflecting concentrator, the absorber tube (photoreactor), the drive-tracking system, and the overall structure. Of these, the latter two are identical to those existing for thermal applications.

The collector structure supports the reflecting concentrator system, which reflects direct radiation onto the receiver tubes. Two-axis PTC consist of a turret with a platform supporting several parallel parabolic trough collectors with focus-located absorber. The two axis tracking system guarantees the collector aperture plane to be always perpendicular to the solar rays,

which are reflected by the parabola onto the reactor tube at the focus. The contaminated water circulates through the reactor tube. More details of this collector are given in section 4.2.2.1.

Typical overall optical efficiency in PTC is in the range of 50 to 75 percent. After all optical losses are considered, the effective concentrating ratio of a PTC is usually between 5 and 20. The optical loss factor and their associated efficiencies are:

-Tracking system: 90%-95%

-Reflector/Concentrator (reflectivity): 80%-90%

-Absorber/Reactor (transmittance): 80%-90%

-Mechanical collector errors: 90%-95%

Parabolic-trough collectors make efficient use of direct solar radiation and, as an additional advantage, the thermal energy collected could be used in parallel for other applications. The reactor is small and receives a large amount of energy per unit of volume. Thus, handling and control of the liquid to be treated is simple and cheap, and the risk of potentially dangerous leaks is low.

4.1.3.2 One-sun collectors

One-sun non-concentrating collectors (CR = 1) are, in principle, cheaper than PTC as they do not have moving parts or solar tracking devices. They do not concentrate radiation, so the efficiency is not affected by concentration and solar-tracking related factors. Manufacturing costs are lower because of their simpler components, which also means easy and low-cost maintenance. The non-concentrating collector-support structures are easier and cheaper to install. Given that they are static and consequently do not project shadows on other collectors, the surface required for their installation is smaller.

Extensive effort in the designing of small non-tracking collectors has led to developing of a wide number of non-concentrating solar reactors for photochemical applications, specially for photocatalytic processes. These reactors can be classified as follows:

-Trickle-down flat plate: based on a tilted plate facing the sun over which the fluid falls slowly. A catalyst is normally fixed on the plate surface.

-Free-falling film: similar to the trickle-down flat plate, but with a higher flow rate. They normally have a catalyst attached to the surface on which the fluid circulates. It is usually open to the atmosphere, so it can be used only when volatile compounds are not present.

-Pressurized flat plate: consisting of two plates between which fluid circulates using a separating wall.

-Tubular: consisting of multiple small tubes connected in parallel that force the flow to circulate faster than in a flat plate reactor.

-Shallow solar ponds: small, low-depth, on-site built pond reactors.

Although one-sun photoreactors present important advantages, the design of a robust system is not trivial, since ultraviolet-transmitting reactors must be weather-resistant and chemically inert. In addition, non-concentrating systems require significantly higher photoreactor area than concentrating photoreactors and, as a consequence, large-scale systems (normally formed by hundred of square meters of collectors) must be designed to withstand the operating pressures anticipated for fluid circulation through a large path. As a consequence, the use of tubular photoreactors has a decided advantage because of the inherent structural efficiency of tubing. Tubing is also available in a large variety of materials and sizes and is a natural choice for a pressurized fluid system.

4.1.3.3 Compound Parabolic Concentrator (CPC)

Compound parabolic collectors are a very interesting cross between trough concentrators and one-sun systems and are one of the best options for solar photocatalytic applications. These collectors have been found to provide the best optics for low-concentrating systems. CPCs are static collectors with a reflective surface describing an involute around a cylindrical reactor tube; it can be designed with a CR=1 (or near one), thus having the advantages of both PTCs and one-sun collectors.

FIGURE 4.8 *Solar reflection on a CPC collector.*

Thanks to the reflector design shown in Figure 4.8, almost all the UV radiation arriving at the CPC aperture area (not only direct, but also diffuse) can be collected being available for the process in the reactor. The UV light reflected by the CPC is distributed around the back of the tubular photoreactor and as a result most of the reactor tube circumference is illuminated. However, due to the ratio of CPC aperture to tube diameter, no single point on the tube receives more than one sun of UV light. The incident light is then very similar to that of a one-sun photoreactor and, as in the case of flat-plate collectors, maximum annual efficiency is obtained at the same collector angle inclination as the local latitude. Performance is very close to that of the simple tubular photoreactor, but only about l/3 of the reactor tube material is required. As in a parabolic trough, the water is more easily piped and distributed than in many one-sun designs. All these factors contribute to excellent CPC-collector performance in solar photocatalytic applications.

Compound parabolic concentrator reflectors are usually made of polished aluminium and the structure can be a simple photoreactor support frame with connecting tubing (Figure 4.10). Since this type of reflector is considerably less expensive than tubing, their use is more cost-effective compared to deploying non-concentrating tubular photoreactors that do not use reflectors. The advantages of using tubing for the active photoreactor area is still preserved in CPCs.

4.1.4 Application of solar photocatalysis to wastewater decontamination

Detoxification is nowadays the most successful photochemical application of solar photons, with several relevant installations and projects already in operation. This is due not only to the fact that solar detoxification, also known as “solardetox” is an outstanding demonstration of how well suited is solar energy for environmental conservation, but also because, contrary to most photochemical processes, it is non-selective and can be employed with complex mixtures of contaminants. During the last decade, the number of references and related patents on heterogeneous photocatalytic removal of toxic and hazardous compounds from water and air can be counted by thousands and the number of applications and target compounds are numerous [10].

Within this context, treatment of industrial wastewater, though difficult to develop, seems one of the most promising application fields of solar detoxification. The only real general rule is that there is no general rule at all, each case being completely different from any other. In some cases, the Photo-Fenton process has demonstrated higher degradation efficiencies than heterogeneous TiO_2 photocatalysis, but in other cases, the Fe cycle is affected by the contaminants and Photo-Fenton does not work at all. As consequence, preliminary research is always required for assessing potential pollutant treatment and to define the best option for any specific problem, nearly on a case-by-case basis.

As indicated above, solar detoxification technology may be considered feasible for industrial effluents containing highly toxic compounds for which biological waste treatment plants are unfeasible at medium or low pollutant concentrations. “Solardetox” is a bidimensional technology that is linearly dependent on energy flux and collector surface. Given the collector surface dependence, land limitations must be considered in planning. An extension of 1000 to 2000 m^2 is usually sufficient for a medium-sized factory. As a conclusion, a reasonable order of magnitude of inflows for a Solar Detoxification plant, with the actual state-of-the-art of the technology, would be in the range from several dozens up to a few hundreds of m^3 per day. At the moment, and from the experience accumulated by many scientists and researchers in the last 10 years [11-15], solar detoxification seems to be a good solution for

destroying industrial wastewater contaminants such us: phenols, agrochemical waste, halogenated hydrocarbons, antibiotics, antineoplastics, and other chemical biocide compounds from the pharmaceutical industry, wood preservative waste, and hazardous metal ions, among others.

In this chapter, all the field experiments presented were carried out at the "Plataforma Solar de Almería (PSA)" in Spain. Metobromuron (MB), isoproturon (IP), and p-nitrotoluene-o-sulfonic acid (p-NTS) were employed as model substances in this study. The following topics are studied: (a) the comparison of two different solar collectors: a medium-concentrating radiation system (Helioman type, HM) and a low-concentrating radiation system (Compound parabolic Collector, CPC), (b) the comparison of different AOP at pilot scale, (c) the efficiency of degradation in a large plant by means of direct solar light, and (d) the feasibility of coupling a CPC photoreactor with a biological system at field pilot scale for the treatment of real biorecalcitrant wastewater.

4.2 Experimental

4.2.1 Materials

All chemicals were used as received. Metobromuron, Isoproturon, and *p*-nitrotoluene-*o*-sulfonic acid were provided by Ciba (Monthey-Switzerland), TiO_2 was Degussa P-25 (mainly anatase with a surface area of 50 m^2g^{-1}), and $FeCl_3.6H_2O$ and H_2O_2 (30% w/w) analysis grade (p.a.) were Fluka. The water used in the experiments was obtained from the PSA desalination plant (evaporation by multi-effect system using solar energy, conductivity < 10 $\mu S\ cm^{-1}$, organic carbon < 0.5 mg l^{-1}).

4.2.2 Solar collectors

Solar experiments were carried out using natural sunlight radiation in two types of reactor: a medium-concentrating radiation system (two-axis parabolic trough collector-type called

Helioman at the PSA) and a low-concentrating system (based on compound parabolic collectors, CPCs).

4.2.2.1 Helioman collector

FIGURE 4.9 *HM-type collector in tracking position.*

A HM collector is shown in Figure 4.9. It consists of a turret with a platform supporting four parabolic trough collectors with focus-absorber tubes. The platform is moved by two motors controlled by a two-axis (azimuth and elevation) tracking system. The tracking system consists of a photoelectric cell keeping the aperture plane perpendicular to the solar rays, which are reflected onto the focus (absorber), through which circulates the water to be treated.

4.2.2.2 Compound parabolic collector

The Compound Parabolic Collector (CPC) consists of 3 modules (collector surface, 3.08 m^2, photoreactor volume 22 l, and total reactor volume 39 l) whereas one module consists of 8

tubes. The three modules of the reactor are mounted on a fixed platform 37^{o} tilted (local latitude). A CPC collector is shown in the Figure 4.10.

FIGURE 4.10 *View of the CPC used for the solar driven experiments at the PSA.*

The 3 modules are connected in series with water directly flowing through them, leading finally to a recirculating tank. A centrifugal pump then returns the water to the collectors. At the beginning of the experiments, with collectors covered, all the chemicals are added to the tank and mixed until homogenisation. The cover is then removed and samples are collected at predetermined times.

In large scale, it was very difficult to dissolve the two herbicides (i.e., MB and IP) because of their very low water solubility. The achieved initial concentrations were 50 and 30 mg l^{-1} of MB and IP, respectively. Aqueous herbicides solutions were prepared within the reactor mixing the components by recirculation of the water. $FeCl_3.6H_2O$ (1.25 mmol l^{-1} Fe^{3+}) was added and a homogenization period of 20 minutes was necessary. Degradation was started by addition of the oxidant (H_2O_2), allowing the first 10 minutes for the dark reaction to take place. Thereafter, solar collector cover was removed at time t=0, and samples were collected at periodic intervals at the outlet of the CPC. During the Fenton reaction the pH of the solution was around 3.0.

4.2.3 Evaluation of solar UV radiation

Solar ultraviolet radiation is a highly important parameter for the correct treatment of data obtained from solar photocatalytic experiments. Radiation was determined during the experiments by means of a global UV radiometer (KIPP&ZONEN, model CUV3) mounted on a 37^{o} fixed-angle platform (the same angle as the CPC's). A direct UV light (International Light-ESD 400) radiometer was also mounted on a sun tracking platform. The sensors provide data in terms of global and direct UV solar energy power incident per unit area, W_{UV} m^{-2} ($UV_{G\text{-}D,n}$) respectively. Solar-UV power varies during experiments, specially when clouds are passing by. Data combination from several days and their comparison with other photocatalytic experiments is done by application of Equation 4.1.

$$Q_{UV,\,n} = Q_{UV,\,n-1} + \Delta t_n \overline{UV}_{G-D,\,n} \frac{A_{collector}}{V_{TOT}} \qquad \textbf{(EQ. 4.1)}$$

Where $\Delta t_n = t_n - t_{n-1}$, t_n is the experimental time for each sample, $\overline{UV}_{G-D,\,n}$ is the average UV_G (global UV radiation) or UV_D (direct UV radiation) during Δt_n. Calculations for experiments in CPC involve UV_G data while HM experiments involve UV_D data. $A_{Collector}$ is the collectors radiated surface, V_{TOT} is the total photoreactor volume, and $Q_{UV,n}$ is the reactor accumulated energy per unit of volume (kJ l^{-1}) for each sample taken. For the HM reactor, $A_{collector} = A_{HM} = 29$ m^2, and $V_{TOT} = 260$ l. For the CPC reactor, $A_{CPC} = 3.08$ m^2 and $V_{TOT} = 39$ l.

4.2.4 Chemical analysis

Compounds concentration were determined using a HPLC (Hewlett-Packard model 1050) equipped with an UV-detector and a RP-18 column (Lichrocart, i.d. 4 mm, 150 mm). The eluent was a methanol/water mixture (50/50 v/v). The DOC was directly measured on slurry by using a Heraeus-Fass Electric TOC-2001 (UV-peroxy-disulphate method). Calibration was achieved by using standards of potassium hydrogen phthalate. The consumption of H_2O_2 during the reaction was followed by the Merckoquant® test for peroxides and by titrating the samples with potassium permanganate in acidic medium. Analysis of ions was performed with a Dionex

DX - 120 ionic chromatograph provided with an Ion Pac column. Aqueous solutions of $NaHCO_3$ (1 mmol l^{-1}) and Na_2CO_3 (3.5 mmol l^{-1}) were used as eluents.

4.3 Results and discussions

4.3.1 Comparison between CPC and HM reactors during the photodegradation of isoproturon and *p*-NTS *via* suspended TiO_2

This part of the study focuses on the comparison of performance of two types of solar collectors, HM and CPC, with regard to the photodegradation of IP and *p*-NTS *via* suspended TiO_2.

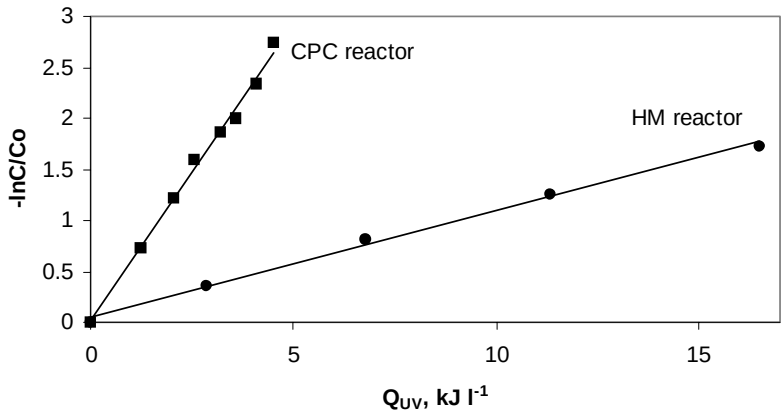

FIGURE 4.11 *Linear transform of the kinetic curves of IP photodegradation in CPC and HM reactors.*
IP(0.15 mmol l^{-1}) and suspended TiO_2 (0.2 g l^{-1}).

Figure 4.11 shows the linear relation between -ln(C/Co) and Q_{UV} for the IP herbicide disappearance in the reactors. In both cases, the kinetics of IP degradation are of apparent first order, with a rate constant (k_{app}) equal to 0.58 and 0.11 lkJ^{-1} for the CPC and HM reactors respectively. The degradation of *p*-NTS in both CPC and HM reactors presents the same

behaviour with rates constants (k_{app}) of 0.13 and 0.045 lkJ^{-1} for the CPC and HM reactors respectively.

Previous research at the PSA indicates that the degradation rate obtained in the CPC collectors are around 3 times higher than those observed in the parabolic HM collectors [16]. We have found the same ratio for the degradation of *p*-NTS [17] but the ratio corresponding to the IP photodegradation is of about 5. This is an indication of the influence of the nature of the compound on the photodegradation as will be explained later.

There are different loss factors (n) that affect the efficiency of both CPC and HM collectors, which could partially explain the difference in the degradation rate of IP and *p*-NTS indicated above. These factors have been previously described in detail by Malato [18]. Definition of each of these loss factors and their values are summarized here:

- n_s is a loss factor originated from the error produced during solar tracking by the collector's control system. The value of this factor is 0.92 for the HM collector. The CPC collector does not have this system and the factor may be considered as 1.0.

- n_c is a loss factor due to the construction features of the solar collectors. 0.91 and 1.0 for HM and CPC, respectively.

- n_r is related with the reflectivity of the aluminized surface of the collectors. 0.60 for HM and 0.90 for CPC.

- n_t is a loss factor due to the transmissivity of the absorber tubes. Its value is 0.90 and 0.91 for HM and CPC, respectively.

In addition, the ratio of photocatalytic reaction rate to radiation intensity, changes with the radiation power in a different way depending on the type and geometry of the photoreactor as explained above (section 4.1.3). It is generally accepted that in a CPC the reaction rate (r) is proportional to the intensity (I) of illumination, with r=kI. In contrast, since the intensity obtained with the HM collectors is about 10.3 suns [2], the reaction rate may be correlated to the square root of the illumination intensity ($r=kI^{0.5}$ or $r^2=k'I$).

Furthermore, the CPC are able to capture both, diffuse and direct UV sunlight. In contrast, a concentrating design like that of the HM reactor, benefits only from the direct UV radiation, which could be drastically decreased on a cloudy day [19, 20]. The diffuse component can represent 50% of the total available UV light, even on a clear day. This phenomenon could influence the photodegradation of a same compound in different ways since photocatalytic reaction pathways and degradation intermediates could be different depending on light incidence. Thus, one could conclude that the nature of the compound is also an important factor to be taken into account when the efficiency of different reactors are compared towards the degradation of organic substances.

All the factors presented above rend the CPC more efficient than the HM collector. This fact, together with low manufacturing, installation, and maintenance costs, and easy operation of CPC collectors compared with HM reactors, suggest that CPCs are the best way to use the solar technology.

4.3.2 Comparison of different advanced oxidation processes in a CPC reactor

Using the CPC photoreactor, various experiments were carried out in order to compare the efficiency of the solar photocatalytic treatment of IP and *p*-NTS based on the photo-Fenton system and TiO_2 photocatalysis.

4.3.2.1 Photodegradation of isoproturon

Figure 4.12 shows the evolution of DOC when a solution of IP (0.15 mmol l^{-1}) is reacted using direct sunlight in different degradation systems under aerobic conditions: UV/TiO_2, UV/TiO_2/H_2O_2, and UV/Fe^{3+}/H_2O_2. It is not plotted as a function of the residence time in the CPC reactor, but as a function of the accumulated energy per unit of volume (kJ l^{-1}), in order to correct any possible variation of the radiant flux. The energy accumulated (Q_{UV}) on the reactor per each sample, was estimated using equation 4.1.

Figure 4.12 shows that the mineralization rate of the IP solution is higher in the photo-Fenton system than in heterogeneous reactions. One of the most important factors that explains these results is the difference of light absorption capabilities between Fe^{3+} and TiO_2 catalyst. The TiO_2 absorbs in the UV light with a wavelength < 387 nm (4% of the solar irradiation) while the Fenton system can be active to wavelengths up to 600 nm (35% of the solar irradiation).

As shown in Figure 4.12, the addition of H_2O_2 to the UV/TiO_2 system does not have a beneficial effect on the mineralization of the IP solution. The effect of this strong electron acceptor depends on its concentration [21]. An optimal H_2O_2/pollutant molar ratio between 10 and 100 has been proposed by several authors [22, 23]. When this ratio is higher than 100, an inhibiting effect is detected. In our case, initial IP and H_2O_2 concentrations of 0.15 and 30 mmol l^{-1} respectively, give an inhibitory ratio of 200.

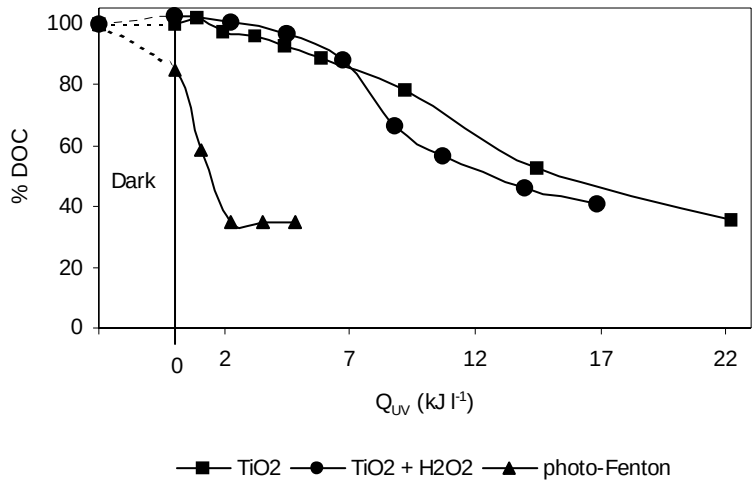

FIGURE 4.12 *Treatment of IP in different degradation systems. Evolution of DOC as a function of accumulated energy. IP (0.15 mmol l^{-1}); H_2O_2 (30 mmol l^{-1}); Fe^{3+} (1 mmol l^{-1}); TiO_2 (0.2 g l^{-1}).*

Even if the photo-Fenton reaction is the most efficient process for the mineralization of the IP solution, both homogeneous and heterogeneous photocatalysis are considered as suitable methods to reach the complete decay of IP in the solution. HPLC analysis indicate that with less than 5 kJ per liter of accumulated energy, the compound responsible for the non-biodegradability of the solution (IP), is completely degraded in all systems.

4.3.2.2 Photodegradation of p-nitrotoluene-o-sulfonic acid

The Figure 4.13 shows the evolution of *p*-NTS when a solution of this compound (0.5 mmol l^{-1}) is reacted using direct sunlight in the same degradation systems compared above: UV/TiO_2, UV/TiO_2/H_2O_2, and UV/Fe^{3+}/H_2O_2.

The curves in Figure 4.13 behave as an apparent first order process as confirmed by the linear transforms shown in the insert. The apparent first order rate constants (k_{app}) for the abatement of *p*-NTS are 0.13, 0.28, and 1.57 l kJ^{-1} for UV/TiO_2, UV/TiO_2/H_2O_2, and UV/Fe^{3+}/ H_2O_2 degradation systems, respectively. These k_{app} values represent the curve slopes in the Figure inset.

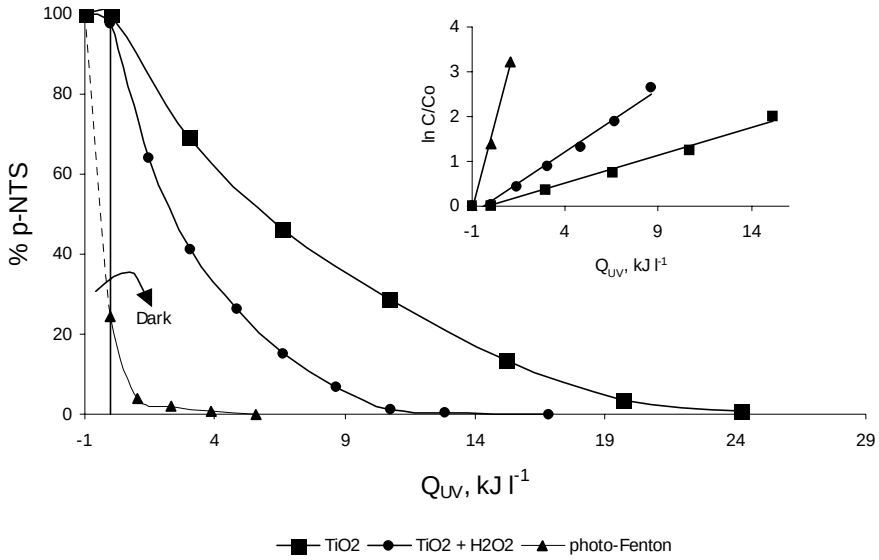

FIGURE 4.13 *Treatment of p-NTS in different degradation systems. Evolution of initial compound as a function of accumulated energy. p-NTS (0.5 mmol l^{-1}); H_2O_2 (25.0 mmol l^{-1}); TiO_2 (0.2 g l^{-1}); Fe^{3+} (1.0 mmol l^{-1}). The inset represents the linear transformation -ln (C/C_o)= f(Q_{UV}).*

As it can be observed, the *p*-NTS degradation rate in the photo-Fenton system is higher than in the heterogeneous reactions. As explained for the case of IP, the different absorption capabilities of Fe^{3+} and TiO_2 catalyst have to be taken into account. Furthermore, in

homogenous solution the depth of light penetration is higher and surface limitations are avoided.

In both homogenous and heterogeneous processes, the $^{\bullet}OH$ radicals are the main responsible for the organic pollutant oxidation. In the key reaction of the photo-Fenton process Fe^{2+} ions are oxidized by H_2O_2 while one equivalent of $^{\bullet}OH$ is produced. The obtained Fe^{3+} acts as the light absorbing species that produces another radical while the initial Fe^{2+} is regenerated (equations 4.2, 4.3).

$$FeOH^{2+} + h\upsilon \rightarrow {}^{\bullet}OH + Fe^{2+} \quad \textbf{(EQ. 4.2)}$$

$$e^{2+} + H_2O_2 \rightarrow {}^{\bullet}OH + {}^{-}OH + Fe^{3+} \quad \textbf{(EQ. 4.3)}$$

In the case of *p*-NTS degradation, as shown in Figure 4.13, the addition of H_2O_2 to the UV/TiO_2 system enhances its photodegradation rate. The k_{app} for the abatement of *p*-NTS in the UV/TiO_2/H_2O_2 system is twice higher than that observed for the UV/TiO_2 system. The H_2O_2/*p*-NTS molar ratio for this experiment is of about 50, which lies in the optimal range as explained above. For the UV/TiO_2 process, the $^{\bullet}OH$ is generated by oxidation reaction involving electron donors (H_2O and ^{-}OH) and a less efficient electron acceptor than H_2O_2 such as O_2. The H_2O_2 is considered as an efficient electron scavenger, which reacts with electrons of the conduction band of the TiO_2 to generate additional $^{\bullet}OH$ radical according to equation 4.4.

$$TiO_2(e^{-}) + H_2O_2 \rightarrow TiO_2 + {}^{-}OH + {}^{\bullet}OH \quad \textbf{(EQ. 4.4)}$$

Photo-Fenton reaction is the most efficient process for *p*-NTS degradation as it was in the case of IP. However, both homogeneous and heterogeneous photocatalysis can be considered as suitable methods to reach the complete degradation of *p*-NTS.

4.3.3 Perspectives for the coupling of a CPC-biological system at field pilot scale

4.3.3.1 The photo-Fenton reaction as pre-treatment.

Photodegradation of MB and IP in the CPC reactor is shown in Figures 4.14a and 4.14b, respectively. The results are given for an accumulated amount of energy per unit of volume (kJ l^{-1}). As shown in the figure, during the first part of the process when the dark reaction (Fenton) takes place after the addition of H_2O_2, both herbicides are rapidly degraded to less than 10% of the initial concentration. This reduction is reached in about 10 minutes of residence time (corresponding to 0 kJ per liter under normal operating conditions).

The DOC reduction for both herbicides is negligible in this dark phase. In contrast, DOC starts to decrease in the presence of solar light (photo-Fenton reaction), reaching up to 50% and 60% of the initial value of MB and IP solutions for the moment when H_2O_2 has been totally consumed. This degree of mineralization is reached in about 10 minutes (corresponding to 0.7 kJ l^{-1} in the Figure 4.14a) in the case of MB degradation and in about 20 minutes (2 kJ l^{-1}, Figure 4.14b) for IP. The concentration of H_2O_2 is monitored, since it induces detrimental physiological effects on bacteria. This means that, after the phototreatment, any residual H_2O_2 in the phototreated solution makes it unsuitable if a coupled photochemical–biological system want to be applied to complete the mineralization.

Results concerning the utilisation of a coupled flow reactor at laboratory scale for the treatment of IP and MB (section 3.3.3.2) show that a phototreated solution of IP is biocompatible if it is completely eliminated and a mineralization of the solution between 50 – 65% is reached. By extrapolation, it can be considered that the solution of IP treated at pilot scale in the CPC photoreactor is also biocompatible if those same conditions are attained. In the case of MB, toxicity and biodegradability analysis of its phototreated solution show that it is not biocompatible. Even though this solution is not appropriate for biological treatment, its

behaviour at a pilot scale under solar irradiation has been determined and included in this section to study the efficacy of the solar treatment.

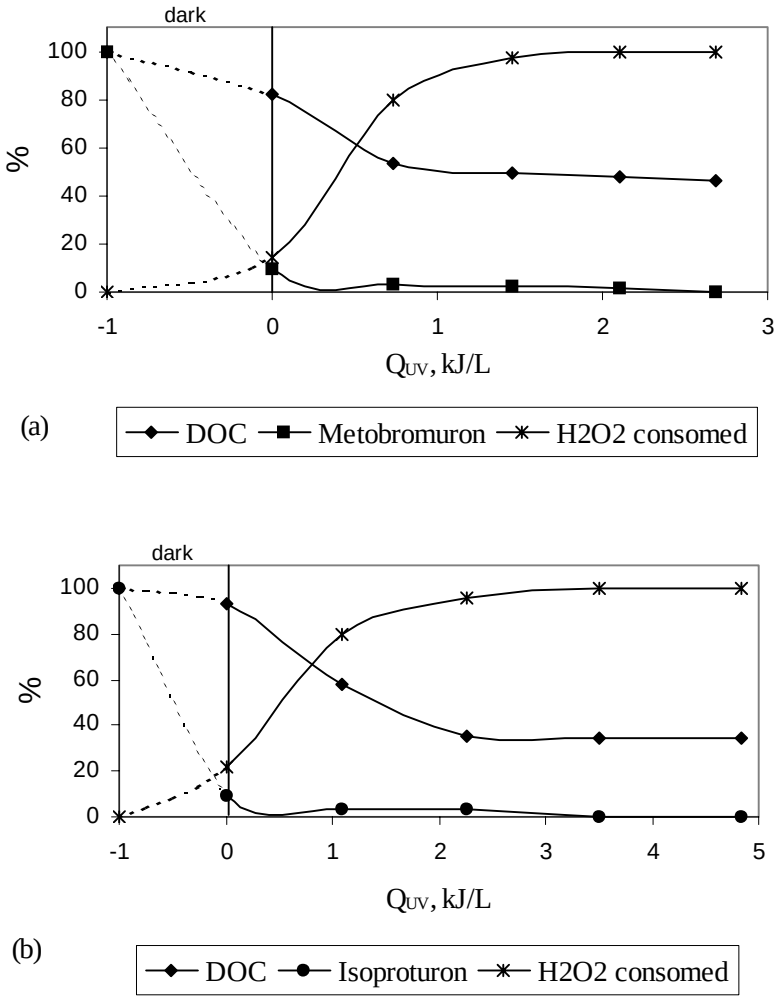

FIGURE 4.14 *Phototreatment of (a) MB and (b) IP in a CPC reactor. Evolution of the initial product, DOC, and H_2O_2 consumption as a function of accumulated energy. MB (50 mg l^{-1}), IP (30 mg l^{-1}), Fe^{3+} (1.25 mmol l^{-1}), and H_2O_2 (30 mmol l^{-1}).*

For IP solution to reach the desired 50–65% DOC degradation, the minimum initial H_2O_2 concentration should be 30 mmol l^{-1} given the DOC reduction dependence on the initial H_2O_2 concentration. As explained before (section 3.3.3.3), once H_2O_2 is consumed the pretreated water may go to a classical biological wastewater treatment plant to achieve the complete mineralization.

Since the phototreated solution of MB is not biocompatible, it has to be mineralized via a single photo-Fenton process. In this case, the quantity of H_2O_2 added must be higher. The time, and consequently, the cost of the phototreatment of MB is also higher compared with the phototreatment time needed to mineralize substances like IP, which can be treated by a coupled system.

Even if the experiments carried out at laboratory scales for the treatment of IP show promising results for the coupling of a photochemical – biological system, further investigations are needed concerning the biological treatment at pilot scale of the solution resulting from the phototreatment of IP. However, it is clearly demonstrated that the solar photo-Fenton treatment *via* CPC reactor is effective for the purification of water contaminated by these herbicides and that the complete mineralization of real bio-recalcitrant wastewater with a coupled system at pilot scale is possible [24].

4.3.3.2 The TiO_2 photo-assisted process as pre-treatment.

The photodegradation of *p*-NTS without addition of H_2O_2 is presented in Figure 4.15. The data correspond to one-day test run using a CPC reactor. The initial *p*-NTS concentration was100 mg l^{-1} corresponding to a DOC of 38.7 mg C l^{-1} and a sulfate content of 44.3 mg l^{-1}. The Figure 4.15a shows the disappearance of *p*-NTS as well as the evolution of NO_3^-, NO_2^-, and $SO_4^=$ during the photodegradation as a function of the accumulated energy. The evolution of DOC and toxicity are shown in Figure 4.15b.

It can be see in Figure 4.15a that in the presence of solar light and TiO_2, *p*-NTS is completely degraded in about 3 hours of residence time, corresponding to 24 kJ per liter under normal operating conditions. Analysis of ions in solution shows that $SO_4^=$ is generated in the stoichiometric value (about 44 mg $SO_4^=$ l^{-1}, corresponding to 100% in the Figure) after about 3 hours of residence time, indicating the absence of sulfo-compounds in solution. As shown in the Figure, the formation of $SO_4^=$ occurs simultaneously with the abatement of *p*-NTS.

The total mineralization of the solution is confirmed by the DOC results. The toxicity tests performed ascertain the average toxicity of the *p*-NTS and that of the phototreatment resulting

solution. The toxicity decrease (expressed as $1/EC_{50}$) displayed in Figure 4.15b exhibits the same shape as the kinetics of the solution mineralization (DOC results), indicating that no other toxic species are formed during the photodegradation process.

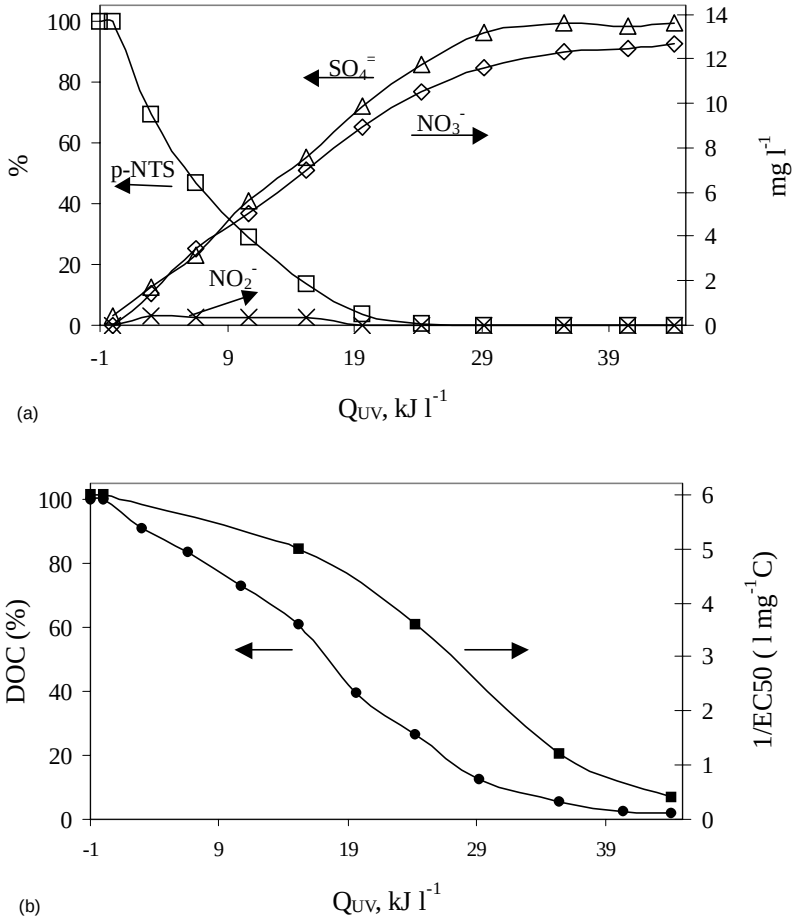

FIGURE 4.15 *Degradation of p-NTS (0.5 mmol l^{-1}) in a CPC reactor with 0.2 g l^{-1} of TiO_2. (a) Evolution of p-NTS, NO_3^-, NO_2^-, and $SO4^=$, (b) Evolution of DOC and toxicity (expressed as 1/EC50) during the phototreatment as a function of accumulated energy.*

Concerning the biodegradability of the treated solution, the ratio BOD_5/COD (representative of the biodegradability) is 0.0 without phototreatment and it increases up to 0.37 after the heterogeneous treatment. As a reference, this parameter is about 0.4 for municipal wastewater [25]. In our previous studies on photodegradation of *p*-NTS by photo-Fenton reaction at laboratory scale (section 3.3.2.2), a similar decrease on the toxicity and increase on the biodegradability was observed. For the complete mineralization of *p*-NTS solution, a

photochemical-biological coupled was efficiently used. Therefore, the experimental results presented here, demonstrate that the heterogeneous catalysis based on TiO_2 is a promising pre-treatment method that can be followed by a biological treatment.

Figure 4.16 shows the degradation of a solution of IP via TiO_2 photocatalysis in the CPC reactor. When IP is completely eliminated, about 80% of the DOC remains in solution. This slow decrease of the DOC indicates an accumulation of intermediates. It was demonstrated that, at laboratory scale, the biocompatibility of the treated solution, by the TiO_2 system, is attained when the initial compound is completely eliminated and the DOC removal is of about 20% (section 3.3.4.3). By extrapolation of these results it can be considered that, at pilot scale a phototreated solution of IP is also biocompatible after 10 kJ l^{-1} of accumulated energy in the CPC reactor. Thus, a coupled CPC–biological system at pilot scale could be envisaged to completely mineralize a solution of IP.

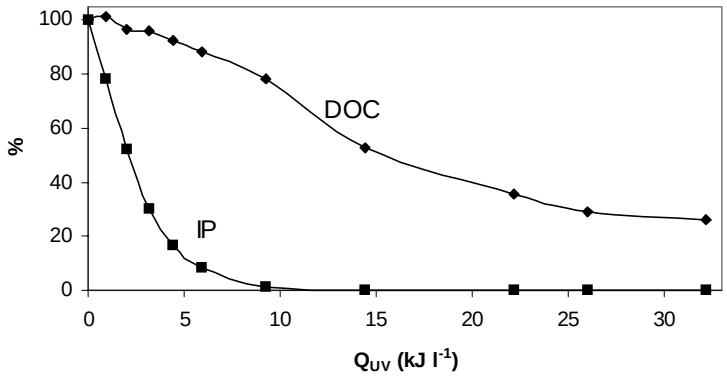

FIGURE 4.16 *Degradation of IP (0.1 mmol l^{-1}) in a CPC reactor. Evolution of the initial compound and the DOC.*

As shown in Figure 4.16, the energy necessary to reach a complete mineralization of the IP solution is more than 3 times the energy necessary for IP elimination. In this context, the implementation of a coupled system could reduce the cost of the treatment. In a sunny day in Almería with solar UV radiation average of 30 Wm^{-2}, 1 kJl^{-1} is equivalent to approximately seven minutes of illumination in the CPC reactor employed for this experiment $1\,\mathrm{kJ\,l^{-1}} = \Delta t \cdot 30\,\mathrm{Wm^{-2}} \cdot 3\,\mathrm{m^2} / 39\,\mathrm{l}$. Thus, 39 l of IP-contaminated water can be treated in

approximately 1 h of phototreatment in a sunny day employing the CPC reactor. Complete mineralization of the same solution, would take longer than 3h.

These encouraging results as well as those concerning the using of immobilized TiO_2 presented in section 3.3.4, open new possibilities for the coupling of TiO_2-photo-assisted and biological processes, at pilot scale, employing both supported TiO_2 and bacteria. The main advantage of this fixed system is that a separation procedure of the catalyst is not necessary rendering more economic and simpler the operation of both reactors.

4.4 Conclusions

The field experiments under direct sunlight using collectors as HM and CPC demonstrate that the solar photocatalytic treatment is effective for the purification of water contaminated by herbicides and other substances of industrial origin. However, different constructive factors, together with low manufacturing, installation, and maintenance costs, and easy operation of CPCs compared with HM collectors, suggest that the former ones are the best way to apply the solar technology.

The efficiency of *p*-NTS and IP solar photocatalytic treatment under direct sunlight in different degradation systems: UV/TiO_2, UV/TiO_2/H_2O_2, and UV/Fe^{3+}/H_2O_2 was studied and compared. Even when the photo-Fenton reaction happened to be the most efficient process, both homogeneous and heterogeneous photocatalysis can be considered as suitable methods to reach the complete mineralization of the solutions. They are also adequate to attain the state of biocompatibility of the phototreated solutions required for further biological treatment. The advantages of the TiO_2-photo-assisted process is that this catalyst is not sacrificed in the reaction and can be recovered from the treated water.

Using the CPC photoreactor, it was demonstrated the utility of the homogeneous (based on photo-Fenton reaction) and heterogeneous photocatalysis (based on TiO_2) as pretreatment methods that can be followed by a biological treatment. Further investigations are needed concerning the biological treatment at pilot scale of solutions resulting from the degradation of the different substances.

4.5 Bibliography

1. Malato, S. *Photocatalysis and Advanced Oxidation Technologies Applied to Water Treatment*. in *Workshop on "Catalytic process for clean chemistry and water and air pollution"*. 2000. Hammamet - Tunisia.

2. Malato, S., *Solar photocatalytic decomposition of pentachlorophenol dissolved in water*, ed. E. CIEMAT. 1999, Madrid.

3. Blanco, J. and S. Malato, *Solar detoxification*, ed. N.S. UNESCO, World Solar Programme 1996-2005. 2001.

4. Hulstrom, R., R. Bird, and C. Riordan, *Spectral solar irradiance data sets for selected terrestial conditions.* Solar Cells, 1985. 15: p. 365-391.

5. Blanco, J., *et al.*, *Compound parabolic concentrator technology development to commercial solar detoxification applications.* Solar Energy, 2000. 67(4-6): p. 317-330.

6. Herrmann, J.M., *Heterogeneous Photocatalysis: an emerging discipline involving multiphase system.* Catalysis Today, 1995. 24: p. 147-164.

7. Ollis, D.F., *Solar-assisted photocatalysis for water purification: issues, data, questions*, in *Photochemical conversion and storage of solar energy.* 1991, Kluwer Academic Publishers. p. 593-622.

8. Kormann, C., D. Bahnemann, and M. Hoffmann, *Photolysis of Chloroform and other organic molecules in aqueous TiO2 suspensions.* Environmental Science and Technology, 1991. 25: p. 494-500.

9. Turchi, C.S. and D.F. Ollis, *Photocatalytic degradation of organic water contaminants: mechanisms involving hydroxyl radical attack.* J. Catal., 1990. 122: p. 178-192.

10. Blake, D., *Bibliography of work on the heterogeneous photocatalytic removal of hazardous compounds from water and air. Update number 3 to january 1999, NREL/TP-570-26797. National Technical Information Service (NTIS), U.S. Department of comerce, Springfield, VA 22161*. 1999.

11. Aguera, A., *et al.*, *Evaluation of Photocatalytic Degradation of Imidacloprid in Industrial Water by GC-MS and LC-MS.* Analusis, 1998. 26(7): p. 245-251.

12. Augugliaro, V., *et al.*, *Photocatalytic oxidation of cyanide in aqueous TiO2 suspensions irradiated by sunlight in mild and strong oxidant conditions.* Catalysis Today, 1999. 54(2-3): p. 245-253.

13. Herrmann, J.M., *et al.*, *Photocatalytic degradation of pesticide pirimiphos-methyl. Determination of the reaction pathway and identification of intermediate products by various analytical methods.* Catalysis Today, 1999. 54(2-3): p. 353-367.

14. Texier, I., *et al.*, *Solar photodegradation of pesticides in water by sodium decatungstate.* Catalysis Today, 1999. 54(2-3): p. 297-307.

15. Malato, S., *et al.*, *Photocatalytic Degradation of Industrial Residual Waters.* Solar Energy, 1996. 56(5): p. 401-410.

16. Blanco, J., S. Malato, and C. Richter, *Solar chemistry technology*, in *Solar Thermal Test Facilities.* 1996, CIEMAT: Madrid. p. 145-164.

17. Parra, S., *et al.*, *Concentrating versus non-concentrating reactors for solar photocatalytic degradation of p-nitrotoluene-o-sulfonic acid.* Water science and technology, 2001. in press.

18. Malato, S., *et al.*, *Solar Photocatalytic Mineralization of Commercial Pesticides - Methamidophos.* Chemosphere, 1999. 38(5): p. 1145-1156.

19. Bockelmann, D., *et al.*, *Concentrating Versus Non-Concentrating Reactors for Solar Water Detoxification.* Solar Energ Mater Solar Cells, 1995. 38(1-4): p. 441-451.

20. Malato, S., *et al.*, *Low-Concentrating CPC Collectors for Photocatalytic Water Detoxification - Comparison with a Medium Concentrating Solar Collector.* Water Sci Technol, 1997. 35(4): p. 157-164.

21. Malato, S., *et al.*, *Enhancement of the Rate of Solar Photocatalytic Mineralization of Organic Pollutants by Inorganic Oxidizing Species.* Applied Catalysis B: Environmental, 1998. 17(4): p. 347-356.

22. Pichat, P., *et al.*, *Assessment of the Importance of the Role of H2O2 and O-2(O-) in the Photocatalytic Degradation of 1,2- Dimethoxybenzene.* Solar Energ Mater Solar Cells, 1995. 38(1-4): p. 391-399.

23. Tanaka, K., H. Teruaki, and K. Harada, *Efficient photocatalytic degradation of chloral hydrate in aqueous semiconductor suspension.* Journal of Photochemistry and Photobiology, A: Chemistry, 1989. 48: p. 155-159.

24. Parra, S., *et al.*, *Photochemical versus coupled photochemical-biological flow system for the treatment of two biorecalcitrant herbicides: metobromuron and isoproturon.* Applied Catalysis B: Environmental, 2000. 27: p. 153-168.

25. Marco, A., S. Esplugas, and G. Saum, *How and Why to Combine Chemical and Biological Processes for Waste-Water Treatment.* Water Sci Technol, 1997. 35(4): p. 321-327.

GENERAL CONCLUSIONS AND PERSPECTIVES

The strategy of coupling photochemical and biological processes is presented as a good alternative to minimize the treatment cost of wastewater containing biorecalcitrant, non-biodegradable and/or toxic pollutants. However, it is not necessarily an universal solution for the detoxification of contaminated wastewater. Chemical, biological, and kinetic studies must be always conducted to ensure that the photochemical pretreatment induces beneficial effect on the biocompatibility of the treated wastewater. The development of this strategy as a new degradation technique of non-biodegradable organic substances in aqueous milieu has implicated among others, the study of some fundamental physicochemical properties, the optimization of a coupled reactor at laboratory scale, and the study of the solar photocatalytic treatment efficacy under direct sunlight using parabolic collectors.

From the fundamental physicochemical study described in the second chapter of this work, it can be conclude that the photoreactivity of substituted phenols and herbicides is affected by the electronic nature of the substituents and their positions in the aromatic ring. The photodegradation is faster when there is a greater electronic density on the aromatic ring. The Hammett constant, which represents the effect that different substituents have on the electronic character of a given aromatic system, appears to be an adequate descriptor of the photocatalytic degradability of the studied *para* substituted phenols. However, Hammett correlations for substrates with higher degree or different pattern of substitution are not reliable since this constant is not representative of all electronic and geometrical phenomena. In this sense, the implementation of predictive models for photoreactivity would requiere additional descriptors.

Further investigations are recommended for the development of models with significant predictive power of photoreactivity using computational quantum chemistry to find global electronic and geometrical descriptors of the molecules such as; zero point energy, total and electronic energy, dipolar moment, atoms charge and moment of inertia among others. These quantitative structure-property relationship studies for predicting the photocatalytic behaviour of different compounds are of great importance to estimate the time and energy necessary for the photocatalytic treatment and the effect of solar irradiation on pollutants present in natural medium.

One important point considered in this work is the role that adsorption of organic compounds on semiconductor particles surface plays on TiO_2-photocatalysed reactions. Although it has been often reported that adsorption is a prerequisite to the photodegradation of organic compounds, its role on the photocatalytic degradation rate is still uncertain. In this work, the dark adsorption isotherms for complete *p*-halophenols series and four herbicides are measured and correlated with their photoreactivity. The results confirm that no direct correlation exists between the measured extents of adsorption and the initial photodegradation rates of the studied compounds. In other words, a large extent of adsorption is not an indication of a highly efficient photodegradation of the herbicides or *vice versa*.

At laboratory scale, two kind of combined systems (of about 2 l) have been developed using in both cases immobilized biomass for the biological step and either diluted Fe^{3+} or TiO_2 supported on glass rings for the photocatalytic pretreatment (Chapter 3). Although both semicontinuous mode operated systems, seem to be efficient for the mineralisation of several compounds in solution, the use of supported TiO_2 is advantageous since the catalyst can be reused, the pH of treated solutions remains neutral, and H_2O_2 is nor necessarily required for the reaction.

The use of immobilized TiO_2 opens new possibilities for the coupling of TiO_2 photo-assisted and biological process, at pilot scale, employing both supported TiO_2 and bacteria. Using a CPC photoreactor, it has been demonstrated the utility of the homogeneous (based on Fe^{3+}/H_2O_2 reaction) and heterogeneous photocatalysis (based on TiO_2 suspension) as pretreatment methods that can be followed by a biological treatment. Further investigations are

needed concerning the biological treatment at pilot scale of solutions resulting from the degradation of the different substances.

The field experiments under direct sunlight using collectors as HM and CPC demonstrate that the solar photocatalytic treatment is effective for the purification of water contaminated by herbicides and other substances of industrial origin (chapter 4). However, different constructive factors, together with low manufacturing, installation, and maintenance costs, and easy operation of CPC compared with HM collectors, suggest that the former ones are, at present, the best way to apply the solar detoxification technology. A remarkable advantage of this kind of technology is that it can be transferred to countries with high sun irradiation levels as the tropical countries in development.

CURRICULUM VITAE

Sandra Patricia PARRA CARDONA

Born on February 8th, 1974 in Zarzal (Valle), COLOMBIA.

Address	EPFL - IGE/LBE Bât. CH-Ecublens CH-1015 Lausanne, Switzerland.
E-mail	sandra.parra@epfl.ch
Phone	++41 21 693 57 58

EDUCATION

1998 - 2001	Doctoral studies at the Laboratory of Environmental Biotechnology, Institute of Environmental Engineering, Department of Rural Engineering, EPFL.
1996 - 1998	Research assistantship at the Laboratory of Environmental Biotechnology, Institute of Environmental Engineering, Department of Rural Engineering, EPFL.
1995 - 1996	Chemist in industry: "Análisis Ambiental", Cali, Valle, Colombia.
1989 - 1995	B. Sc. Chemistry Universidad del Valle, Cali, Colombia.

LANGUAGES

Spanish: mother tongue

French: fluent

English: good knowledge

PUBLICATIONS

Journals

1. C. Pulgarín, M. Invernizzi, S. Parra, V. Sarria, R. Polanía, and P. Péringer. *Strategy for the coupling of photochemical and biological flow reactors useful in mineralization of biorecalcitrant industrial polluants*.Catalysis Today: (1999) 54. 341-352.

2. S. Parra, V. Sarria, S. Malato, P. Péringer, C. Pulgarín. *Photochemical versus photochemical-biological flow system for the treatment of two biorecalcitrant herbicides: metobromuron and isoproturon*. Applied Catalysis B: Environmental. 27 (2000) 153-168.

3. D. Robert, S. Parra, C. Pulgarín, A. Krzton and J.V. Weber. *Chemisorption of phenols and acids on TiO_2 surface*. Applied Surface Science. 167 (2000) 51-58.

4. S. Parra, S. Malato, J. Blanco, P. Péringer, C. Pulgarín. *Concentrating versus non-concentrating reactors for solar photocatalytic degradation of p-nitrotoluene-o-sulfonic acid*. Water Science and Technology. 44 (2001) 219-227.

5. V. Sarria, S. Parra, M. Invernizzi, P. Péringer, C. Pulgarín. *Photochemical - Biological treatment of a real industrial biorecalcitrant wastewater containing 5-amino-6-methyl-2-benzimidazolone*. Water Science and Technology. 44 (2001) 93-101.

6. S. Parra, S. Malato, C. Pulgarín. *New integrated photocatalytic-biological system using supported TiO_2 and fixed bacteria for the mineralization of isoproturon*. Applied Catalysis B: Environmental: in press.

7. S. Parra, J. Olivero, C. Pulgarín. *Relationship between physicochemical properties and photoreactivity of four biorecalcitrant phenylurea herbicides in aqueous TiO_2 suspension*. Applied Catalysis B: Environmental: in press.

Conferences

1. S. Parra, E. Hemmer, P. Péringer, C. Pulgarín. *Effect of the nature of substituent on the photoreactivity of the aromatics rings.* The Third International Conference on TiO_2 Photocatalytic Purification and Treatment of Water and Air, Orlando, Florida, USA, 1997.

2. S. Parra, C. Pulgarín, I. Rappaz, and P. Péringer. *Photocatalytic degradation of Isoproturon and Metobromuron in aqueous solution* The fourth International Conference on Advanced Oxidation Technologies for Water and Air Remediation, Orlando Orlando, Florida, USA, 1997.

3. S. Parra, E. Hemmer, P. Péringer, C. Pulgarín. *Effect of the nature of substituents in aromatic rings on the biodegradability and toxicity of photodegradated solutions.* International Symposium on Solar Chemistry:. Baden, Switzerland, 1997.

4. C. Pulgarín, M. Invernizzi, S. Parra, V. Sarria, P. Péringer. *Photochemical treatment vs continuous coupled photophenton-biological process for the degradation of a biorecalcitrant pollutant. Kinetics and economics aspects.* AWT98 -Advanced Wastewater Treatment, Recycling and Reuse, Milan, Italy, p. 919 – 922, 1998.

5. S. Parra, R. Polanía, V. Sarria, P. Péringer, C. Pulgarín. *Photoreactivity of phenolic compounds in TiO_2 suspension. Structure – reactivity relationship observations*. AWT98 -Advanced Wastewater Treatment, Recycling and Reuse, Milan, Italy, pp. 923 – 926, 1998.

6. S. Parra, R. Polanía, P. Péringer, C. Pulgarín. *Photoreactivity of industrial phenolic compounds in TiO_2 aqueous suspension: Biological and chemical characterictics of photodegradated solutions.* Water and Air treatment by Advanced oxidation technologies: Innovative and Commercial Applications, Lausanne, Switzerland, 1998.

7. C. Pulgarín, M. Invernizzi, S. Parra, V. Sarria and P. Péringer. *Photochemical Stand-Alone Reactor versus Integrated photophenton-biological flow systems for the mineralization of biorecalcitrant p-nitrotoluene-o-sulfonic acid.* Water and Air treatment by Advanced oxidation technologies: Innovative and Commercial Applications, Lausanne, Switzerland, 1998.

8. S. Parra, D. Robert, A. Krzton, J.V. Weber, C. Pulgarín. *Relationship between the structure and the adsorption of phenolic compounds: Diffuse reflectance FTIR study.* Water and Air treatment by Advanced oxidation technologies: Innovative and Commercial Applications, Lausanne, Switzerland, 1998.

9. C. Pulgarín, M. Invernizzi, S. Parra, V. Sarria, R. Polanía, and P. Péringer. *Strategy for the coupling of photochemical and biological flow reactors useful in mineralization of biorecalcitrant industrial polluants*. Proceedings of the 2nd users workshop: Training and Mobility of Researchers Programme at Plataforma Solar de Almeria, Almeria, Spain, p. 93-99, 1998.

10. S. Parra, C. Pulgarín, S. Malato, J. Blanco, P. Péringer. *Concentrating vs. non-concentrating reactor for solar photocatalytic degradation of p-NTS.* Proceedings of "Premières Journées: Chimie, Energie et Environnement". Saint-Avold, France, 2000.

11. S. Parra, V. Sarria, C. Pulgarín, S. Malato, P. Péringer. *Photochemical pre-treatment of two herbicides as a way to improve the biodegradability of their treated solutions.* Proceedings of "Premières Journées: Chimie, Energie et Environnement". Saint-Avold, France, 2000.

12. S. Parra, C. Pulgarín, S. Malato, J. Blanco, P. Péringer. *Concentrating vs non-concentrating reactor for solar photocatalytic degradation of p-nitrotoluene-o-sulfonic acid*. Abstract R-066. 2nd International Conference : Oxidation Technologies for Water and Wastewater treatment. Clausthal-Zellerfeld, Germany, 2000.

13. V. Sarria, M. Invernizzi, S. Parra, P. Péringer, C. Pulgarín. *Biological vs. Coupled photochemical-biological flow systems for degradation of an industrial wastewater.* Abstract R-073. 2nd International Conference : Oxidation Technologies for Water and Wastewater treatment. Clausthal-Zellerfeld, Germany, 2000.

14. K. Ng, S. Parra, P. Péringer, C. Pulgarín. *Photocatalytic degradation of para-halophenols in aqueous TiO_2 suspensions : influence of dissolved copper ions.* The fifth international conference on TiO_2 photocatalytic purification and treatment of water and air. London, Ontario, Canada, 2000.

15. S. Parra. V. Sarria. P. Péringer, C. Pulgarín. *Photochemical pre-treatment of two herbicides as a way to improve the biodegradability of their treated solutions.* The sixth international Conference on Advanced Oxidation Technologies for water and air remediation. London, Ontario, Canada, 2000.

16. S. Parra, V. Sarria, G. Rincón, R. Torres, C. Pulgarín. *Research and development of electrochemical and photochemical systems for the treatment of drinking and wastewater.* Water 2000, International Conference Water and Sanitation in Small Systems. Santiago de Cali, Colombia, October 2000.

17. L. Menkari, S. Parra, P. Péringer, C. Pulgarín. *Integrated photocatalytic – biological flow system for mineralization of the biorecalcitrant chlorotoluron herbicide.* Joint meeting of Italian, French, and Swiss photochemistry groups. Lausanne, Switzerland, February 2001.

18. S. Parra, G. Rincón, P. Péringer, C. Pulgarín. *Photocatalytical treatment via TiO_2 of four biorecalcitrant herbicides: metobromuron, isoproturon, chlorotoluron, and chlorobromuron.* The second European workshop on water, air and soil treatment by advanced oxidation technologies: Innovative and commercial applications. Poitiers, France, February 2001.